2018

DISTRIBUTION SYSTEM OPTIMIZATION WITH INTEGRATED DISTRIBUTED GENERATION

Sarmad Khaleel Ibrahim
University of Kentucky, sarmad_ibrahim1975@uky.edu
Digital Object Identifier: https://doi.org/10.13023/ETD.2018.132

STUDENT AGREEMENT:

I represent that my thesis or dissertation and abstract are my original work. Proper attribution has been given to all outside sources. I understand that I am solely responsible for obtaining any needed copyright permissions. I have obtained needed written permission statement(s) from the owner(s) of each third-party copyrighted matter to be included in my work, allowing electronic distribution (if such use is not permitted by the fair use doctrine) which will be submitted to UKnowledge as Additional File.

I hereby grant to The University of Kentucky and its agents the irrevocable, non-exclusive, and royalty-free license to archive and make accessible my work in whole or in part in all forms of media, now or hereafter known. I agree that the document mentioned above may be made available immediately for worldwide access unless an embargo applies.

I retain all other ownership rights to the copyright of my work. I also retain the right to use in future works (such as articles or books) all or part of my work. I understand that I am free to register the copyright to my work.

REVIEW, APPROVAL AND ACCEPTANCE

The document mentioned above has been reviewed and accepted by the student's advisor, on behalf of the advisory committee, and by the Director of Graduate Studies (DGS), on behalf of the program; we verify that this is the final, approved version of the student's thesis including all changes required by the advisory committee. The undersigned agree to abide by the statements above.

Sarmad Khaleel Ibrahim, Student

Dr. Aaron M. Cramer, Major Professor

Dr. Caicheng Lu, Director of Graduate Studies

DISTRIBUTION SYSTEM OPTIMIZATION WITH INTEGRATED DISTRIBUTED GENERATION

DISSERTATION

A dissertation submitted in partial fulfillment of the
requirements for the degree of Doctor of Philosophy in the
College of Engineering at the University of Kentucky

By

Sarmad Khaleel Ibrahim

Lexington, Kentucky

Director: Dr. Aaron M. Cramer , Associate Professor of Electrical Engineering

Lexington, Kentucky

2018

ABSTRACT OF DISSERTATION

DISTRIBUTION SYSTEM OPTIMIZATION WITH INTEGRATED DISTRIBUTED GENERATION

In this dissertation, several volt-var optimization methods have been proposed to improve the expected performance of the distribution system using distributed renewable energy sources and conventional volt-var control equipment:photovoltaic inverter reactive power control for chance-constrained distribution system performance optimisation, integrated distribution system optimization using a chance-constrained formulation, integrated control of distribution system equipment and distributed generation inverters, and coordination of PV inverters and voltage regulators considering generation correlation and voltage quality constraints for loss minimization. Distributed generation sources (DGs) have important benefits, including the use of renewable resources, increased customer participation, and decreased losses. However, as the penetration level of DGs increases, the technical challenges of integrating these resources into the power system increase as well. One such challenge is the rapid variation of voltages along distribution feeders in response to DG output fluctuations, and the traditional volt-var control equipment and inverter-based DG can be used to address this challenge.

These methods aim to achieve an optimal expected performance with respect to the figure of merit of interest to the distribution system operator while maintaining appropriate system voltage magnitudes and considering the uncertainty of DG power injections. The first method is used to optimize only the reactive power output of DGs to improve system performance (e.g., operating profit) and compensate for variations in active power injection while maintaining appropriate system voltage magnitudes and considering the uncertainty of DG power injections over the interval of interest. The second method proposes an integrated volt-var control based on a control action ahead of time to find the optimal voltage regulation tap settings and inverter reactive control parameters to improve the expected system performance (e.g., operating profit) while keeping the voltages across the system within specified ranges and considering the uncertainty of DG power injections over the interval of interest. In the third method, an integrated control strategy is formulated for the coordinated control of both distribution system equipment and inverter-based DG. This control strategy combines the use of inverter reactive power capability with the operation of voltage regulators to improve the expected value of the desired figure of merit (e.g., system losses) while maintaining appropriate system voltage magnitudes. The fourth method

proposes a coordinated control strategy of voltage and reactive power control equipment to improve the expected system performance (e.g., system losses and voltage profiles) while considering the spatial correlation among the DGs and keeping voltage magnitudes within permissible limits, by formulating chance constraints on the voltage magnitude and considering the uncertainty of PV power injections over the interval of interest.

The proposed methods require infrequent communication with the distribution system operator and base their decisions on short-term forecasts (i.e., the first and second methods) and long-term forecasts (i.e., the third and fourth methods). The proposed methods achieve the best set of control actions for all voltage and reactive power control equipment to improve the expected value of the figure of merit proposed in this dissertation without violating any of the operating constraints. The proposed methods are validated using the IEEE 123-node radial distribution test feeder.

KEYWORDS: Distributed power generation, chance-constrained programming, renewable integration, reactive power optimization, voltage control

Sarmad Khaleel Ibrahim
Author's signature

May 4, 2018
Date

DISTRIBUTION SYSTEM OPTIMIZATION WITH INTEGRATED DISTRIBUTED GENERATION

By

Sarmad Khaleel Ibrahim

Aaron M. Cramer
Director of Dissertation

Caicheng Lu
Director of Graduate Studies

May 4, 2018
Data

To my parents and family.

ACKNOWLEDGEMENTS

To my advisor Dr. Aaron M. Cramer, thank you for the advice and support. I have been lucky to work with Dr. Cramer for the past four years. I would also like to thank Dr. Liao for providing help, ideas, and co-authoring a couple of papers with me. I would like to thank my committee members Dr. Yuan Liao, Dr. Paul A. Dolloff, and Dr. Joseph Sottile for their insightful comments and their advice and willingness to serve on my dissertation advisory committee. I have to thank my outside examiner Prof. Zongming Fei for his valuable time. I would like to thank my wife for her encouragement and support through my Ph.D. studies. I have to thank my parents for their support and encouragement. They are always supporting me and encouraging me with their best wishes. This work was supported by the Ministry of Higher Education and Scientific Research and the University of Babylon, Iraq.

TABLE OF CONTENTS

LIST OF TABLES

LIST OF FIGURES

Chapter 1

Introduction

1.1 Introduction

A traditional power distribution system is a part of a power delivery system which serves as a link between the transmission system and customers. It has been initially designed and operated based on many essential assumptions in which the reliability and efficiency of distribution systems can be evaluated by designers or customers. It is designed to deliver power from the high voltage side of the electrical grid to last customers connected on the low voltage side. It is also designed based on unidirectional power flow, low energy losses, minimum consumption, voltages and currents within allowable limits, and centralized generating [1]. Although non-renewable energy sources are considered the primary source of energy in most electric power systems, they are also considered a source of environmental pollution because of waste materials such as carbon dioxide and sulfur dioxide, which contribute to increasing rates of greenhouse gas emissions in our atmosphere. Greenhouse gas emissions and polluting materials have necessitated research into new sources of producing electricity with less environmental impact. Renewable energy is an efficient solution to reduce global warming.

1.2 Distributed Generator Sources (DGs)

The increase of environmental pollution produced from conventional energy resources has stimulated the electric utilities to think of alternative energy sources to improve the tra-

ditional electric power system. This necessity of finding alternative energy sources with less environmental impact and production cost has dramatically increased in recent years. This need also gives a motivation to look for new small and large-scale power generation technologies that are able to be located at any point of consumption to reduce resources and improve system performance. These generating techniques are known as distributed generation or renewable energy distributed generation sources and can be easily installed into distribution systems by customers or electric utilities. However, these power generation sources fluctuate over the course of the day because they can only produce electricity when their energy source is available [2].

1.3 The Challenges Associated with Integration of DGs

When the number of DGs, which are mostly connected near the loads, increases with a high-level penetration, the challenges of integrating DGs into a power grid increase as well. With both a bidirectional power flow and fluctuated nature of DGs that cause a voltage fluctuation [3], the imperative challenge is how to control and mitigate the adverse effects of DGs such as a maximum voltage deviation. Also, all voltage control devices in traditional distribution systems have been mainly designed to operate without DGs, and voltage magnitudes decrease along the distribution feeder from the substation to the end-users. The presence of DGs makes this assumption no longer valid because the change of power flow (e.g., the bidirectional power flow) causes the node phase voltage magnitudes along the distribution feeder to violate these assumptions [4].

The DG impacts relatively increase or decrease depending on the location and size of a penetration level of the DGs generation. These impacts can significantly reduce the life of equipment that is used in a distribution feeder for controlling issues. Some of the significant impacts and challenges have been addressed by researchers for the implementation of distribution networks with DGs including voltage magnitude levels, power flow, thermal equipment ratings, fault current levels, and protection issues [5].

1.4 The Benefits Associated with Integration of DGs

The contribution of increasing benefits by DGs to the electric utilities is dramatically increased during the last few decades. Most electric utilities have found that the economic cost of injecting reactive power into distribution systems can be obtained by using DGs, and efficient use of the DGs will highly benefit the electric utilities. Many advantages have been mainly obtained by using DGs into distribution systems such as supporting the network voltage, minimizing feeder losses, increasing the system reliability, and reducing greenhouse gas emissions [6–8]. The DGs are also capable to assist the energy supply for distribution system loads. Once DGs are connected near the loads, the electric utilities and users who own the DGs can obtain some good benefits such as loss reduction and increased operating profit [9].

1.5 Volt-var Control in Distribution Systems with DGs

The primary advantages of using the volt-var control in distribution systems are to maintain appropriate system voltages and consider the uncertainty of power injections and loads by injecting or consuming reactive power as necessary. In the traditional distribution system, volt-var control actions have been performed based on the voltage and reactive power equipment such as switchable capacitor banks, on load tap changer transformers, and step voltage regulators. This volt-var control equipment is designed to operate based on assumptions such as unidirectional power flow in which the voltages decrease along the distribution system within the American National Standards Institute (ANSI) standard.

Coordinated volt-var control methods using the traditional voltage and reactive power equipment in distribution systems to minimize the energy consumption or system losses have been widely investigated and studied by researchers. For example, a step voltage regulator and shunt capacitor are coordinated to keep the system voltage within acceptable limits under various load conditions [10]. Another researcher has discovered that finding

optimal scheduling of on-load tap changer position and capacitor bank status for some hours in advance can minimize the real power losses [11]. Voltage stability of the system can be improved by controlling the operational decision of the voltage regulator devices [12]. Different control approaches in the distribution system are reviewed based on volt-var control strategies [13].

Due to falling costs and increasing interest in alternative energy sources rather than fossil-fuel-based sources, using DGs has increased significantly in recent years with the transmission and distribution system [14]. The connection of DGs into the distribution system has increased the challenges of traditional volt-var control equipment to match the assumptions for which the distribution system is designed. With increasing the penetration level and intermittent nature of DGs, traditional feeder volt-var controls are too slow to react to fast fluctuations in the power output of DGs. Traditional voltage control systems, which are considered local static var sources and too expensive, cannot respond to a fast variation in the power output of DGs [15].

With fast development in DG inverter technologies, the electric utilities have found that power electronic inverter-based DGs are an excellent alternative to solve the problem associated with a rapid response to a voltage variation. Since inverter-based DGs are power electronic devices, they can provide the reactive power needed in less than 50 milliseconds to avoid fast voltage fluctuations caused by transient cloud passing [16, 17]. Using this feature, inverter-based DGs have reduced the dependency on the traditional distribution system control such as on-load tap changers, capacitor banks, and static var compensators. For example, shunt capacitors can only support the system voltage by injecting reactive power, but cannot absorb reactive power. On the other hand, DG inverters have fast response times and simply provide dynamic values, and can efficiently provide faster and more flexible reactive power support that is capable of generating or absorbing and assisting in controlling voltage [18].

Coordinated reactive power compensation, which can be obtained from DG inverters

and traditional volt-var control devices, can provide significant economic benefits for electric utilities and can improve the system efficiency and reliability [19, 20]. For example, significant advantages can be obtained using PV inverters such as minimizing system losses and increasing line capacities [21]. The optimal volt-var control is proposed using the capability of PV inverters to generate and absorb the reactive power to minimize system losses and energy consumption while maintaining the voltage magnitudes within desired ranges [22].

The volt-var control also aims to keep the voltage deviation within an acceptable range by using system control devices, such as on-load tap changer transformers and PV inverters, and to regulate voltage magnitudes for either local control or global control along the distribution feeder [23]. PV inverters can provide a reactive power compensation that can be utilized in supplying voltage support when fluctuations in generation occur [24]. The volt-var control can also be used to conserve energy by maintaining the voltage magnitudes within acceptable levels [25]. The electric utility company can deliver energy more efficiently by controlling voltage magnitudes based on the ANSI standards [26]. As a result, the electric utilities will save money by reducing total power losses in a distribution feeder [27].

There are many other methods to support voltage optimization in the distribution system using DGs. Many electric utility companies have efficiently used an accurate power prediction method for fluctuating solar power production to improve the accuracy of volt-var control methods. An accurate prediction is essential for electric utilities because efficient use of the fluctuating solar power production could provide a strong economic impact on total generation costs and a substantial improvement associated with the integration of DGs into the distribution feeder [28].

This dissertation provides supervisory control methods focusing on improving the expected system performance concerning a figure of the merit of interest to the distribution system operator (e.g., operating profits, system losses, and voltage profiles) while con-

straining the probability of unacceptable voltage magnitudes occurring during the interval of interest. The integrated control strategies proposed herein are used to coordinate existing inverter-based DG and voltage control equipment (e.g., voltage regulators) based on the current communication infrastructure of traditional power distribution networks. For instance, it is assumed that supervisory control and data acquisition (SCADA) systems can be used for communicating and coordinating between the distribution system operator and the available voltage and reactive power control equipment. These control strategies also require both infrequent communication with the distribution system operator and infrequent changes to voltage control equipment. However, they can respond to rapidly changing conditions by providing control parameters to the inverters to allow them to respond to such changes in real time, a capability that is available in smart inverters.

1.6 Dissertation Outline

The remainder of this dissertation is organized as follows: The literature review related to the contribution of DG inverters and traditional voltage regulator devices in volt-var control methods into the distribution system is described in Chapter 2. Photovoltaic inverter reactive power control for chance-constrained distribution system performance optimisation is proposed in Chapter 3. Integrated distribution system optimization using a chance-constrained formulation is discussed in Chapter 4. Integrated control of distribution system equipment and distributed generation inverters is discussed in Chapter 5. Coordination of PV inverters and voltage regulators considering generation correlation and voltage quality constraints for loss minimization is discussed in Chapter 6. Conclusions and the future work are discussed in Chapter 7.

Chapter 2

Literature Review

With more PV installations being implemented in distribution systems, due to falling costs and increasing interest in alternative energy sources rather than fossil-fuel-based sources, the technical challenges associated with high penetration levels are becoming ever more critical [29]. Despite the potential benefits of DGs [30], such as PV and wind generation, high penetration of these resources also reduces the effectiveness of existing methods that are used to maintain system voltage magnitudes and reduce system losses in distribution systems [31]. Mitigation of the problems associated with the intermittency of PV sources when clouds pass is a difficult technical challenge that distribution system operators must address. PV output changes both over the course of a day and much shorter periods due to cloud transient. Cloud transient caused by the passage of shadows over a PV source can result in changes in solar irradiance as much as $60\%/s$ [32, 33]. Therefore, PV inverters, which perform maximum power point tracking on the order of 50 milliseconds [16, 34], will quickly vary the amount of active power being injected into the distribution system. These transients cause voltage magnitudes in distribution systems to fluctuate rapidly. The rapid variation of voltages along distribution feeders in response to PV output fluctuations remains one of the challenges that has increased with rising PV penetration levels in the distribution feeder [35]. While facing this issue, distribution system operators are still charged with improving system performance by reducing system losses or total demand.

Many studies have proposed that PV inverters, with their reactive power capability that

can be largely controlled independently [36], can be used to improve distribution system operations [37, 38]. PV inverters, in addition to feeding active power, are capable of absorbing reactive power from or providing it to the distribution system [39]. PV inverters, unlike other distribution system devices, are necessary to inject power from PV sources into the distribution system and are typically purchased by the PV owner. PV inverters can efficiently reduce the dependency on traditional distribution system control equipment such as OLTC transformers, capacitor banks, and static var compensators [31, 40]. Traditional voltage regulator devices either do not have the capability to respond to voltage fluctuations, due to fast variation in the power output of PV sources (in the case of mechanical devices), or are very expensive (in the case of power electronic devices) [41]. Many published studies have addressed the use of static var compensators, capacitor banks, on-load tap changer transformers (OLTC), etc., for volt-var optimization [42,43]. A voltage and var control (VCC) with DGs is used to find the optimal setting for the feeder control variables using traditional voltage control and a PV inverter [44].

Many studies have proposed that PV inverters and traditional volt-var control devices can provide significant economic benefits for electric utilities and can improve the system efficiency and reliability. For example, improving the operating profit using the distribution system losses and the voltage profile as important factors to measure the growth in the operating profit is shown in [45–47]. The goodness factor of DGs based on the calculation of the incremental contribution of DGs to distribution system losses is proposed in [45]. Increasing financial benefits and managing the load demand by optimizing short-term activities for a distribution system operator is considered in [46]. Financial benefits can be obtained by using the nodal pricing on the distribution network [47]. The PV inverters can be used to improve the efficiency of power distribution systems by reducing line losses. For example, in [48], a decentralized controller is proposed to reduce system losses by controlling the reactive power being injected by PV inverters. System losses can be reduced by injecting most of the PV power produced into the phase with the highest power consumption [49].

In [50], a real-time volt-var controller is proposed to reduce feeder losses by controlling the traditional voltage regulation devices along with a PV inverter. The integration of DGs used to maximize the system performance and maintain a voltage regulation with uncertain power injections is presented in [51, 52]. Minimizing the operating cost and eliminating voltage violations are proposed in [53]. Based on predictive outputs of wind turbines and photovoltaic generators, volt/var control considers the integration of distributed generators and load-to-voltage sensitivities [54]. The optimal allocation of DGs can reduce system losses in the distribution system while maintaining the system voltages within acceptable limits [55]. While such studies show a benefit from reactive power injection, they do not address the challenges associated with fluctuations in active power injection.

To limit the voltage fluctuations that can cause a number of technical challenges, many volt-var control approaches have been studied in distribution systems. For example, the enhanced utilization of voltage control resources in order to increase DG capacity and reduce the negative impact on the voltage levels in a transmission system side is proposed in [56]. Different control strategies to coordinate multiple voltage regulating devices with PV inverters can be used to mitigate the voltage fluctuation and improve the power quality [57, 58]. A volt-var control with DGs is used to find the optimal settings of reactive power provided by distributed energy resources for the system control variables using traditional voltage control and PV inverters [59]. The optimal control of distribution voltage magnitudes with coordination of voltage regulation devices is considered in [60]. The central and local methods used to control the distribution voltage and the amount of curtailed active power using PV inverters are proposed in [61].

A high penetration level of DGs in a distribution system may also result in voltage rise because of a bi-directional power flow. Multiple methods to avoid a voltage rise have been studied in distribution systems. For example, a voltage control loop can be used by absorbing or injecting reactive power from PV inverters to mitigate the effect of the reverse power flow caused by PV inverters [62]. An adaptive algorithm for reactive power

control is proposed to manage the bus voltage along the distribution feeder and reduce the feeder losses with high-level penetration in [63]. A smart VVC is used to perform power flow analysis based on intelligent meter measurements and wireless communication systems to maintain voltages within acceptable voltage limits along the distribution feeder, minimize system losses, and coordinate the traditional voltage regulators [64]. To mitigate an unwanted voltage rise at the load bus when DGs with high penetration are installed on the distribution feeder, voltage magnitudes at the substation can be adjusted within acceptable limits [65].

A consequence of wide-scale deployment of DGs is also voltage variations. Many studies have been conducted to address voltage magnitude variations. For example, DG inverters can perform fast and flexible voltage regulation to mitigate the impacts of sudden voltage fluctuations and reduce system losses [66]. Voltage deviations caused by variation in the output of DGs are too fast to be effectively remedied by traditional distribution system equipment and can cause excessive wear and tear on such devices [67–69]. Voltage deviation problems can be mitigated using adaptive droop-based control algorithms to control the active and reactive power of PV inverters [70]. Another study to mitigate unwanted voltage variations has shown that voltage quality can be improved if the reactive power output is substituted for active power output during periods of fluctuation [71]. Multiple control modes (voltage support, mitigating the voltage rise, and mitigating the voltage fluctuation) are considered in [72–74].

A method for controlling the reactive power capability of PV inverters has two primary concerns for the distribution system operator. First, the voltage magnitudes throughout the distribution system must remain within acceptable limits, despite fluctuations in PV active power output. Second, the method should improve the performance of the distribution system as quantified by some figure of merit of interest to the distribution system operator. Most of the studies above have focused on one or the other of these two concerns, with relatively little work on the combined problem. Even the dual-layer approach proposed

in [75], solves the second concern in its outer layer, reserving a margin to address the first concern in its inner layer. Although reactive power control to improve voltage quality or system performance had been investigated in previous studies, the full capability of all control devices is not being used either because of lack of coordination between these devices or because of separate consideration of reactive power control and voltage control that causes suboptimal solutions.

By analogy to microgrid control systems, the volt-var control methods proposed in this dissertation are most similar to a tertiary level control [76]. Similar control ideas are employed in microgrids [77]. The proposed control methods use a chance-constrained approach.

Chance-constrained approaches have been proposed recently to achieve a certain level of reliability under the uncertainty associated with DG output. For example, minimization of capital and operating costs under uncertainty can be posed as a chance-constrained problem [78, 79]. A robust chance-constrained optimal power flow is used to minimize an uncertainty in the parameters of probability distributions and model uncertainty of supply in [80]. Chance-constrained optimal power flow can be used to maximize system performance [81–83]. In very recent studies, the idea of chance-constrained optimal power flow is considered for similar problems [84]. In [84], a similar approach to that proposed in [85] is applied to optimal power flow problems in which forecasting errors can occur in future time steps and in which there are devices with intertemporal constraints (e.g., energy storage). The approach proposed in [85] is used to solve a chance-constrained optimal control problem. In this proposed approach, unlike existing literature, a similar approach is applied to a conceptually different problem. While [84] considers uncertainty at future time steps, the proposed method in [85] consider uncertainty that can occur between control time steps, allowing for suitable operation with relatively infrequent communication. Unlike methods in other studies, an integrated control strategy proposed in [85] for the coordinated control of DGs and voltage control devices (e.g., voltage regulators) requires only infrequent

communication with the distribution system operator.

In this dissertation, the proposed methods perform the supervisory control methods of voltage and reactive power devices in the distribution system. These controls use a large time step (i.e., 1 second for inverter reactive power control and 15 minutes for voltage regulator tap operations and communication with the distribution system operator) using low bandwidth communication. At this level, these controls are primarily focused on optimizing the performance of the system in terms of voltage magnitudes, operating profits, losses, and voltage profiles.

Chapter 3

Photovoltaic Inverter Reactive Power Control for Chance-Constrained Distribution System Performance Optimisation

3.1 Introduction

In this chapter, a method of achieving optimal expected performance with respect to a figure of merit of interest to the distribution system operator while keeping voltage magnitudes within acceptable ranges is proposed. A figure of merit, as used herein, represents a numerical quantity for which a distribution system operator has an interest in maximizing the expected value. In this proposed method, the operating profit serves as an example, but other figures (e.g., losses, total demand) could also be used with this method. Such a method would preferably not rely on high-bandwidth communication between the distribution system operator and the PV inverters.

Specifically, this method utilizes reactive power injections in PV phases both to improve expected system performance and to compensate for variations in active power injection during an upcoming interval in which no further system control decisions are possible and yet in which considerable uncertainty regarding PV power injections remains. It operates at a relatively slow time step (e.g.,15 minutes), requiring relatively infrequent communication between the distribution system operator and the PV inverters. For instance, the current communication infrastructure of classic power distribution networks, via SCADA

system, can be used for communication so that the distribution system operator can control the PV inverters [86]. The implementation of the proposed strategy assumes that short-term forecasts of the expected real power generated by the PV plant and the expected load are known with sufficient accuracy. As well, it bases its decisions on short-term forecasts that include the mean and variance of the active power injection over the interval (e.g., every 15 minutes), and formulates the voltage magnitude requirements as chance constraints. By utilizing the reactive power capability of the inverters in this manner, it reduces wear-and-tear of traditional mechanical voltage regulation equipment while achieving faster control of voltage magnitudes during a period of PV power injection variation. The work mentioned in this chapter has been published in [85].

The remainder of this chapter is organized as follows. The system description and methods of approximating the figure of merit and the system voltage magnitudes and their sensitivity with respect to the active and reactive power injected into each PV phase are presented in Section 3.2. In Section 3.3, the specific problem formulation considered herein and the proposed solution method are described. The test system, based on the IEEE 123-node radial distribution test feeder [87], is detailed in Section 3.4. In Section 3.5, the results of the proposed method and three benchmark methods are compared for three cases (cloudy, sunny, and transient). Conclusions are drawn in Section 3.6.

3.2 System Description and Approximation

The problem considered herein is to maximize the expected value of a figure of merit U associated with the operation of the distribution system while constraining the probability of unacceptable voltage magnitudes. The performance of the distribution system will vary with load and other factors, but the primary concern addressed herein is the rapid fluctuation of power injection from PV sources (e.g., due to cloud transients). An example figure

of merit considered herein is operating profit, which can be expressed as

$$U = \sum_{i=1}^{N_{load}} C^{load} P_{load,i} - \sum_{i=1}^{N_{pv}} C^{pv} P_{pv,i} - \sum_{i=1}^{N_{in}} C^{in} P_{in,i}, \tag{3.1}$$

where N_{load}, N_{pv}, and N_{in} are the numbers of load, PV, and input (i.e., substation) node phases, respectively, C^{load} is the price received for power delivered to loads, C^{pv} is the price paid for power received from PV sources, C^{in} is the price paid for power received from the input, $P_{load,i}$ is power delivered to a load phase i, $P_{pv,i}$ is power received from a PV phase i, and $P_{in,i}$ is power received from an input phase i.

The first part of (3.1) is the revenue associated with the active power consumed by the loads. The second part is the cost of the active power supplied by the PV sources. The third part is the cost of power purchased by the distribution system operator from an external source, such as the transmission system. In this study, the prices are considered to be known in advance for an upcoming time interval. When the output power of the PV sources change, the load demand and the power supplied from the transmission system vary as well.

The active power produced in each PV phase is represented by the vector $\mathbf{P}_{pv} \in \mathbb{R}^{N_{pv}}$. PV inverters are also capable of producing reactive power, and the reactive power produced in each PV phase is represented by $\mathbf{Q}_{pv} \in \mathbb{R}^{N_{pv}}$. It is possible to use linearization to describe the behavior of the distribution system about an operating point. For a given operating point represented as $*$ where $\mathbf{P}_{pv} = \mathbf{P}_{pv0}$ and $\mathbf{Q}_{pv} = \mathbf{Q}_{pv0}$, Taylor series expansion can be used around the operation point.

The figure of merit can be approximated as

$$U(\mathbf{P}_{pv}, \mathbf{Q}_{pv}) \approx \underbrace{U|_*}_{U_0} + \underbrace{\left.\frac{\partial U}{\partial \mathbf{P}_{pv}}\right|_*}_{\mathbf{U}_P^{\mathrm{T}}} (\mathbf{P}_{pv} - \mathbf{P}_{pv0}) \underbrace{\left.\frac{\partial U}{\partial \mathbf{Q}_{pv}}\right|_*}_{\mathbf{U}_Q^{\mathrm{T}}} (\mathbf{Q}_{pv} - \mathbf{Q}_{pv0}), \tag{3.2}$$

where U_0 is the figure of merit evaluated at the operating point and $\mathbf{U}_P$ and $\mathbf{U}_Q$ represent the sensitivity of the figure of merit with respect to the active and reactive power injected

into each PV phase. The operating profit herein considered as an example figure of merit,

$$U_0 = \sum_{i=1}^{N_{load}} C^{load} P_{load,i}|_* - \sum_{i=1}^{N_{pv}} C^{pv} P_{pv,i}|_* - \sum_{i=1}^{N_{in}} C^{in} P_{in,i}|_* \tag{3.3}$$

$$\mathbf{U}_P^{\mathrm{T}} = \sum_{i=1}^{N_{load}} C^{load} \frac{\partial P_{load,i}}{\partial \mathbf{P}_{pv}}\bigg|_* - \sum_{i=1}^{N_{pv}} C^{pv} \frac{\partial P_{pv,i}}{\partial \mathbf{P}_{pv}}\bigg|_* - \sum_{i=1}^{N_{in}} C^{in} \frac{\partial P_{in,i}}{\partial \mathbf{P}_{pv}}\bigg|_* \tag{3.4}$$

$$\mathbf{U}_Q^{\mathrm{T}} = \sum_{i=1}^{N_{load}} C^{load} \frac{\partial P_{load,i}}{\partial \mathbf{Q}_{pv}}\bigg|_* - \sum_{i=1}^{N_{pv}} C^{pv} \frac{\partial P_{pv,i}}{\partial \mathbf{Q}_{pv}}\bigg|_* - \sum_{i=1}^{N_{in}} C^{in} \frac{\partial P_{in,i}}{\partial \mathbf{Q}_{pv}}\bigg|_* . \tag{3.5}$$

The node phase voltages along the distribution feeder can be represented using the vector $\tilde{\mathbf{V}} \in \mathbb{C}^{N_{node}}$, where N_{node} is the number of node phases within the system. The node voltage magnitudes are a function of the active and reactive power injected into each PV phase:

$$|\tilde{\mathbf{V}}| = \mathbf{f}(\mathbf{P}_{pv}, \mathbf{Q}_{pv}), \tag{3.6}$$

and this function can be evaluated while performing load flow. Taylor series expansion is used around the operation point $*$, and the voltage magnitudes can be approximated as

$$|\tilde{\mathbf{V}}| \approx \underbrace{\mathbf{f}|_*}_{\mathbf{V}_0} + \underbrace{\frac{\partial \mathbf{f}}{\partial \mathbf{P}_{pv}}\bigg|_*}_{\mathbf{V}_P} (\mathbf{P}_{pv} - \mathbf{P}_{pv0}) + \underbrace{\frac{\partial \mathbf{f}}{\partial \mathbf{Q}_{pv}}\bigg|_*}_{\mathbf{V}_Q} (\mathbf{Q}_{pv} - \mathbf{Q}_{pv0}), \tag{3.7}$$

where $\mathbf{V}_0$ is the voltage magnitudes evaluated at the operating point and $\mathbf{V}_P$ and $\mathbf{V}_Q$ represent the sensitivity of the voltage magnitudes with respect to the active and reactive power injected into each PV phase and can be evaluated while performing load flow. In this work, it is assumed that the PV injections are provided by three-phase sources (i.e., $N_{pv} = 3N_{source}$), where N_{source} is the number of sources. Furthermore, it is assumed that the active power from these sources is being injected equally in each phase. Thus, the power being injected into each PV phase can be expressed as

$$\mathbf{P}_{pv} = \mathbf{H}\mathbf{P}_{source}, \tag{3.8}$$

where $\mathbf{H} = \frac{1}{3}(\mathbf{I}_{N_{source}} \otimes \mathbf{1}_{3\times 1})$, $\mathbf{I}_n$ is the $n \times n$ identity matrix, $\otimes$ is the Kronecker product operator, $\mathbf{1}_{m\times n}$ is the $m \times n$ matrix filled with unity, and $\mathbf{P}_{source} \in \mathbb{R}^{N_{source}}$ is the vector describing the power being injected from each PV source.

The reactive power output of each PV phase can be adjusted based on the active power output of the phase. The reactive power injected into each PV phase can be expressed using an affine control equation:

$$\mathbf{Q}_{pv} = \boldsymbol{\alpha} + \boldsymbol{\beta} \circ \mathbf{P}_{pv}, \tag{3.9}$$

where $\boldsymbol{\alpha} \in \mathbb{R}^{N_{pv}}$ and $\boldsymbol{\beta} \in \mathbb{R}^{N_{pv}}$ are vectors of the control parameters describing the behavior of each PV phase, and the $\circ$ is the Hadamard product operator. The nth Hadamard root of a matrix $\mathbf{A}$ is denoted $\mathbf{A}^{\circ\frac{1}{n}}$, and the nth Hadamard power is denoted $\mathbf{A}^{\circ n}$. Substituting (3.8) into (3.9) yields

$$\mathbf{Q}_{pv} = \boldsymbol{\alpha} + \boldsymbol{\beta} \circ (\mathbf{H}\mathbf{P}_{source}). \tag{3.10}$$

Substituting (3.8) and (3.10) into (3.2) yields

$$\begin{aligned} U \approx\ & U_0 + \mathbf{U}_P^{\mathrm{T}}(\mathbf{H}\mathbf{P}_{source} - \mathbf{P}_{pv0}) + \mathbf{U}_Q^{\mathrm{T}}((\boldsymbol{\alpha} + \boldsymbol{\beta} \circ (\mathbf{H}\mathbf{P}_{source})) - \mathbf{Q}_{pv0}) \\ =\ & U_0 + \mathbf{U}_P^{\mathrm{T}}(\mathbf{H}\mathbf{P}_{source} - \mathbf{P}_{pv0}) - \mathbf{U}_Q^{\mathrm{T}}\mathbf{Q}_{pv0} + \mathbf{U}_Q^{\mathrm{T}}\boldsymbol{\alpha} + \mathbf{U}_Q^{\mathrm{T}}\operatorname{diag}[\mathbf{H}\mathbf{P}_{source}]\boldsymbol{\beta}, \end{aligned} \tag{3.11}$$

where the diagonal operator $\operatorname{diag}[\mathbf{x}]$ on a vector $\mathbf{x} \in \mathbb{R}^n$ is an $n \times n$ matrix with the elements of $\mathbf{x}$ on the diagonal. Substituting (3.8) and (3.10) into (3.7) gives

$$\begin{aligned} |\tilde{\mathbf{V}}| \approx\ & \mathbf{V}_0 + \mathbf{V}_P(\mathbf{H}\mathbf{P}_{source} - \mathbf{P}_{pv0}) + \mathbf{V}_Q\left((\boldsymbol{\alpha} + \boldsymbol{\beta} \circ (\mathbf{H}\mathbf{P}_{source})) - \mathbf{Q}_{pv0}\right) \\ =\ & \mathbf{V}_0 + \mathbf{V}_P(\mathbf{H}\mathbf{P}_{source} - \mathbf{P}_{pv0}) - \mathbf{V}_Q\mathbf{Q}_{pv0} + \mathbf{V}_Q\boldsymbol{\alpha} + \mathbf{V}_Q\operatorname{diag}[\mathbf{H}\mathbf{P}_{source}]\boldsymbol{\beta}. \end{aligned} \tag{3.12}$$

3.3 Problem Formulation

The problem considered herein is to maximize the expected value of a figure of merit while constraining the probability of unacceptable voltage magnitudes over some interval of time:

$$\begin{array}{ll} \max_{\boldsymbol{\alpha},\boldsymbol{\beta}} & \mathrm{E}[U] \\ \text{subject to} & \Pr[|\tilde{V}_i| \le V_{min}] \le p_{max} \\ \forall i \in \{1,2,\ldots,N_{node}\} & \Pr[|\tilde{V}_i| \ge V_{max}] \le p_{max}, \end{array} \tag{3.13}$$

where V_i is the voltage at node phase i and p_{max} is the maximum acceptable probability for a node phase voltage magnitude to leave the acceptable range of $[V_{min}, V_{max}]$. It is

assumed that the expected value and the variance of each source power are both known, i.e., $\mathrm{E}[\mathbf{P}_{source}]$ and $\mathrm{Var}[\mathbf{P}_{source}]$. This nonlinear problem is solved iteratively (as described below) and is solved based on a linearization about the previous solution estimate (i.e., $\boldsymbol{\beta}_0$).

For given control parameters $\boldsymbol{\alpha}$ and $\boldsymbol{\beta}$, it is possible to approximate $\mathrm{E}[U]$ using (3.2):

$$\begin{aligned}\mathrm{E}[U] &\approx U_0 + \mathbf{U}_P^{\mathrm{T}}(\mathbf{H}\mathrm{E}[\mathbf{P}_{source}] - \mathbf{P}_{pv0}) - \mathbf{U}_Q^{\mathrm{T}}\mathbf{Q}_{pv0} + \mathbf{U}_Q^{\mathrm{T}}\boldsymbol{\alpha} + \mathbf{U}_Q^{\mathrm{T}}\,\mathrm{diag}[\mathbf{H}\mathrm{E}[\mathbf{P}_{source}]]\boldsymbol{\beta} \\ &= \mathbf{c}_0 + \mathbf{c}_\alpha^{\mathrm{T}}\boldsymbol{\alpha} + \mathbf{c}_\beta^{\mathrm{T}}\boldsymbol{\beta}, \end{aligned} \tag{3.14}$$

where

$$\mathbf{c}_0 = U_0 + \mathbf{U}_P^{\mathrm{T}}(\mathbf{H}\mathrm{E}[\mathbf{P}_{source}] - \mathbf{P}_{pv0}) - \mathbf{U}_Q^{\mathrm{T}}\mathbf{Q}_{pv0}, \tag{3.15}$$

$$\mathbf{c}_\alpha = \mathbf{U}_Q, \tag{3.16}$$

$$\mathbf{c}_\beta = \mathrm{diag}[\mathbf{H}\mathrm{E}[\mathbf{P}_{source}]]\mathbf{U}_Q. \tag{3.17}$$

The expected voltage magnitudes along the distribution feeder can be expressed from (3.7) as

$$\begin{aligned}\mathrm{E}[|\tilde{\mathbf{V}}|] &\approx \mathbf{V}_0 + \mathbf{V}_P(\mathbf{H}\mathrm{E}[\mathbf{P}_{source}] - \mathbf{P}_{pv0}) - \mathbf{V}_Q\mathbf{Q}_{pv0} + \mathbf{V}_Q\boldsymbol{\alpha} + \mathbf{V}_Q\,\mathrm{diag}[\mathbf{H}\mathrm{E}[\mathbf{P}_{source}]]\boldsymbol{\beta} \\ &= \mathbf{N}_0 + \mathbf{N}_\alpha\boldsymbol{\alpha} + \mathbf{N}_\beta\boldsymbol{\beta}, \end{aligned} \tag{3.18}$$

where

$$\mathbf{N}_0 = \mathbf{V}_0 + \mathbf{V}_P(\mathbf{H}\mathrm{E}[\mathbf{P}_{source}] - \mathbf{P}_{pv0}) - \mathbf{V}_Q\mathbf{Q}_{pv0} \tag{3.19}$$

$$\mathbf{N}_\alpha = \mathbf{V}_Q \tag{3.20}$$

$$\mathbf{N}_\beta = \mathbf{V}_Q\,\mathrm{diag}[\mathbf{H}\mathrm{E}[\mathbf{P}_{source}]]. \tag{3.21}$$

Assuming that the source powers are independently distributed over the interval of interest, the variance of the voltage magnitudes can be expressed from (3.7) as

$$\mathrm{Var}[|\tilde{\mathbf{V}}|] \approx (\mathbf{V}_P\mathbf{H} + \mathbf{V}_Q\,\mathrm{diag}(\boldsymbol{\beta})\mathbf{H})^{\circ 2}\,\mathrm{Var}[\mathbf{P}_{source}], \tag{3.22}$$

and the standard deviation can be written as

$$(\mathrm{Var}[|\tilde{\mathbf{V}}|])^{\circ\frac{1}{2}} \approx ((\mathbf{V}_P\mathbf{H} + \mathbf{V}_Q\,\mathrm{diag}(\boldsymbol{\beta})\mathbf{H})^{\circ 2}\mathrm{Var}[\mathbf{P}_{source}])^{\circ\frac{1}{2}}. \tag{3.23}$$

The standard deviation can be further approximated using a Taylor series around a previous estimate of $\boldsymbol{\beta}$ (i.e., $\boldsymbol{\beta}_0$):

$$\begin{aligned}(\mathrm{Var}[|\mathbf{V}|])^{\circ\frac{1}{2}} \approx{}& (((\mathbf{V}_P + \mathbf{V}_Q \,\mathrm{diag}[\boldsymbol{\beta}_0])\mathbf{H})^{\circ 2}\,\mathrm{Var}[\mathbf{P}_{source}])^{\circ\frac{1}{2}} \\ &+ (((\mathbf{V}_P + \mathbf{V}_Q \,\mathrm{diag}[\boldsymbol{\beta}_0])\mathbf{H}\,\mathrm{diag}[\mathrm{Var}[\mathbf{P}_{source}]] \\ &\cdot \mathbf{H}^{\mathrm{T}}) \circ \mathbf{V}_Q \circ ((((\mathbf{V}_P + \mathbf{V}_Q \,\mathrm{diag}[\boldsymbol{\beta}_0])\mathbf{H})^{\circ 2} \\ &\cdot \mathrm{Var}[\mathbf{P}_{source}])^{\circ\frac{1}{2}}\mathbf{1}_{1\times N_{pv}})^{\circ(-1)})(\boldsymbol{\beta} - \boldsymbol{\beta}_0) \\ ={}& \mathbf{M}_0 + \mathbf{M}_\beta \boldsymbol{\beta}, \end{aligned} \tag{3.24}$$

where

$$\begin{aligned}\mathbf{M}_0 = {}& (((\mathbf{V}_P + \mathbf{V}_Q \,\mathrm{diag}[\boldsymbol{\beta}_0])\mathbf{H})^{\circ 2}\,\mathrm{Var}[\mathbf{P}_{source}])^{\circ\frac{1}{2}} \\ &- (((\mathbf{V}_P + \mathbf{V}_Q \,\mathrm{diag}[\boldsymbol{\beta}_0])\mathbf{H}\,\mathrm{diag}[\mathrm{Var}[\mathbf{P}_{source}]]\mathbf{H}^{\mathrm{T}}) \\ &\circ \mathbf{V}_Q \circ ((((\mathbf{V}_P + \mathbf{V}_Q \,\mathrm{diag}[\boldsymbol{\beta}_0])\mathbf{H})^{\circ 2}\,\mathrm{Var}[\mathbf{P}_{source}])^{\circ\frac{1}{2}} \\ &\cdot \mathbf{1}_{1\times N_{pv}})^{\circ(-1)})\boldsymbol{\beta}_0 \end{aligned} \tag{3.25}$$

$$\begin{aligned}\mathbf{M}_\beta = {}& ((\mathbf{V}_P + \mathbf{V}_Q \,\mathrm{diag}[\boldsymbol{\beta}_0])\mathbf{H}\,\mathrm{diag}[\mathrm{Var}[\mathbf{P}_{source}]]\mathbf{H}^{\mathrm{T}}) \\ &\circ \mathbf{V}_Q \circ ((((\mathbf{V}_P + \mathbf{V}_Q \,\mathrm{diag}[\boldsymbol{\beta}_0])\mathbf{H})^{\circ 2}\,\mathrm{Var}[\mathbf{P}_{source}])^{\circ\frac{1}{2}} \\ &\cdot \mathbf{1}_{1\times N_{pv}})^{\circ(-1)} \end{aligned} \tag{3.26}$$

If the node voltage magnitudes are assumed to be normally distributed over the interval of interest, then the probability constraints in (3.13), which are equivalent to

$$\Pr[|\tilde{V}_i| \leq V_{min}] \leq p_{max} \tag{3.27}$$

$$\Pr[|\tilde{V}_i| \leq V_{max}] \geq 1 - p_{max}, \tag{3.28}$$

can be expressed as

$$\Phi\left(\frac{V_{min} - \mathrm{E}[|\tilde{V}_i|]}{\sqrt{\mathrm{Var}[|\tilde{V}_i|]}}\right) \leq p_{max} \tag{3.29}$$

$$\Phi\left(\frac{V_{max} - \mathrm{E}[|\tilde{V}_i|]}{\sqrt{\mathrm{Var}[|\tilde{V}_i|]}}\right) \geq 1 - p_{max}, \tag{3.30}$$

where $\Phi(\cdot)$ is the cumulative distribution function of the standard normal distribution. By substitution of (3.18) and (3.24), these constraints $\forall i \in \{1,2,\ldots,N_{node}\}$ can be expressed as

$$\mathbf{V}_{min} - (\mathbf{N}_0 + \mathbf{N}_\alpha \boldsymbol{\alpha} + \mathbf{N}_\beta \boldsymbol{\beta}) \leq \Phi^{-1}(p_{max})(\mathbf{M}_0 + \mathbf{M}_\beta \boldsymbol{\beta}), \tag{3.31}$$

$$\mathbf{V}_{max} - (\mathbf{N}_0 + \mathbf{N}_\alpha \boldsymbol{\alpha} + \mathbf{N}_\beta \boldsymbol{\beta}) \geq \Phi^{-1}(1-p_{max})(\mathbf{M}_0 + \mathbf{M}_\beta \boldsymbol{\beta}), \tag{3.32}$$

where $\mathbf{V}_{min} = V_{min}\mathbf{1}_{N_{node}\times 1}$ and $\mathbf{V}_{max} = V_{max}\mathbf{1}_{N_{node}\times 1}$. The approximation in (3.24) is only valid for $\boldsymbol{\beta}$ sufficiently close to $\boldsymbol{\beta}_0$. In particular, an additional constraint is introduced to ensure that the approximate standard deviation is nonnegative:

$$\mathbf{M}_0 + \mathbf{M}_\beta \boldsymbol{\beta} \geq \mathbf{0}. \tag{3.33}$$

The maximum expected reactive power being injected by the PV inverter is also limited by the apparent power limits of the PV phases:

$$-(\mathbf{S}_{max}^{\circ 2} - \mathbf{P}_{pv0}^{\circ 2})^{\circ \frac{1}{2}} \leq (\boldsymbol{\alpha} + \boldsymbol{\beta} \circ \mathbf{P}_{pv0}) \leq (\mathbf{S}_{max}^{\circ 2} - \mathbf{P}_{pv0}^{\circ 2})^{\circ \frac{1}{2}}, \tag{3.34}$$

where $\mathbf{S}_{max} \in \mathbb{R}^{N_{pv}\times 1}$ is a vector of the apparent power limits of the PV phases.

By combining (3.14) and (3.31)–(3.34), the solution to the optimization problem in (3.13) can be approximated by the solution of a linear programming problem of the form

$$\begin{aligned} &\max_{\mathbf{x}} && \mathbf{c}^{\mathrm{T}}\mathbf{x} \\ &\text{subject to} && \mathbf{A}\mathbf{x} \leq \mathbf{b}, \end{aligned} \tag{3.35}$$

where $\mathbf{x} = [\boldsymbol{\alpha}^{\mathrm{T}}\ \boldsymbol{\beta}^{\mathrm{T}}]^{\mathrm{T}}$, $\mathbf{c} = [\mathbf{c}_\alpha^{\mathrm{T}}\ \mathbf{c}_\beta^{\mathrm{T}}]^{\mathrm{T}}$, and

$$\mathbf{A} = \begin{bmatrix} -\mathbf{N}_\alpha & -(\mathbf{N}_\beta + \Phi^{-1}(p_{max})\mathbf{M}_\beta) \\ \mathbf{N}_\alpha & \mathbf{N}_\beta + \Phi^{-1}(1-p_{max})\mathbf{M}_\beta \\ \mathbf{0}_{3N_{node}\times N_{pv}} & -\mathbf{M}_\beta \\ \mathbf{I}_{N_{pv}} & \mathrm{diag}[\mathbf{P}_{pv0}] \\ -\mathbf{I}_{N_{pv}} & -\mathrm{diag}[\mathbf{P}_{pv0}] \end{bmatrix}$$

$$\mathbf{b} = \begin{bmatrix} \Phi^{-1}(p_{max})\mathbf{M}_0 - \mathbf{V}_{min} + \mathbf{N}_0 \\ -\Phi^{-1}(1-p_{max})\mathbf{M}_0 + \mathbf{V}_{min} - \mathbf{N}_0 \\ \mathbf{M}_0 \\ (\mathbf{S}_{max}^{\circ 2} - \mathbf{P}_{pv0}^{\circ 2})^{\circ \frac{1}{2}} \\ (\mathbf{S}_{max}^{\circ 2} - \mathbf{P}_{pv0}^{\circ 2})^{\circ \frac{1}{2}} \end{bmatrix},$$

where $\mathbf{0}_{m\times n}$ is the $m \times n$ matrix filled with zero.

The problem is solved relatively infrequently for the interval of interest over which load and traditional regulating device characteristics are approximately constant but in which there can be significant PV fluctuation. Likewise, it is assumed that the statistical characteristics of the source power over the interval of interest (i.e., $\mathrm{E}[\mathbf{P}_{source}]$ and $\mathrm{Var}[\mathbf{P}_{source}]$) are known. Therefore,

$$\mathbf{P}_{pv0} = \mathbf{H}\mathrm{E}[\mathbf{P}_{source}] \tag{3.36}$$

is a suitable value of active PV phase power about which to linearize the system. If, in addition to $\boldsymbol{\beta}_0$, a previous estimate of $\boldsymbol{\alpha}$ is available (i.e., $\boldsymbol{\alpha}_0$), then

$$\mathbf{Q}_{pv0} = \boldsymbol{\alpha}_0 + \boldsymbol{\beta}_0 \circ (\mathbf{H}\mathrm{E}[\mathbf{P}_{source}]) \tag{3.37}$$

is a suitable value of reactive PV phase power about which to linearize the system. In this work, it is not strictly necessary to limit the values of $\boldsymbol{\alpha}$ and $\boldsymbol{\beta}$ because they are constrained by the apparent power limits in (3.34).

Because the linear programming problem described by (3.35) is based on a previous estimate of the solution of the optimization problem in (3.13), the solution to the problem may not be optimal or even be feasible. However, if the previous estimate of the solution is feasible, then it can be shown that the solution to (3.35) indicates a direction in which the solution quality can be improved. In order to implement an algorithm using this approach, it is necessary to locate an initial feasible solution. Starting from any initial solution (e.g., $\boldsymbol{\alpha}_0 = \mathbf{0}$ and $\boldsymbol{\beta}_0 = \mathbf{0}$), it is possible to linearize the system and solve for a point that is near the initial solution that satisfies the linear inequality constraints associated with the initial

solution. Because the solution is near the initial solution, it is more likely to be feasible with the constraints being obtained from a nearby point. This problem can be expressed as a quadratic programming problem:

$$\begin{aligned} &\min_{\mathbf{x}} && \tfrac{1}{2}\mathbf{x}^{\mathrm{T}}\mathbf{Q}\mathbf{x}+\mathbf{f}^{\mathrm{T}}\mathbf{x} \\ &\text{subject to} && \mathbf{A}\mathbf{x}\leq\mathbf{b}, \end{aligned} \tag{3.38}$$

where

$$\frac{1}{2}\mathbf{x}^{\mathrm{T}}\mathbf{Q}\mathbf{x}+\mathbf{f}^{\mathrm{T}}\mathbf{x}+C=\frac{1}{2}(\boldsymbol{\alpha}-\boldsymbol{\alpha}_0)^{\mathrm{T}}\,\mathrm{diag}[\mathbf{S}_{max}^{\circ(-1)}](\boldsymbol{\alpha}-\boldsymbol{\alpha}_0)+\frac{1}{2}(\boldsymbol{\beta}-\boldsymbol{\beta}_0)^{\mathrm{T}}(\boldsymbol{\beta}-\boldsymbol{\beta}_0). \tag{3.39}$$

By repetitively solving this quadratic programming problem, an initial feasible solution can be found. Once an initial feasible solution is found, the linear programming problem in (3.35) can be solved to determine a direction in which the solution quality can be improved. By searching in this direction, a feasible solution that improves the solution quality can be located. This process can be repeated until the solution converges. A flowchart illustrating this process is shown in Figure 3.1. In this flowchart, the top portion shows the process of finding an initial feasible solution (i.e., $\bar{\boldsymbol{\alpha}}$ and $\bar{\boldsymbol{\beta}}$). Throughout the remainder of the algorithm, $\bar{\boldsymbol{\alpha}}$ and $\bar{\boldsymbol{\beta}}$ represent the current feasible candidate solution. By solving the linear programming problem, a new, possibly infeasible, candidate solution represented by $\boldsymbol{\alpha}$ and $\boldsymbol{\beta}$, is found. The feasibility and solution quality of points between the current candidate solution and the new candidate solution are evaluated (using a step size constriction coefficient $\delta \in (0,1)$) in order to update the current candidate solution. When no further feasible improvement to the solution can be made (in terms of relative step size $0<\varepsilon\ll 1$), the algorithm terminates with the values $\bar{\boldsymbol{\alpha}}$ and $\bar{\boldsymbol{\beta}}$.

3.4 Test System Description

In order to evaluate the performance of the proposed method, the IEEE 123-node radial distribution test feeder is used in this study [87]. The system is shown in Figure 3.2 and consists of 123 nodes in a low-voltage feeder connected through a step-down transformer

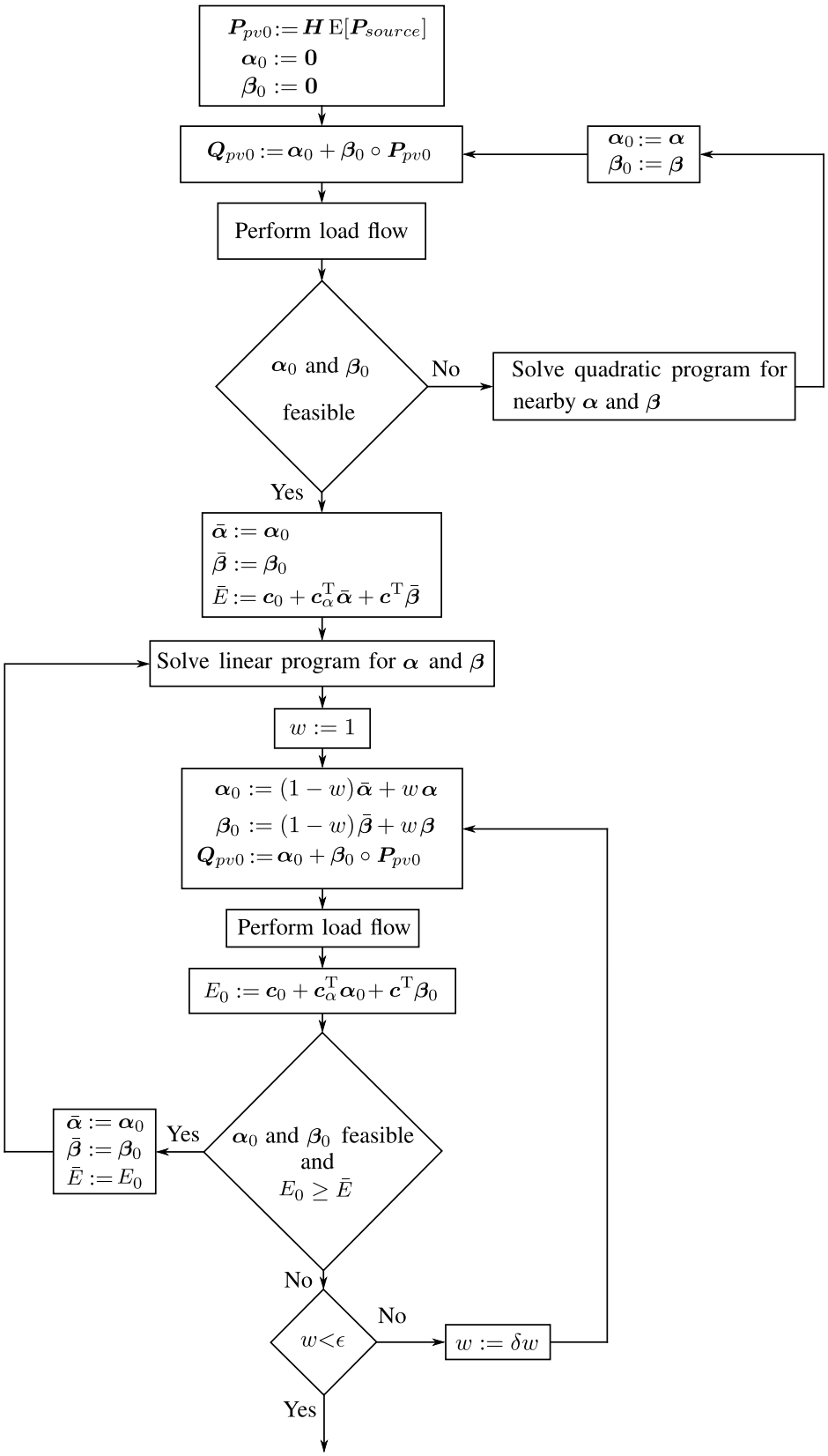

Figure 3.1: Flowchart of proposed solution algorithm

Table 3.1: Inverter parameters

Node Location	Rated Solar Power (kW)	Irradiance Data Source
1	200	DH1
7	200	DH2
8	200	DH3
13	200	DH4
18	200	DH5
52	200	DH6
53	200	DH7
54	200	DH8
55	200	DH9
56	200	DH10

to a transmission system, four capacitor banks, and four voltage regulators. These four voltage regulators can be used to control voltage magnitudes along the distribution feeder, and they are placed between Nodes 150 and 149, 9 and 14, 25 and 26, and 160 and 67. The nominal voltage used for the analysis is 4.16 kV. The loads in this system are unbalanced and are classified as constant impedance, constant current, and constant power loads in either a wye or delta configuration [87]. To validate the proposed method, ten three-phase PV inverters are connected to Nodes 1, 7, 8, 13, 18, 52, 53, 54, 55, and 56. The placement of these inverters is based on a previous study [71] in which it was found that inverters situated in these locations with spatially correlated irradiance can cause very significant voltage fluctuations. The power output of these inverters is based on the 1-s global horizontal irradiance data collected by the National Renewable Energy Laboratory Solar Measurement Grid in Oahu, Hawaii [88]. In particular, each inverter is associated with one of the sensors in the grid. The active power output of each inverter is proportional to the irradiance with the rated power output at an irradiance of 1000 W/m^2. The inverter locations, ratings, and data sources are given in Table 3.1.

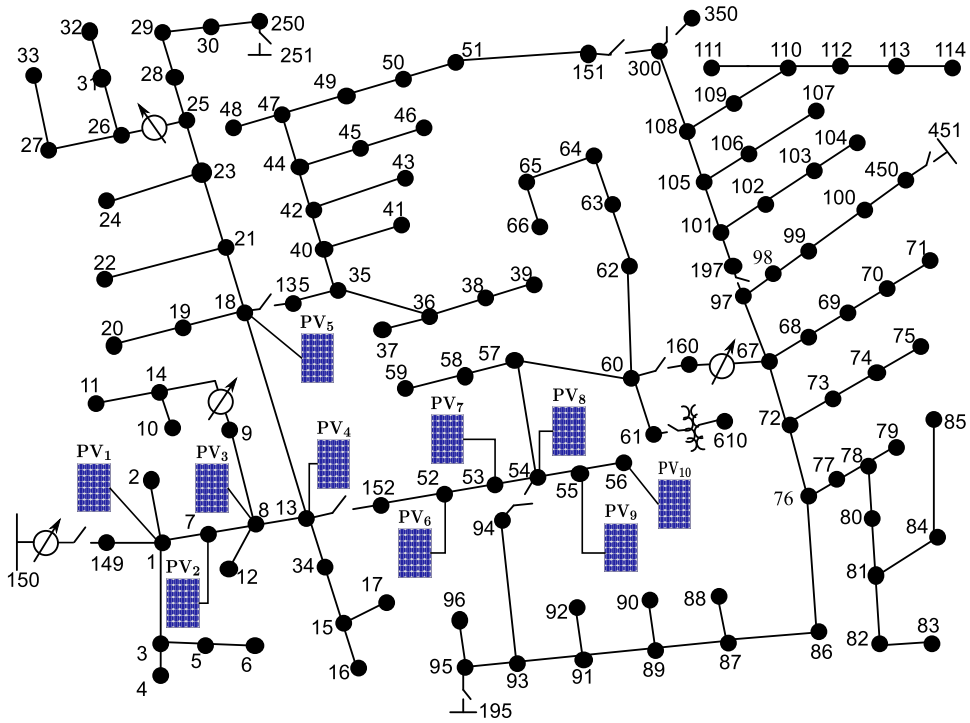

Figure 3.2: IEEE 123-node radial distribution test feeder. The PV source location nodes are indicated with PV panels.

3.5 Simulation Results and Discussion

Three different cases are studied to understand the performance of the proposed method under various conditions. Each of these cases represents a 15-minute interval over which the operation of traditional voltage regulation equipment (i.e., capacitor banks and voltage regulators) is considered fixed. Case 1 is cloudy with data from 1:50 pm to 2:05 pm on 13 July 2010. Case 2 is sunny with data from 2:40 pm to 2:55 pm on 10 July 2011. Case 3 is transient with data from 11:00 am to 11:15 am on 1 March 2010. Representative irradiance data are shown in Figure 3.3 to convey the nature of the three cases. From Figure 3.3, it can be seen that there is significant correlation among the PV sources. For each of the cases, voltage regulator tap settings shown in Table 3.2 are used.

All of the optimization problems are solved using an open-source linear programming solver (Coin-OR Linear Programming (CLP)) and an open-source quadratic programming solver (Object Orientated Quadratic Programming (OOQP)). The average CPU time to find

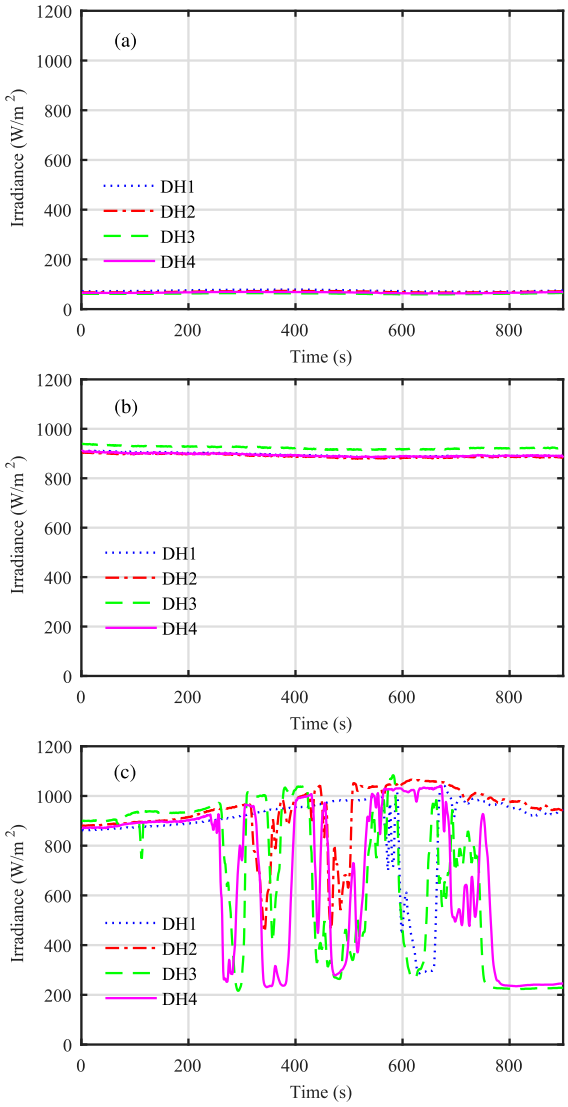

Figure 3.3: Irradiance data for (a) Case 1 (Cloudy), (b) Case 2 (Sunny), and (c) Case 3 (Transient).

$\bar{\boldsymbol{\alpha}}$ and $\bar{\boldsymbol{\beta}}$ for three cases is recorded as 85 seconds for the IEEE 123-node radial distribution test feeder. The values $\delta = 0.5$ and $\varepsilon = 10^{-4}$ are used in this work. A workstation with an Intel Core i7-3770 processor operating at 3.40 GHz with 8 GB of memory was used to perform the results and simulations.

The proposed chance-constrained optimization (CCO) method is tested against three other methods. The baseline method involves the inverters providing active power without any reactive power.

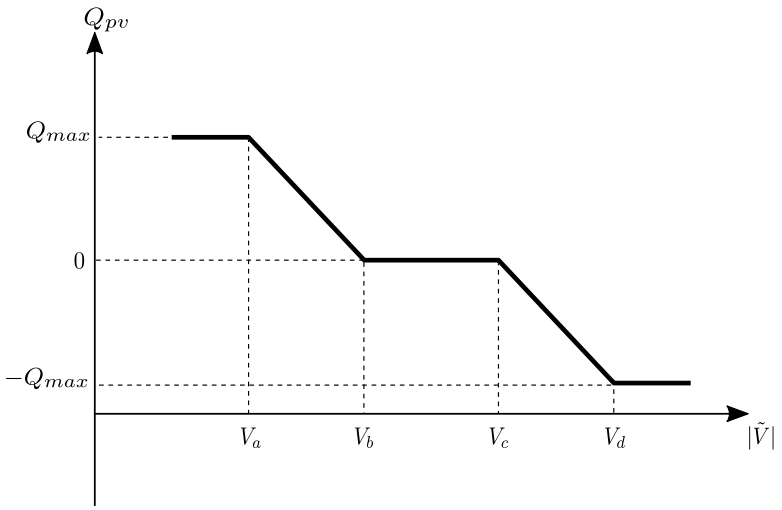

Figure 3.4: Volt/var control using droop control function.

The local voltage control (LVC) method involves the conventional droop function as shown in Figure 3.4. This method proposes volt-var control to maintain the system voltage magnitudes within acceptable limits and coordinate the injecting or the absorbing of reactive power among several distributed generators with a piecewise linear droop characteristic. This characteristic determines and adjusts the reactive power output of the PV inverters as a function of the voltage magnitude at the PV inverter terminals [62], but it does not seek to maximize a figure of merit. The predetermined piecewise linear droop characteristic is used with the parameters $V_a = 119$ V, $V_b = 120$ V, $V_c = 125$ V, and $V_d = 126$ V. The maximum reactive power available to the PV inverter phase is a function of the present real power injection:

$$Q_{max} = \sqrt{(S_{max})^2 - (P_{pv})^2},$$

while the LVC method is based on node voltages, the global violation unbalanced (GVU) method from [71] is based on real power injections and provides independent injections of reactive power into each phase to mitigate voltage violations, but it also does not seek to maximize a figure of merit.

The CCO method uses a maximum acceptable probability of voltage magnitude violation p_{max} of 5%. The retail price used in this study for power delivered to loads is 30¢/kWh,

Table 3.2: Voltage regulator tap settings

Node	150	9	25		160		
Phase	*a*,*b*,*c*	*a*	*a*	*c*	*a*	*b*	*c*
Case 1 (Cloudy)	7	−2	0	−2	8	2	5
Case 2 (Sunny)	6	−3	0	−2	6	1	4
Case 3 (Transient)	5	0	1	0	8	3	5

the wholesale price for power received from the transmission system is 20¢/kWh, and the price for power received from PV sources is 20¢/kWh, based on prices obtained from the U.S. Energy Information Administration [89]. For this study, the acceptable voltage magnitude limits of all nodes are 118–126 V on a 120 V scale based on American National Standards Institute limits [26].

While research on short-term forecasting exists (e.g., [90,91]), an idealized forecasting model is assumed herein. With this model, the expected values and variances of the PV sources are known over the next period of time (e.g., 15 minutes), but the moment-by-moment source power injections are not assumed to be known in advance.

The voltage regulator tap settings in Table 3.2 are selected such that all of the node phase voltage magnitudes are acceptable if the expected active power is injected with no reactive power injection, a prerequisite for using the benchmark GVU method. No further adjustment of the voltage regulator tap settings is performed during each case. Both the GVU method and the proposed CCO method are executed to determine the reactive power control parameters for each case, and these parameters are held constant during the case.

In this study, a modified version of the ladder iterative power flow technique [1] is used both for evaluating the characteristics of the system about the expected active power injection (in order to execute the GVU and CCO methods) and for determining the voltages and currents in each time step.

The baseline, LVC, GVU, and CCO methods are evaluated for the system in each of the three cases described above and the results for each case are described below. Each method is compared with the others on the basis of several metrics. The number of violated node

Table 3.3: Simulation results for Case 1 (Cloudy)

Method	Violated node phases	Violation time (s)	Violation percentage (%)	Mean U (¢/s)	Mean loss (kW)
Baseline	0	0	0.0	9.29	91.9
LVC	0	0	0.0	9.30	91.7
GVU	0	0	0.0	9.29	91.9
CCO	0	0	0.0	9.35	86.9

U represents the figure of merit.

phases is the number of node phases in which a voltage magnitude outside of the acceptable limits is experienced during the case. The violation time is the time for which at least one node phase experienced a voltage magnitude outside of the acceptable limits during the case. Each node phase voltage magnitude is over the acceptable limit a certain fraction of time during the case and under the acceptable limit a certain fraction of time. The largest such fraction is the violation percentage, corresponding to the worst-case satisfaction of the chance-constraints in (3.13). The mean figure of merit and system loss over the cases are also calculated.

3.5.1 Case 1 (Cloudy)

In Case 1, there is relatively little active power injection from the PV sources due to cloud cover and also relatively low variability in the active power injections as seen in Figure 3.3 (a). The resulting voltage magnitude at the a phase of Node 83 is shown as an example in Figure 3.5 (a) for each of the four methods. It can be seen that for this node phase, none of the methods cause the voltage magnitude to leave the acceptable range. It can also be seen that the CCO method moves the average voltage magnitude closer to the upper limit (to reduce feeder losses), which is possible to do without violating the constraints because of the low variability. The overall performance of the methods for this case is shown in Table 3.3. It can be seen that no node phases experience any voltage magnitude violations. Therefore, the performances of the baseline and GVU methods are nearly iden-

Table 3.4: Simulation results for Case 2 (Sunny)

Method	Violated node phases	Violation time (s)	Violation percentage (%)	Mean U (¢/s)	Mean loss (kW)
Baseline	0	0	0.0	9.47	56.4
LVC	0	0	0.0	9.47	56.4
GVU	0	0	0.0	9.47	56.4
CCO	0	0	0.0	9.55	51.5

U represents the figure of merit.

tical, and the performance of the LVC has very little improvement. In comparison with the baseline method, the CCO method is able to reduce the mean loss by 5.44%, resulting in an improvement in the mean figure of merit of 0.65%. It can be seen that due to the relatively high efficiency of the feeder, a modest improvement in the figure of merit corresponds with a more sizable improvement in system losses.

3.5.2 Case 2 (Sunny)

In Case 2, there is relatively high active power injection from the PV sources, but there is also relatively low variability in the active power injections. The resulting voltage magnitude at the *a* phase of Node 83, the same node phase as above, is shown in Figure 3.5 (b) for each of the four methods. The resulting voltage magnitudes are similar to those shown for Case 1. The voltage magnitudes are relatively constant and do not leave the allowable range during the case for any of the methods. As with Case 1, the CCO method reduces losses by moving the average voltage magnitude closer to the upper limit. The overall performance of the methods for this sunny case is shown in Table 3.4. As with the previous case, all voltage magnitudes are within acceptable limits for the duration of the case for each method. Also, the performance of the baseline, LVC, and GVU methods are nearly identical in terms of the figure of merit and losses, In comparison with the baseline method, the mean figure of merit is improved by 0.84% under the CCO method, corresponding to an 8.69% reduction in losses. As with Case 1, a relatively modest improvement in the figure

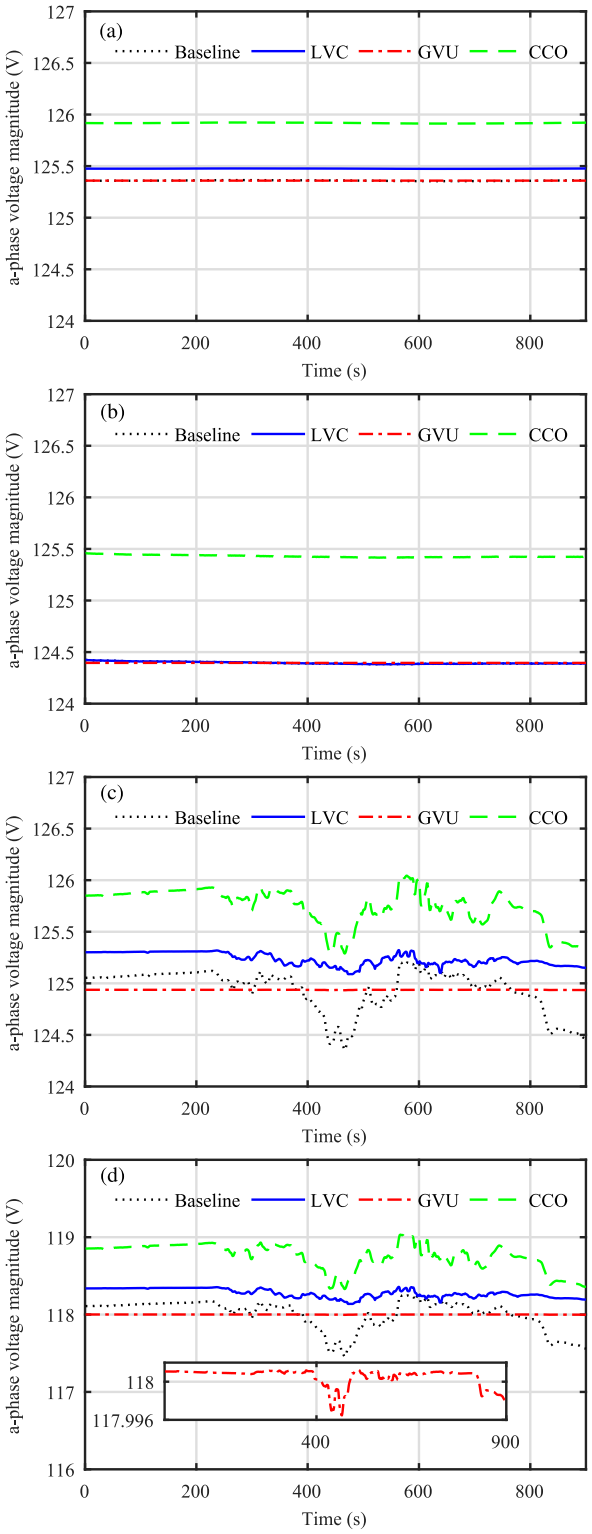

Figure 3.5: Node 83 *a*-phase voltage magnitude for (a) Case 1 (Cloudy), (b) Case 2 (Sunny), and (c) Case 3 (Transient), and (d) Node 65 *a*-phase voltage magnitude for Case 3 (Transient).

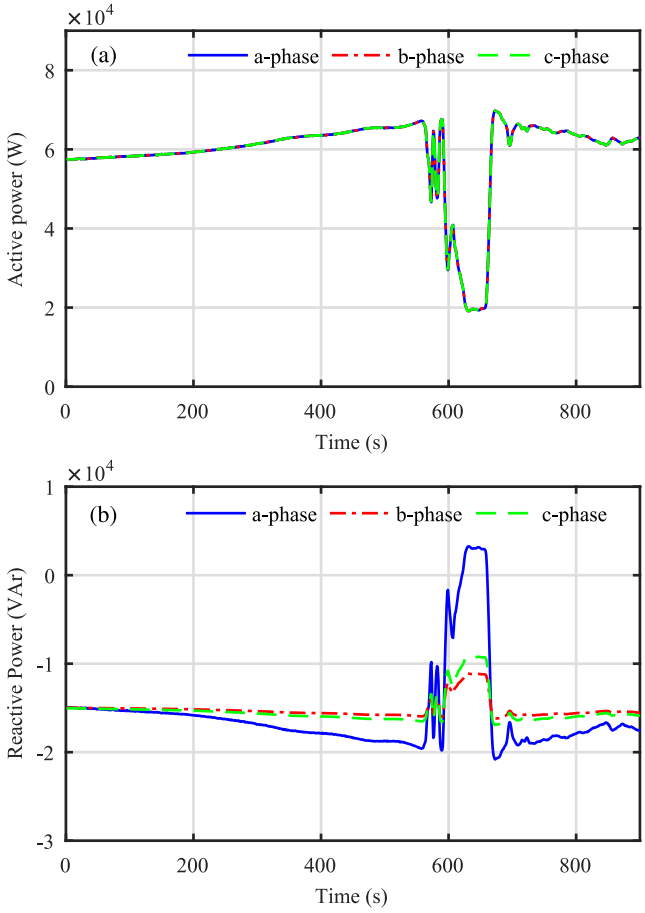

Figure 3.6: Sample of PV inverter active power set points in (a) and optimal reactive power set points in (b) for a time interval at Node 1 for *a*-phase, *b*-phase, and *c*-phase for the CCO method in Case 3 (Transient).

of merit is associated with a more substantial improvement in losses.

3.5.3 Case 3 (Transient)

In Case 3, the active power injection varies significantly over the case, exhibiting high variance and spatial correlation between nearby PV sources as shown in Figure 3.3 (c). Figure 3.6 illustrates a sample of the action of the CCO method at Node 1. It can be seen that even when the active power output is equally injected into each PV phase as shown in Figure 3.6 (a), the reactive power being injected into each PV phase as shown in Figure 3.6 (b) depends on the generation patterns of the PV sources and the CCO method.

The voltage magnitude of the *a* phase of Node 83 is shown in Figure 3.5 (c) for each of the four methods. It can be seen in this case that the voltage magnitude for the baseline, LVC and CCO methods exhibit visibly greater variation than for the GVU method. It can also be seen that the voltage magnitude for the CCO method makes a brief excursion above the acceptable upper limit (126 V).

The overall performance of the methods during this transient are shown in Table 3.5. It can be seen that the baseline method results in 14 node phases having voltage magnitude violations at some point during the case and that the time during which at least one voltage magnitude is unacceptable is more than one third of the total case duration. In this case, this corresponds to the violation percentage, the largest fraction of time over which a node phase voltage magnitude is over or under the acceptable limits. It can also be seen that LVC method results in none of node phases having a voltage magnitude violation during this case. The GVU method uses reactive power injection to reduce the occurrence of voltage magnitude violations. For the GVU method, only one node phase (*a* phase of Node 65) experiences a violation, but this violation occurs for nearly one sixth of the total case duration, corresponding to the violation percentage. The voltage magnitude of this phase is shown in Figure 3.5 (d). It can be seen in this figure that the voltage magnitude remains very close to the lower limit of 118 V, but that it often makes small excursions below this voltage. This is the worst-case phase for the GVU method. The CCO method seeks to limit the probability of voltage magnitude violations while maximizing the desired figure of merit. Like the GVU method, the CCO method also results in a single node phase (*a* phase of Node 83) experiencing a violation. This is the phase voltage shown in Figure 3.5 (a)–(c) and represents the worst-case phase for the CCO method. This phase experiences a violation for approximately one thirtieth of the total case duration.

For this case, the mean figures of merit for the baseline and GVU methods are approximately equal, with the GVU method only resulting in slightly higher losses. The mean figure of merit and the mean loss of the LVC method have little improvement. Alterna-

Table 3.5: Simulation results for Case 3 (Transient)

Method	Violated node phases	Violation time (s)	Violation percentage (%)	Mean U (¢/s)	Mean loss (kW)
Baseline	14	305	33.9	9.42	60.1
LVC	0	0	0.0	9.43	59.7
GVU	1	146	16.2	9.42	60.2
CCO	1	29	3.2	9.48	56.1

U represents the figure of merit.

tively, the mean figure of merit of the CCO method is improved by 0.64%, corresponding to a reduction in losses of 6.66%, with respect to the baseline method.

This result is consistent with the formulations of the LVC, GVU, and CCO methods. The GVU and LVC methods only seek to reduce voltage violations. It is clear from the reductions in the number of violated node phases, violation time, and violation percentage that the GVU and LVC methods effectively use reactive power injection to achieve this goal. It can be seen in Figure 3.5 (d) that even when the GVU method results in a voltage magnitude violation, the violation is relatively small. It can also be seen in Figure 3.5 (d) that even when the LVC method results in no voltage magnitude violation, the improvement in the figure of merit and loss reduction is still very little. Alternatively, the proposed CCO method does not seek only to reduce voltage violations; it seeks to limit voltage violations while improving a desired figure of merit. The CCO method was performed using a maximum acceptable probability of voltage magnitude violation p_{max} of 5% at any moment in time. It can be seen in Table 3.5 that the violation percentage, which corresponds to the worst-case frequency of voltage magnitude violation, is 3.2%, which is less than p_{max}. This means that the chance constraints in (3.13) are satisfied. At the same time, the CCO method results in substantial improvement of the figure of merit and loss reduction.

Table 3.6: Performance of proposed method for Case 3 (Transient)

	Violated node phases	Violation time (s)	Violation percentage (%)	Mean U (¢/s)	Mean loss (kW)
Expected	–	–	5.0	9.48	56.0
Synthetic	3	44	4.9	9.48	56.0
Actual	1	29	3.2	9.48	56.1

U represents the figure of merit.

3.5.4 Sensitivity to Distribution Assumptions

The most significant assumptions made by the proposed method are the normality and independence of the PV source powers. In this section, the sensitivity of the proposed CCO method is evaluated with respect to these assumptions using Case 3, the transient case. The Anderson-Darling normality test is performed [92] and can reject the hypothesis that the irradiance during this interval is normally distributed. Furthermore, the Pearson correlation coefficient (i.e., Pearson's r) is calculated to examine the linear correlation between PV source powers, and values as high as 0.7 are observed between PV sources, indicating strong linear correlation. These tests indicate that the assumptions do not actually hold for the PV source powers in Case 3, and yet the results in Table 3.5 seem to indicate acceptable performance by the proposed CCO method in this case.

To evaluate the "cost" of failing to satisfy the assumptions, synthetic PV source powers are constructed that have the same statistical characteristics (i.e., mean values and variances) as those in Case 3. However, the synthetic values are constructed to be independent and normally distributed. For such data, the input to the CCO method is identical (i.e., mean values and variances), and the resulting solution is identical. It is possible to compare the expected values (considered when computing the CCO solution) to the simulation performances of CCO in both the synthetic Case 3 and the actual Case 3. These values are shown in Table 3.6.

It can be seen that the CCO method in the synthetic Case 3 actually results in more

node phases having voltage magnitude violations at some point during the case and a greater period of time in which at least one node phase experiences an unacceptable voltage magnitude. In terms of the violation percentage, the synthetic Case 3 more carefully approaches the expected violation percentage of 5% when compare with the actual Case 3. This is expected because the synthetic Case 3 more carefully matches the assumptions upon which the expected value is calculated. The lower value during the actual Case 3 indicates improved voltage quality, but it also represents a more conservative solution to the optimization problem because p_{max} is 5%.

In terms of figure-of-merit performance, the expected value of U matches the mean value in both the synthetic and actual cases. The mean loss in the actual Case 3 is slightly greater than the expected value or the mean value from the synthetic Case 3. When taken together, the results indicate that the CCO method is not highly sensitive to the assumptions regarding the normality and independence of the PV source powers. The CCO method may be slightly conservative and may be capable of modest improvement by a more exact representation of the distributions of the PV source powers.

3.6 Conclusion

A method of achieving optimal expected performance with respect to a figure of merit of interest to the distribution system operator while maintaining appropriate system voltage magnitudes and considering the uncertainty of PV power injections is proposed. It is based on short-term forecasts that include the mean and variance of the active power injection and formulates the voltage magnitude requirements as chance constraints. Reactive power injections in PV phases are used both to improve expected system performance and to compensate for variations in active power injection. The method requires relatively infrequent communication between the distribution system operator and the PV inverters.

Operating profit is used herein as an example figure of merit. The proposed CCO method is compared with a baseline method without reactive power control, the LVC,

which varies reactive power based on a piecewise linear droop characteristic of the voltage magnitude, and the GVU method, which similarly varies reactive power based on an affine function of the reactive power injection. These methods are compared on the IEEE 123-node radial distribution feeder. Three cases are considered, corresponding to cloudy, sunny, and transient conditions. In each of these cases, the CCO method is able to improve the average operating profit over the other methods, while maintaining acceptable voltage magnitudes and reducing distribution system losses by 5.4–8.7%. The sensitivity of the CCO method to the distribution assumptions is considered, and it is found that the method is not highly sensitive to these assumptions. Because the proposed method is able to utilize short-term forecasts, to consider uncertainty of PV power injections, and to operate without high-bandwidth communication, it can be used to maintain voltage magnitudes throughout the distribution system and to improve the performance of the distribution system.

Chapter 4

Integrated Distribution System Optimization Using a Chance-Constrained Formulation

4.1 Introduction

In this chapter, a method of achieving optimal voltage regulation tap settings and optimal expected performance with respect to a figure of merit of interest to the distribution system operator while maintaining voltage magnitudes within acceptable limits and considering the uncertainty of PV power injections are proposed. In this work, the integrated chance-constrained optimization (ICCO) is proposed to combine the conventional voltage control devices (e.g., voltage regulators) and the capability of PV inverters to inject reactive power along with active power for maximizing the expected value of a figure of merit while constraining the probability of unacceptable voltage magnitudes. The optimal voltage regulator tap settings and PV inverter set point values including optimal reactive power parameters can be transmitted periodically from a centralized control center (e.g., each 15 minutes) via local communication channels. The proposed method uses short-term forecasts that include the expected mean and variance of the active power injection and expected load

with sufficient accuracy over the interval of interest and formulates the voltage magnitude requirements as chance constraints. The work suggested in this chapter has been published in [93].

The remainder of this chapter is arranged as follows. Section 4.2 provides the system description and approximations for the figure of merit and the system voltage magnitudes. Section 4.3 presents the problem formulation and solution approach. Section 4.4 presents the description of the distribution system and case studies. The simulation results are presented in Section 4.5. Finally, conclusions are drawn in Section 4.6.

4.2 System Description and Approximation

The operating profit serves, in this study, as example of figure of merit, which is expressed as

$$U = \sum_{i=1}^{N_{load}} C^{load} P_{load,i} - \sum_{i=1}^{N_{pv}} C^{pv} P_{pv,i} - \sum_{i=1}^{N_{in}} C^{in} P_{in,i}. \tag{4.1}$$

where N_{load}, N_{pv}, and N_{in} are the numbers of load, PV, and input (i.e., substation) node phases, respectively, C^{load} is the price received for power delivered to loads, C^{pv} is the price paid for power received from PV sources, C^{in} is the price paid for power received from the input, $P_{load,i}$ is power delivered to a load phase i, $P_{pv,i}$ is power received from a PV phase i, and $P_{in,i}$ is power received from an input phase i. The first part of (4.1) is the revenue received from the loads. The second part is the cost of the active power provided by the PV sources. The third part is the cost of the active power purchased from external source. In this study, the prices are considered known in advance over the interval of interest.

The active and reactive power produced in each PV phase are represented by the vectors $\mathbf{P}_{pv} \in \mathbb{R}^{N_{pv}}$ and $\mathbf{Q}_{pv} \in \mathbb{R}^{N_{pv}}$. The vector $\mathbf{T} \in \mathbb{Z}^{N_t}$ represents tap settings of voltage regulators, where N_t denotes the number of regulator tap settings. To approximate (4.1), Taylor series expansion is used around the desired operation point represented as $*$ where

$\mathbf{P}_{pv} = \mathbf{P}_{pv0}$, $\mathbf{Q}_{pv} = \mathbf{Q}_{pv0}$, and $\mathbf{T} = \mathbf{T}_0$. The figure of merit can be approximated as

$$U(\mathbf{P}_{pv}, \mathbf{Q}_{pv}, \mathbf{T}) \approx \underbrace{U|_*}_{U_0} + \underbrace{\frac{\partial U}{\partial \mathbf{P}_{pv}}\bigg|_*}_{\mathbf{U}_P^{\mathrm{T}}} (\mathbf{P}_{pv} - \mathbf{P}_{pv0}) + \underbrace{\frac{\partial U}{\partial \mathbf{Q}_{pv}}\bigg|_*}_{\mathbf{U}_Q^{\mathrm{T}}} (\mathbf{Q}_{pv} - \mathbf{Q}_{pv0}) + \underbrace{\frac{\partial U}{\partial \mathbf{T}}\bigg|_*}_{\mathbf{U}_T^{\mathrm{T}}} (\mathbf{T} - \mathbf{T}_0), \quad (4.2)$$

where U_0 is the figure of merit evaluated at the operating point, $\mathbf{U}_P$, $\mathbf{U}_Q$, and $\mathbf{U}_T$ are the sensitivity of the figure of merit with respect to the active and reactive power injected into each PV phase and voltage regulation tap settings—calculated using the power flow algorithm.

The node voltage magnitudes are a function of the active and reactive power injected into each PV phase and voltage regulator tap settings:

$$|\tilde{\mathbf{V}}| = \mathbf{f}(\mathbf{P}_{pv}, \mathbf{Q}_{pv}, \mathbf{T}), \quad (4.3)$$

where $\tilde{\mathbf{V}} \in \mathbb{C}^{N_{node}}$ is a vector of node phase voltages along the distribution feeder, and N_{node} is the number of node phases within the system, and this function can be calculated using power flow algorithm. Taylor series expansion is used around the operation point $*$, and the voltage magnitudes can be approximated as

$$|\tilde{\mathbf{V}}| \approx \underbrace{\mathbf{f}|_*}_{\mathbf{V}_0} + \underbrace{\frac{\partial \mathbf{f}}{\partial \mathbf{P}_{pv}}\bigg|_*}_{\mathbf{V}_P^{\mathrm{T}}} (\mathbf{P}_{pv} - \mathbf{P}_{pv0}) + \underbrace{\frac{\partial \mathbf{f}}{\partial \mathbf{Q}_{pv}}\bigg|_*}_{\mathbf{V}_Q^{\mathrm{T}}} (\mathbf{Q}_{pv} - \mathbf{Q}_{pv0}) + \underbrace{\frac{\partial \mathbf{f}}{\partial \mathbf{T}}\bigg|_*}_{\mathbf{V}_T^{\mathrm{T}}} (\mathbf{T} - \mathbf{T}_0), \quad (4.4)$$

where $\mathbf{V}_0$ is the voltage magnitudes evaluated at the operating point and $\mathbf{V}_P$,$\mathbf{V}_Q$, and $\mathbf{V}_T$ represent the sensitivity of the voltage magnitudes with respect to the active and reactive power injected into each PV phase and voltage regulator tap settings— calculated using power flow algorithm.

Three-phase PV inverters (i.e., $N_{pv} = 3N_{source}$) are used, and the active power from these sources is being injected equally in each phase:

$$\mathbf{P}_{pv} = \mathbf{H}\mathbf{P}_{source}, \quad (4.5)$$

where $\mathbf{H} = \frac{1}{3}(\mathbf{I}_{N_{source}} \otimes \mathbf{1}_{3\times 1})$, $\mathbf{I}_n$ is the $n \times n$ identity matrix, $\otimes$ is the Kronecker product operator, $\mathbf{1}_{m\times n}$ is the $m \times n$ matrix filled with unity, and $\mathbf{P}_{source} \in \mathbb{R}^{N_{source}}$ is the vector describing the power being injected from each PV source.

The proposed method allows reactive power output of each PV phase to be adjusted based on the active power output of the phase. Thus, an affine control equation is used to control the reactive power injected into each PV:

$$\mathbf{Q}_{pv} = \boldsymbol{\alpha} + \boldsymbol{\beta} \circ \mathbf{P}_{pv}, \tag{4.6}$$

where $\boldsymbol{\alpha} \in \mathbb{R}^{N_{pv}}$ and $\boldsymbol{\beta} \in \mathbb{R}^{N_{pv}}$ are vectors of the control parameters, and the $\circ$ is the Hadamard product operator. The nth Hadamard root of a matrix $\mathbf{A}$ is denoted $\mathbf{A}^{\circ\frac{1}{n}}$, and the nth Hadamard power is denoted $\mathbf{A}^{\circ n}$. Substituting (4.5) into (4.6) yields

$$\mathbf{Q}_{pv} = \boldsymbol{\alpha} + \boldsymbol{\beta} \circ (\mathbf{H}\mathbf{P}_{source}). \tag{4.7}$$

Substituting (4.5) and (4.7) into (4.2) yields

$$\begin{aligned} U \approx\ & U_0 + \mathbf{U}_P^{\mathrm{T}}(\mathbf{H}\mathbf{P}_{source} - \mathbf{P}_{pv0}) + \mathbf{U}_Q^{\mathrm{T}}((\boldsymbol{\alpha} + \boldsymbol{\beta} \circ (\mathbf{H}\mathbf{P}_{source})) - \mathbf{Q}_{pv0}) + \mathbf{U}_T^{\mathrm{T}}(\mathbf{T} - \mathbf{T}_0) \\ =\ & U_0 + \mathbf{U}_P^{\mathrm{T}}(\mathbf{H}\mathbf{P}_{source} - \mathbf{P}_{pv0}) - \mathbf{U}_Q^{\mathrm{T}}\mathbf{Q}_{pv0} + \mathbf{U}_Q^{\mathrm{T}}\boldsymbol{\alpha} + \mathbf{U}_Q^{\mathrm{T}}\mathrm{diag}[\mathbf{H}\mathbf{P}_{source}]\boldsymbol{\beta} + \mathbf{U}_T^{\mathrm{T}}\mathbf{T} - \mathbf{U}_T^{\mathrm{T}}\mathbf{T}_0. \end{aligned} \tag{4.8}$$

where the diagonal operator $\mathrm{diag}[\mathbf{x}]$ on a vector $\mathbf{x} \in \mathbb{R}^n$ is an $n \times n$ matrix with the elements of $\mathbf{x}$ on the diagonal. Substituting (4.5) and (4.7) into (4.4) yields

$$\begin{aligned} |\tilde{\mathbf{V}}| \approx\ & \mathbf{V}_0 + \mathbf{V}_P^{\mathrm{T}}(\mathbf{H}\mathbf{P}_{source} - \mathbf{P}_{pv0})\mathbf{V}_Q^{\mathrm{T}}\left((\boldsymbol{\alpha} + \boldsymbol{\beta} \circ (\mathbf{H}\mathbf{P}_{source})) - \mathbf{Q}_{pv0}\right) + \mathbf{V}_T^{\mathrm{T}}\left(\mathbf{T} - \mathbf{T}_0\right) \\ =\ & \mathbf{V}_0 + \mathbf{V}_P^{\mathrm{T}}(\mathbf{H}\mathbf{P}_{source} - \mathbf{P}_{pv0}) - \mathbf{V}_Q^{\mathrm{T}}\mathbf{Q}_{pv0} + \mathbf{V}_Q^{\mathrm{T}}\boldsymbol{\alpha} + \mathbf{V}_Q^{\mathrm{T}}\mathrm{diag}[\mathbf{H}\mathbf{P}_{source}]\boldsymbol{\beta} + \mathbf{V}_T^{\mathrm{T}}\mathbf{T} - \mathbf{V}_T^{\mathrm{T}}\mathbf{T}_0. \end{aligned} \tag{4.9}$$

4.3 Problem Formulation

The main goal of the proposed method is to maximize the expected value of a figure of merit by selecting optimal PV control parameters and optimal voltage regulator settings,

while constraining the probability of unacceptable voltage magnitudes over the interval of interest:

$$\begin{array}{ll} \max_{\boldsymbol{\alpha},\boldsymbol{\beta},\mathbf{T}} & \mathrm{E}[U] \\ \text{subject to} & \Pr[|\tilde{V}_i| \leq V_{min}] \leq p_{max} \\ \forall i \in \{1,2,\ldots,N_{node}\} & \Pr[|\tilde{V}_i| \geq V_{max}] \leq p_{max}. \end{array} \tag{4.10}$$

where V_i is the voltage at node phase i and p_{max} is the maximum acceptable probability for a node phase voltage magnitude to leave the acceptable range of $[V_{min}, V_{max}]$. It is assumed that the expected value and the variance of each source power are known, i.e., $\mathrm{E}[\mathbf{P}_{source}]$ and $\mathrm{Var}[\mathbf{P}_{source}]$ over the interval of interest. This nonlinear problem is solved iteratively based on a linearization about the previous solution estimate (i.e., $\boldsymbol{\beta}_0$). For the given control parameters $\boldsymbol{\alpha}$, $\boldsymbol{\beta}$, and $\mathbf{T}$, it is possible to approximate $\mathrm{E}[U]$ using (4.2):

$$\mathrm{E}[U] = \mathbf{c}_0 + \mathbf{c}_\alpha^{\mathrm{T}}\boldsymbol{\alpha} + \mathbf{c}_\beta^{\mathrm{T}}\boldsymbol{\beta} + \mathbf{c}_T^{\mathrm{T}}\mathbf{T}, \tag{4.11}$$

where

$$\mathbf{c}_0 = U_0 + \mathbf{U}_P^{\mathrm{T}}(\mathbf{H}\,\mathrm{E}[\mathbf{P}_{source}] - \mathbf{P}_{pv0}) - \mathbf{U}_Q^{\mathrm{T}}\mathbf{Q}_{pv0} - \mathbf{U}_T^{\mathrm{T}}\mathbf{T}_0, \tag{4.12}$$

$$\mathbf{c}_\alpha = \mathbf{U}_Q, \tag{4.13}$$

$$\mathbf{c}_\beta = \mathrm{diag}[\mathbf{H}\,\mathrm{E}[\mathbf{P}_{source}]]\mathbf{U}_Q, \tag{4.14}$$

$$\mathbf{c}_T = \mathbf{U}_T. \tag{4.15}$$

The expected voltage magnitudes along the distribution feeder can be expressed from (4.4) as

$$\mathrm{E}[|\tilde{\mathbf{V}}|] = \mathbf{N}_0 + \mathbf{N}_\alpha\boldsymbol{\alpha} + \mathbf{N}_\beta\boldsymbol{\beta} + \mathbf{N}_T\mathbf{T}, \tag{4.16}$$

where

$$\mathbf{N}_0 = \mathbf{V}_0 + \mathbf{V}_P^{\mathrm{T}}(\mathbf{H}\,\mathrm{E}[\mathbf{P}_{source}] - \mathbf{P}_{pv0}) - \mathbf{V}_Q^{\mathrm{T}}\mathbf{Q}_{pv0} - \mathbf{V}_T^{\mathrm{T}}\mathbf{T}_0, \tag{4.17}$$

$$\mathbf{N}_\alpha = \mathbf{V}_Q^{\mathrm{T}}, \tag{4.18}$$

$$\mathbf{N}_\beta = \mathbf{V}_Q^{\mathrm{T}}\,\mathrm{diag}[\mathbf{H}\,\mathrm{E}[\mathbf{P}_{source}]], \tag{4.19}$$

$$\mathbf{N}_T = \mathbf{V}_T^{\mathrm{T}}. \tag{4.20}$$

If the source powers are assumed to be distributed independently over the interval of interest, the variance of the voltage magnitudes can be expressed from (4.4) as

$$\mathrm{Var}[|\tilde{\mathbf{V}}|] \approx (\mathbf{V}_P^{\mathrm{T}}\mathbf{H} + \mathbf{V}_Q^{\mathrm{T}}\,\mathrm{diag}(\boldsymbol{\beta})\mathbf{H})^{\circ 2}\,\mathrm{Var}[\mathbf{P}_{source}], \tag{4.21}$$

and the standard deviation can be written as

$$(\mathrm{Var}[|\tilde{\mathbf{V}}|])^{\circ\frac{1}{2}} \approx ((\mathbf{V}_P^{\mathrm{T}}\mathbf{H} + \mathbf{V}_Q^{\mathrm{T}}\,\mathrm{diag}(\boldsymbol{\beta})\mathbf{H})^{\circ 2}\mathrm{Var}[\mathbf{P}_{source}])^{\circ\frac{1}{2}}. \tag{4.22}$$

The standard deviation can be further approximated using a Taylor series around a previous estimate of $\boldsymbol{\beta}$ (i.e., $\boldsymbol{\beta}_0$):

$$(\mathrm{Var}[|\mathbf{V}|])^{\circ\frac{1}{2}} = \mathbf{M}_0 + \mathbf{M}_\beta\boldsymbol{\beta}, \tag{4.23}$$

where

$$\begin{aligned}
\mathbf{M}_0 = {} & (((\mathbf{V}_P^{\mathrm{T}} + \mathbf{V}_Q^{\mathrm{T}}\,\mathrm{diag}[\boldsymbol{\beta}_0])\mathbf{H})^{\circ 2}\,\mathrm{Var}[\mathbf{P}_{source}])^{\circ\frac{1}{2}} \\
& - (((\mathbf{V}_P^{\mathrm{T}} + \mathbf{V}_Q^{\mathrm{T}}\,\mathrm{diag}[\boldsymbol{\beta}_0])\mathbf{H}\,\mathrm{diag}[\mathrm{Var}[\mathbf{P}_{source}]]\mathbf{H}^{\mathrm{T}}) \\
& \circ \mathbf{V}_Q^{\mathrm{T}} \circ ((((\mathbf{V}_P^{\mathrm{T}} + \mathbf{V}_Q^{\mathrm{T}}\,\mathrm{diag}[\boldsymbol{\beta}_0])\mathbf{H})^{\circ 2}\,\mathrm{Var}[\mathbf{P}_{source}])^{\circ\frac{1}{2}} \\
& \cdot \mathbf{1}_{1\times N_{pv}})^{\circ(-1)})\boldsymbol{\beta}_0
\end{aligned} \tag{4.24}$$

$$\begin{aligned}
\mathbf{M}_\beta = {} & ((\mathbf{V}_P^{\mathrm{T}} + \mathbf{V}_Q^{\mathrm{T}}\,\mathrm{diag}[\boldsymbol{\beta}_0])\mathbf{H}\,\mathrm{diag}[\mathrm{Var}[\mathbf{P}_{source}]]\mathbf{H}^{\mathrm{T}}) \\
& \circ \mathbf{V}_Q^{\mathrm{T}} \circ ((((\mathbf{V}_P^{\mathrm{T}} + \mathbf{V}_Q^{\mathrm{T}}\,\mathrm{diag}[\boldsymbol{\beta}_0])\mathbf{H})^{\circ 2}\,\mathrm{Var}[\mathbf{P}_{source}])^{\circ\frac{1}{2}} \\
& \cdot \mathbf{1}_{1\times N_{pv}})^{\circ(-1)}.
\end{aligned} \tag{4.25}$$

If the node voltage magnitudes are assumed to be normally distributed over the interval of interest, the probability constraints in (4.10), which are equivalent to

$$\Pr[|\tilde{V}_i| \le V_{min}] \le p_{max} \tag{4.26}$$

$$\Pr[|\tilde{V}_i| \le V_{max}] \ge 1 - p_{max}, \tag{4.27}$$

can be expressed as

$$\Phi\left(\frac{V_{min}-\mathrm{E}[|\tilde{V}_i|]}{\sqrt{\mathrm{Var}[|\tilde{V}_i|]}}\right) \leq p_{max} \tag{4.28}$$

$$\Phi\left(\frac{V_{max}-\mathrm{E}[|\tilde{V}_i|]}{\sqrt{\mathrm{Var}[|\tilde{V}_i|]}}\right) \geq 1-p_{max}. \tag{4.29}$$

where $\Phi(\cdot)$ is the cumulative distribution function of the standard normal distribution. By substitution of (4.16) and (4.23), these constraints $\forall i \in \{1,2,\ldots,N_{node}\}$ can be expressed as

$$\mathbf{V}_{min}-(\mathbf{N}_0+\mathbf{N}_\alpha\boldsymbol{\alpha}+\mathbf{N}_\beta\boldsymbol{\beta}+\mathbf{N}_T\mathbf{T}) \leq \Phi^{-1}(p_{max})(\mathbf{M}_0+\mathbf{M}_\beta\boldsymbol{\beta}), \tag{4.30}$$

$$\mathbf{V}_{max}-(\mathbf{N}_0+\mathbf{N}_\alpha\boldsymbol{\alpha}+\mathbf{N}_\beta\boldsymbol{\beta}+\mathbf{N}_T\mathbf{T}) \geq \Phi^{-1}(1-p_{max})(\mathbf{M}_0+\mathbf{M}_\beta\boldsymbol{\beta}), \tag{4.31}$$

where $\mathbf{V}_{min}=V_{min}\mathbf{1}_{N_{node}\times 1}$ and $\mathbf{V}_{max}=V_{max}\mathbf{1}_{N_{node}\times 1}$. The approximation in (4.23) is only valid for $\boldsymbol{\beta}$ sufficiently close to $\boldsymbol{\beta}_0$. In particular, an additional constraint is introduced to ensure that the approximate standard deviation is nonnegative:

$$\mathbf{M}_0+\mathbf{M}_\beta\boldsymbol{\beta} \geq \mathbf{0}. \tag{4.32}$$

The maximum expected reactive power being injected by the PV inverter is limited by the apparent power limits of the PV phases:

$$-(\mathbf{S}_{max}^{\circ 2}-\mathbf{P}_{pv0}^{\circ 2})^{\circ\frac{1}{2}} \leq (\boldsymbol{\alpha}+\boldsymbol{\beta}\circ\mathbf{P}_{pv0}) \leq (\mathbf{S}_{max}^{\circ 2}-\mathbf{P}_{pv0}^{\circ 2})^{\circ\frac{1}{2}}. \tag{4.33}$$

where $\mathbf{S}_{max}\in\mathbb{R}^{N_{pv}\times 1}$ is a vector of the apparent power limits of the inverter phases. To ensure that the voltage regulator tap settings are within allowable limits, an additional constraint is introduced,

$$\mathbf{T}_{min} \leq \mathbf{T} \leq \mathbf{T}_{max}, \tag{4.34}$$

where $\mathbf{T}_{max}$ and $\mathbf{T}_{min}$ are maximal and minimal allowable voltage regulator tap settings. By combining (4.11) and (4.30)–(4.34), the solution to the optimization problem in (4.10) can be approximated by the solution of a linear programming problem in the form of

$$\begin{aligned} &\max_{\mathbf{x}} && \mathbf{c}^{\mathrm{T}}\mathbf{x} \\ &\text{subject to} && \mathbf{A}\mathbf{x} \leq \mathbf{b}, \end{aligned} \tag{4.35}$$

where $\mathbf{x} = [\boldsymbol{\alpha}^{\mathrm{T}}\ \boldsymbol{\beta}^{\mathrm{T}}\ \mathbf{T}^{\mathrm{T}}]^{\mathrm{T}}$, $\mathbf{c} = [\mathbf{c}_{\alpha}^{\mathrm{T}}\ \mathbf{c}_{\beta}^{\mathrm{T}}\ \mathbf{c}_{T}^{\mathrm{T}}]^{\mathrm{T}}$, and

$$\mathbf{A} = \begin{bmatrix} -\mathbf{N}_{\alpha} & -(\mathbf{N}_{\beta} + \Phi^{-1}(p_{max})\mathbf{M}_{\beta}) & -\mathbf{N}_{T} \\ \mathbf{N}_{\alpha} & \mathbf{N}_{\beta} + \Phi^{-1}(1-p_{max})\mathbf{M}_{\beta} & -\mathbf{N}_{T} \\ \mathbf{0}_{3N_{node}\times N_{pv}} & -\mathbf{M}_{\beta} & \mathbf{0}_{3N_{node}\times N_{t}} \\ \mathbf{I}_{N_{pv}} & \mathrm{diag}[\mathbf{P}_{pv0}] & \mathbf{0}_{N_{pv}\times N_{t}} \\ -\mathbf{I}_{N_{pv}} & -\mathrm{diag}[\mathbf{P}_{pv0}] & \mathbf{0}_{N_{pv}\times N_{t}} \end{bmatrix}$$

$$\mathbf{b} = \begin{bmatrix} \Phi^{-1}(p_{max})\mathbf{M}_{0} - \mathbf{V}_{min} + \mathbf{N}_{0} \\ -\Phi^{-1}(1-p_{max})\mathbf{M}_{0} + \mathbf{V}_{min} - \mathbf{N}_{0} \\ \mathbf{M}_{0} \\ (\mathbf{S}_{max}^{\circ 2} - \mathbf{P}_{pv0}^{\circ 2})^{\circ \frac{1}{2}} \\ (\mathbf{S}_{max}^{\circ 2} - \mathbf{P}_{pv0}^{\circ 2})^{\circ \frac{1}{2}} \end{bmatrix},$$

where $\mathbf{0}_{m\times n}$ is the $m \times n$ matrix filled with zero.

The problem is solved relatively infrequently, once for each interval, over the length of which load and traditional regulating device characteristics are approximately constant but in which there can be significant PV fluctuation.

The first part of the proposed solution method is to locate an initial feasible solution as shown in first portion of Figure 4.1. This problem can be expressed as a quadratic programming problem:

$$\begin{aligned} &\min_{\mathbf{x}} && \tfrac{1}{2}\mathbf{x}^{\mathrm{T}}\mathbf{Q}\mathbf{x} + \mathbf{f}^{\mathrm{T}}\mathbf{x} \\ &\text{subject to} && \mathbf{A}\mathbf{x} \leq \mathbf{b}, \end{aligned} \tag{4.36}$$

where

$$\begin{aligned} \frac{1}{2}\mathbf{x}^{\mathrm{T}}\mathbf{Q}\mathbf{x} + \mathbf{f}^{\mathrm{T}}\mathbf{x} + C = {} & \frac{1}{2}(\boldsymbol{\alpha} - \boldsymbol{\alpha}_0)^{\mathrm{T}}\,\mathrm{diag}[\mathbf{S}_{max}^{\circ(-1)}](\boldsymbol{\alpha} - \boldsymbol{\alpha}_0) \\ & + \frac{1}{2}(\boldsymbol{\beta} - \boldsymbol{\beta}_0)^{\mathrm{T}}(\boldsymbol{\beta} - \boldsymbol{\beta}_0) + \frac{1}{2}(\mathbf{T} - \mathbf{T}_0)^{\mathrm{T}}\,\mathrm{diag}[\mathbf{T}_{max}^{\circ(-1)}](\mathbf{T} - \mathbf{T}_0). \end{aligned} \tag{4.37}$$

Starting from any initial solution (e.g., $\boldsymbol{\alpha}_0 = \mathbf{0}$, $\boldsymbol{\beta}_0 = \mathbf{0}$, and $\mathbf{T}_0 = \mathbf{0}$) and repetitively solving this quadratic programming problem, an initial feasible solution can be found rep-

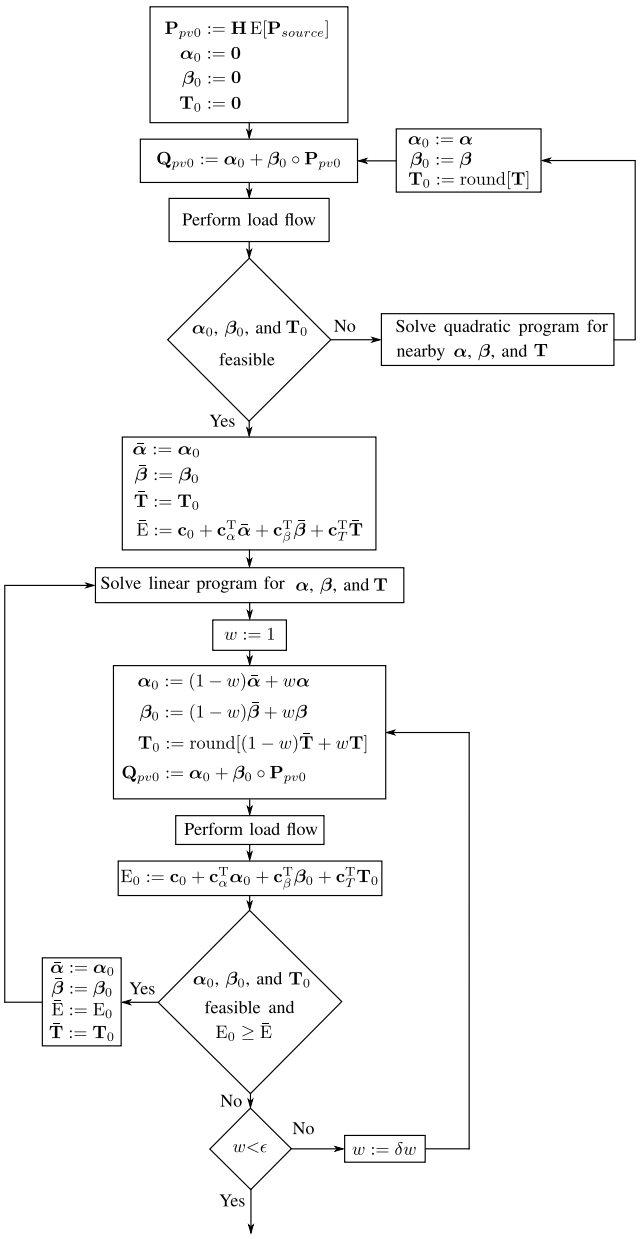

Figure 4.1: Flowchart of proposed solution algorithm

resented by $\bar{\boldsymbol{\alpha}}$, $\bar{\boldsymbol{\beta}}$, and $\bar{\mathbf{T}}$. In the second portion, the linear programming problem in (4.35) is used to find a direction in which the solution quality can be improved. By searching in this direction, a feasible solution represented by $\boldsymbol{\alpha}_0$, $\boldsymbol{\beta}_0$, and $\mathbf{T}_0$ that improves the solution quality can be located. This process can be repeated until the solution converges. The discrete variables (e.g. voltage regulator tap settings) are treated herein as discrete variables by rounding them.

4.4 Description of the distribution system and case studies

The IEEE 123-node radial distribution test feeder is used from [87] to test the proposed methodology. This test system as shown in Figure 3.2 consists of 123 nodes, four capacitor banks, the nominal voltage is 4.16 kV, unbalanced loads, and four voltage regulators which are located between Nodes 150 and 149, 9 and 14, 25 and 26, and 160 and 67 [87]. In this work, ten three-phase PV inverters are considered in the locations shown in Figure 3.2 based on a previous study [71] in which inverters situated in these locations with spatially correlated irradiance can cause significant voltage fluctuations. The power output of these inverters is based on the 1-s global horizontal irradiance data collected by the National Renewable Energy Laboratory Solar Measurement Grid in Oahu, Hawaii [88]. The active power output of each inverter in proportional to the irradiance with the rated power output at an irradiance of 1000 W/m^2. In this work, the rated solar power for all the PV sources is chosen to be 200 kW.

In order to examine the proposed method, three cases are considered. Each case represents a 15-minute interval over which the operation of traditional voltage regulation equipment (i.e., capacitor banks and voltage regulators) is considered fixed. Example irradiance data used are shown in Figure 3.3.

The proposed ICCO method is examined against three other methods. The baseline method involves the PV inverters providing active power without reactive power. The chance-constrained optimization (CCO) method involves finding optimal expected performance with respect to a figure of merit of interest while maintaining appropriate system voltage magnitudes without considering the optimal voltage regulator tap settings. The dual global violation unbalanced (DGVU) method involves calculating the optimal control settings in the first layer (e.g., voltage regulation tap settings and reference reactive power of PV inverters), and they are kept constant for the second layer. In the second layer, PV inverter reactive power is used to to mitigate voltage variations [75]. In the ICCO method,

it is assumed that a p_{max} of 5%, the price received from loads is 30¢/kWh, the price paid to PV sources is 20¢/kWh, the price paid to the input source is 20¢/kWh, and the acceptable voltage magnitude limits are assumed to be 118–126 V on a 120-V scale.

The optimal control parameters and optimal voltage regulator tap settings for DGVU and ICCO methods are held to be constant over the interval of interest in each case. Likewise, the optimal control parameters for CCO method are held to be constant over the interval of interest in each case. A modified version of the ladder iterative power flow technique [1] is used to simulate the baseline, CCO, DGVU, and ICCO methods. The baseline, CCO, DGVU, and ICCO methods are examined in each of the three cases (i.e., cloudy, sunny, and transient). The number of node phases in which a voltage magnitude outside of the acceptable limits is experienced during the case and the time for which at least one node phase experienced a voltage magnitude outside of the acceptable limits during the case are used as performance metrics. Also, each node phase voltage magnitude is over the acceptable limit a certain fraction of time during the case and under the acceptable limit a certain fraction of time. The largest such fraction is the violation percentage, corresponding to the worst-case satisfaction of the chance-constraints in (4.10). The mean figure of merit and system loss over the case are also considered.

4.5 Simulation results

In order to understand the proposed method, three cases are investigated for comparison purposes as shown in Figure 3.3. The potential benefits of this approach are clearly discernible from the three cases as shown in Table 4.1. As can be seen, the larger improvement in the mean of the figure of merit of interest (e.g. 1.2–1.6%.) is observed in ICCO method in all cases with a corresponding 6.64–10.5% reduction in losses. The improvement of losses is generally correlated with an improvement in the figure of merit. However, in Case 1, the ICCO method has slightly worse losses than the DGVU method (0.23% more), but it is still able to improve the mean value of the figure of merit. Only Case 3 presents voltage

Table 4.1: Simulation Results for Cases

Cases	Method	Violated node phases	Violation time (s)	Violation percentage (%)	Mean U (¢/s)	Mean loss (kW)
Cloudy	Baseline	0	0	0.0	9.29	91.9
	CCO	0	0	0.0	9.35	86.9
	DGVU	0	0	0.0	9.39	85.6
	ICCO	0	0	0.0	9.40	85.8
Sunny	Baseline	0	0	0.0	9.47	56.4
	CCO	0	0	0.0	9.55	51.5
	DGVU	0	0	0.0	9.57	51.9
	ICCO	0	0	0.0	9.58	51.2
Transient	Baseline	14	305	33.9	9.42	60.1
	CCO	1	29	3.2	9.48	56.1
	DGVU	0	0	0.0	9.56	54.5
	ICCO	0	0	0.0	9.57	53.8

U represents the figure of merit.

magnitude challenges due to highly variable PV injection. To understand the effects of the ICCO method on voltage violations, the worst two node phases in Case 3 are shown in Figure 4.2. For the a-phase of Node 65, the voltage magnitudes associated with the four methods are shown in Figure 4.2 (a). It can be seen that for this node phase, the baseline method causes voltage magnitude violations. It can also be seen that the ICCO method moves the average voltage magnitude closer to the upper limit (to reduce feeder losses), which is possible to do without violating the constraints because of consideration of the chance constraints.

The voltage magnitudes associated with the four methods for the a-phase of Node 83 are shown in Figure 4.2 (b). It can be seen that for this node phase, the CCO method causes the voltage magnitude to exceed the acceptable upper limit (126 V). While the CCO method only violates this limit for an acceptable fraction of the interval ($p_{max} = 5\%$), the ICCO method is able to adjust the voltage regulator settings to eliminate this violation. The ICCO method maintains the voltage magnitudes within acceptable limits while improving

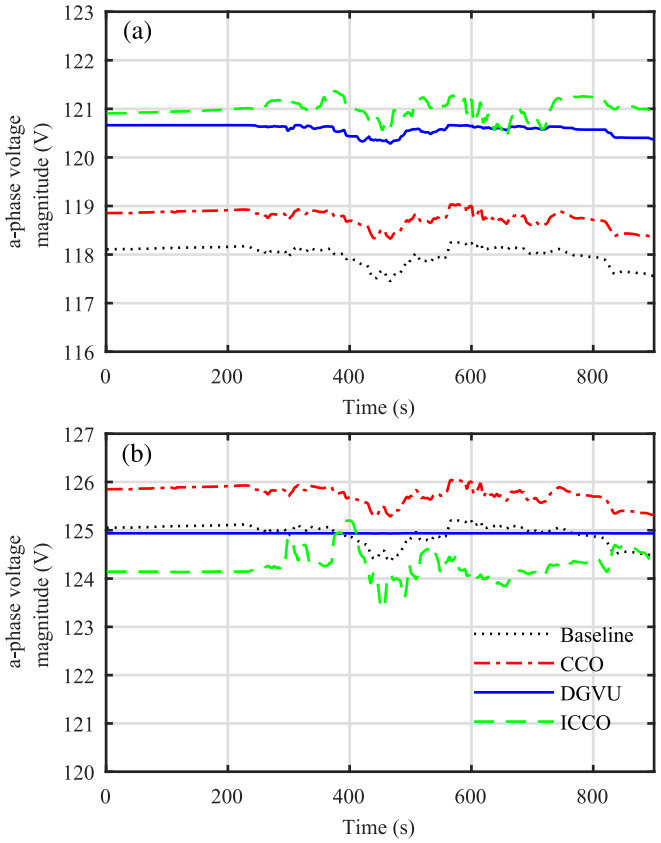

Figure 4.2: Node 65 *a*-phase voltage magnitude for (a) Case 3 (Transient) and Node 83 *a*-phase voltage magnitude for (b) Case 3 (Transient).

the figure of merit.

4.6 Conclusion

The proposed ICCO method aims to maximize the expected value of a given figure of merit while constraining the probability of voltage magnitudes leaving acceptable limits. This method combines control of traditional voltage regulation equipment with control of PV inverter reactive power capability in an integrated optimization formulation. It considers short-term uncertainty in PV power injections and formulates chance constraints in terms of short-term forecasts of the statistical characteristics of these injections. Because it operates over relatively long intervals of interest, only low bandwidth communication is required.

The proposed approach is compared to baseline, CCO, and DGVU methods on the IEEE 123-node radial distribution feeder under various generation conditions. Three cases were considered, corresponding to cloudy, sunny, and transient conditions. The results showed that the ICCO method was effective in both improving performance with respect to the figure of merit and constraining the probability of voltage magnitude violations.

Chapter 5

Integrated Control of Voltage Regulators and Distributed Generation Inverters

5.1 Introduction

In this chapter, an integrated control strategy is formulated for the coordinated control of both distribution system equipment and inverter-based DG. The control strategy combines the use of inverter reactive power capability with the operation of voltage regulators in order to improve the expected value of a desired figure of merit (e.g., system losses) while maintaining appropriate system voltage magnitudes, by formulating chance constraints on the voltage magnitudes. The control strategy requires both infrequent communication with the distribution system operator and infrequent changes to voltage regulator settings. However, it can respond to rapidly changing conditions by providing control parameters to the inverters to allow them to respond to such changes in real time. The control strategy is formulated as a mixed-integer, nonlinear, chance-constrained optimization problem, and a heuristic approach using power flow solutions and linearization is used to find solutions. The proposed method builds on the progress in [85], where such a method is used to optimize only the reactive power output of DGs, and in [93] where distribution system equipment is considered. An initial study that considered coordination of DGs and voltage regulators was performed in [93]. The current work includes an improved solution

algorithm to the mixed-integer problem that accounts for the discrete nature of voltage regulator tap settings and accelerates the process of finding initial feasible points. The current work also evaluates the performance of the proposed method more thoroughly by consideration of longer periods of time and by comparison with existing methods. Although the proposed method does not explicitly seek to reduce the number of tap change operations, the proposed control method uses an efficient approach to limit the number of tap change operations indirectly. The strategy used herein helps the voltage regulators to be infrequently adjusted (i.e., every 15 minutes over the 14-hour period) and proposes restarting the algorithm from the previous solution, helping with reducing tap change operations as well.

The remainder of this chapter is arranged as follows. Section 5.2 provides the system description and approximation for the figure of merit and the system voltage magnitudes. The problem formulation is presented in Section 5.3. Section 5.4 presents the test system description based on the IEEE 123-node radial distribution test feeder [87]. Simulation results and discussion are presented in Section 5.5. Finally, conclusions are drawn in Section 5.6.

5.2 System Description and Approximation

To formulate the integrated control method, the system behavior and suitable approximations are introduced. The system behavior is evaluated using power flow solutions, while the approximations, which are derived from power flow solutions, are used in a heuristic method to identify optimal solutions, which will be described in Section 5.4. In particular, the behavior of the system with respect to changes in active and reactive power injections from DG and to changes in the settings of voltage regulation equipment is of interest. The control method seeks to minimize the expected value of a figure of merit that is of interest to the distribution system operator. Herein, network loss is used as an example figure of

merit and can be expressed as

$$U = \sum_{i=1}^{N_{in}} P_{in,i} + \sum_{i=1}^{N_{inv}} P_{inv,i} - \sum_{i=1}^{N_{load}} P_{load,i}, \tag{5.1}$$

where N_{load}, N_{inv}, and N_{in} denote the numbers of load, inverter, and input (i.e., substation) node phases, respectively, $P_{load,i}$ denotes power to a load phase i, $P_{inv,i}$ denotes power from an inverter phase i, and $P_{in,i}$ denotes power from an input phase i.

The active and reactive power produced in each inverter phase are represented by the vectors $\mathbf{P}_{inv} \in \mathbb{R}^{N_{inv}}$ and $\mathbf{Q}_{inv} \in \mathbb{R}^{N_{inv}}$. The vector $\mathbf{K} \in \mathbb{Z}^{N_t}$ represents tap settings of voltage regulators, where N_t denotes the number of regulator tap settings.

The proposed solution approach uses a linear approximation of (5.1), which can be obtained by Taylor series expansion around a specified operating point represented as $*$ and where $\mathbf{P}_{inv} = \mathbf{P}_{inv0}$, $\mathbf{Q}_{inv} = \mathbf{Q}_{inv0}$, and $\mathbf{K} = \mathbf{K}_0$. The figure of merit can be approximated as

$$\begin{aligned} U(\mathbf{P}_{inv}, \mathbf{Q}_{inv}, \mathbf{K}) \approx \underbrace{U|_*}_{U_0} + \underbrace{\left.\frac{\partial U}{\partial \mathbf{P}_{inv}}\right|_*}_{\mathbf{U}_P^{\mathrm{T}}} (\mathbf{P}_{inv} - \mathbf{P}_{inv0}) \\ + \underbrace{\left.\frac{\partial U}{\partial \mathbf{Q}_{inv}}\right|_*}_{\mathbf{U}_Q^{\mathrm{T}}} (\mathbf{Q}_{inv} - \mathbf{Q}_{inv0}) + \underbrace{\left.\frac{\partial U}{\partial \mathbf{K}}\right|_*}_{\mathbf{U}_K^{\mathrm{T}}} (\mathbf{K} - \mathbf{K}_0), \end{aligned} \tag{5.2}$$

where U_0 is the figure of merit evaluated at the operating point and $\mathbf{U}_P$, $\mathbf{U}_Q$, and $\mathbf{U}_K$ are the sensitivities of the figure of merit with respect to the active and reactive power injected into each inverter phase and voltage regulation tap settings.[1] The values of U_0, $\mathbf{U}_P$, $\mathbf{U}_Q$, and $\mathbf{U}_K$ can be estimated from power flow solution and numerical perturbations [94].

All else being equal, the node voltage magnitudes along the distribution feeder are a function of the active and reactive power injected into each inverter phase and voltage regulator tap settings:

$$|\tilde{\mathbf{V}}| = \mathbf{f}(\mathbf{P}_{inv}, \mathbf{Q}_{inv}, \mathbf{K}), \tag{5.3}$$

where $\tilde{\mathbf{V}} \in \mathbb{C}^{N_{node}}$ is a vector of node phase voltages along the distribution feeder, and N_{node} is the number of node phases within the system. A similar linear approximation is

[1] T is the transpose operator.

employed:

$$|\tilde{\mathbf{V}}| \approx \underbrace{\mathbf{f}|_*}_{\mathbf{V}_0} + \underbrace{\left.\frac{\partial \mathbf{f}}{\partial \mathbf{P}_{inv}}\right|_*}_{\mathbf{V}_P} (\mathbf{P}_{inv} - \mathbf{P}_{inv0}) + \underbrace{\left.\frac{\partial \mathbf{f}}{\partial \mathbf{Q}_{inv}}\right|_*}_{\mathbf{V}_Q} (\mathbf{Q}_{inv} - \mathbf{Q}_{inv0}) + \underbrace{\left.\frac{\partial \mathbf{f}}{\partial \mathbf{K}}\right|_*}_{\mathbf{V}_K} (\mathbf{K} - \mathbf{K}_0), \quad (5.4)$$

where $\mathbf{V}_0$ is the voltage magnitudes evaluated at the operating point and $\mathbf{V}_P$,$\mathbf{V}_Q$, and $\mathbf{V}_K$ are the sensitivities of the voltage magnitudes with respect to the active and reactive power injected into each inverter phase and voltage regulator tap settings. These values can also be obtained from power flow solution and numerical perturbations.

The inverters considered in this work are three-phase inverters (i.e., $N_{inv} = 3N_{source}$), where N_{source} is the number of sources, and the active power from these sources is being injected equally in each phase. Thus, the power being injected into each inverter phase can be expressed as

$$\mathbf{P}_{inv} = \mathbf{H}\mathbf{P}_{source}, \quad (5.5)$$

where $\mathbf{H} = \frac{1}{3}(\mathbf{I}_{N_{source}} \otimes \mathbf{1}_{3\times 1})$, $\mathbf{I}_n$ is the $n \times n$ identity matrix, $\mathbf{1}_{m\times n}$ is the $m \times n$ matrix filled with unity, and $\mathbf{P}_{source} \in \mathbb{R}^{N_{source}}$ is a vector describing the power being injected from each PV source.[2]

The local reactive power control method allows reactive power output of each inverter phase to be adjusted based on the active power output of the phase. The reactive power injected into each inverter phase can be expressed using an affine control equation:

$$\mathbf{Q}_{inv} = \boldsymbol{\alpha} + \boldsymbol{\beta} \circ \mathbf{P}_{inv}, \quad (5.6)$$

where $\boldsymbol{\alpha} \in \mathbb{R}^{N_{inv}}$ and $\boldsymbol{\beta} \in \mathbb{R}^{N_{inv}}$ are vectors of the inverter control parameters (i.e., the fixed and variable reactive power output of the PV inverters) describing the behavior of each inverter phase.[3] Substituting (5.5) into (5.6) yields

$$\mathbf{Q}_{inv} = \boldsymbol{\alpha} + \boldsymbol{\beta} \circ (\mathbf{H}\mathbf{P}_{source}). \quad (5.7)$$

[2] $\otimes$ is the Kronecker product operator.

[3] $\circ$ is the Hadamard product operator. The nth Hadamard root of a matrix $\mathbf{A}$ is denoted $\mathbf{A}^{\circ\frac{1}{n}}$, and the nth Hadamard power is denoted $\mathbf{A}^{\circ n}$.

Substituting (5.5) and (5.7) into (5.2) yields[4]

$$\begin{aligned} U \approx\ & U_0 + \mathbf{U}_P^{\mathrm{T}}(\mathbf{HP}_{source} - \mathbf{P}_{inv0}) + \mathbf{U}_Q^{\mathrm{T}}((\boldsymbol{\alpha} + \boldsymbol{\beta} \circ (\mathbf{HP}_{source})) - \mathbf{Q}_{inv0}) + \mathbf{U}_K^{\mathrm{T}}(\mathbf{K} - \mathbf{K}_0) \\ & = U_0 + \mathbf{U}_P^{\mathrm{T}}(\mathbf{HP}_{source} - \mathbf{P}_{inv0}) - \mathbf{U}_Q^{\mathrm{T}}\mathbf{Q}_{inv0} - \mathbf{U}_K^{\mathrm{T}}\mathbf{K}_0 + \mathbf{U}_Q^{\mathrm{T}}\boldsymbol{\alpha} + \mathbf{U}_Q^{\mathrm{T}}\,\mathrm{diag}[\mathbf{HP}_{source}]\boldsymbol{\beta} + \mathbf{U}_K^{\mathrm{T}}\mathbf{K}. \end{aligned} \tag{5.8}$$

Substituting (5.5) and (5.7) into (5.4) gives

$$\begin{aligned} |\tilde{\mathbf{V}}| \approx\ & \mathbf{V}_0 + \mathbf{V}_P(\mathbf{HP}_{source} - \mathbf{P}_{inv0}) + \mathbf{V}_Q\left((\boldsymbol{\alpha} + \boldsymbol{\beta} \circ (\mathbf{HP}_{source})) - \mathbf{Q}_{inv0}\right) + \mathbf{V}_K\left(\mathbf{K} - \mathbf{K}_0\right) \\ & = \mathbf{V}_0 + \mathbf{V}_P(\mathbf{HP}_{source} - \mathbf{P}_{inv0}) - \mathbf{V}_Q\mathbf{Q}_{inv0} - \mathbf{V}_K\mathbf{K}_0 + \mathbf{V}_Q\boldsymbol{\alpha} + \mathbf{V}_Q\,\mathrm{diag}[\mathbf{HP}_{source}]\boldsymbol{\beta} + \mathbf{V}_K\mathbf{K}. \end{aligned} \tag{5.9}$$

5.3 Problem Formulation

The proposed integrated control method is formulated as a nonlinear, mixed-integer, chance-constrained problem. Values of the inverter control parameters and voltage regulator tap settings are sought to minimize the expected value of a figure of merit (e.g., system loss) while constraining the probability of unacceptable voltage magnitudes occurring during the interval of interest[5]:

$$\begin{aligned} \min_{\boldsymbol{\alpha},\boldsymbol{\beta},\mathbf{K}} \quad & \mathrm{E}\left[U\right] \\ \text{subject to} \quad & \Pr[|\tilde{V}_i| \leq V_{min}] \leq p_{max} \\ \forall i \quad & \Pr[|\tilde{V}_i| \geq V_{max}] \leq p_{max} \\ & \boldsymbol{\alpha}_{min} \leq \boldsymbol{\alpha} \leq \boldsymbol{\alpha}_{max} \\ & \boldsymbol{\beta}_{min} \leq \boldsymbol{\beta} \leq \boldsymbol{\beta}_{max} \\ & \mathbf{K}_{min} \leq \mathbf{K} \leq \mathbf{K}_{max}, \end{aligned} \tag{5.10}$$

where $\tilde{V}_i$ is the voltage at node phase i, $\forall i \in \{1, 2, \ldots, N_{node}\}$, p_{max} is the maximum acceptable probability for a node phase voltage magnitude to exceed V_{max} or to fall below V_{min}, $\boldsymbol{\alpha}_{min}$, $\boldsymbol{\beta}_{min}$, $\boldsymbol{\alpha}_{max}$, $\boldsymbol{\beta}_{max}$ are minimal and maximal allowable inverter control parameters,

[4]The diagonal operator diag[$\mathbf{x}$] on the vector $\mathbf{x} \in \mathbb{R}^n$ is the $n \times n$ matrix with the elements of $\mathbf{x}$ on the diagonal.

[5]E is the expectation operator

and $\mathbf{K}_{min}$ and $\mathbf{K}_{max}$ are minimal and maximal allowable voltage regulator tap settings. It is assumed that the expected value and the variance of each source power, i.e., $\mathrm{E}[\mathbf{P}_{source}]$ and $\mathrm{Var}[\mathbf{P}_{source}]$, are known over the interval of interest. This nonlinear problem is solved iteratively and is solved based on a linearization about the previous solution estimate (i.e., $\boldsymbol{\alpha}_0$, $\boldsymbol{\beta}_0$, and $\mathbf{K}_0$).

It is possible to approximate $\mathrm{E}[U]$ using (5.8):

$$\begin{aligned}\mathrm{E}[U] &\approx U_0 + \mathbf{U}_P^{\mathrm{T}}(\mathbf{H}\mathrm{E}[\mathbf{P}_{source}] - \mathbf{P}_{inv0}) - \mathbf{U}_Q^{\mathrm{T}}\mathbf{Q}_{inv0} - \mathbf{U}_K^{\mathrm{T}}\mathbf{K}_0 \\ &\quad + \mathbf{U}_Q^{\mathrm{T}}\boldsymbol{\alpha} + \mathbf{U}_Q^{\mathrm{T}}\mathrm{diag}[\mathbf{H}\mathrm{E}[\mathbf{P}_{source}]]\boldsymbol{\beta} + \mathbf{U}_K^{\mathrm{T}}\mathbf{K} \\ &= \mathbf{c}_0 + \mathbf{c}_\alpha^{\mathrm{T}}\boldsymbol{\alpha} + \mathbf{c}_\beta^{\mathrm{T}}\boldsymbol{\beta} + \mathbf{c}_K^{\mathrm{T}}\mathbf{K}, \end{aligned} \tag{5.11}$$

where

$$\mathbf{c}_0 = U_0 + \mathbf{U}_P^{\mathrm{T}}(\mathbf{H}\mathrm{E}[\mathbf{P}_{source}] - \mathbf{P}_{inv0}) - \mathbf{U}_Q^{\mathrm{T}}\mathbf{Q}_{inv0} - \mathbf{U}_K^{\mathrm{T}}\mathbf{K}_0 \tag{5.12}$$

$$\mathbf{c}_\alpha = \mathbf{U}_Q \tag{5.13}$$

$$\mathbf{c}_\beta = \mathrm{diag}[\mathbf{H}\mathrm{E}[\mathbf{P}_{source}]]\mathbf{U}_Q \tag{5.14}$$

$$\mathbf{c}_K = \mathbf{U}_K. \tag{5.15}$$

The expected voltage magnitudes along the distribution feeder can be expressed from (5.9) as

$$\begin{aligned}\mathrm{E}[|\tilde{\mathbf{V}}|] &\approx \mathbf{V}_0 + \mathbf{V}_P(\mathbf{H}\mathrm{E}[\mathbf{P}_{source}] - \mathbf{P}_{inv0}) - \mathbf{V}_Q\mathbf{Q}_{inv0} - \mathbf{V}_K\mathbf{K}_0 \\ &\quad + \mathbf{V}_Q\boldsymbol{\alpha} + \mathbf{V}_Q\,\mathrm{diag}[\mathbf{H}\mathrm{E}[\mathbf{P}_{source}]]\boldsymbol{\beta} + \mathbf{V}_K\mathbf{K} \\ &= \mathbf{N}_0 + \mathbf{N}_\alpha\boldsymbol{\alpha} + \mathbf{N}_\beta\boldsymbol{\beta} + \mathbf{N}_K\mathbf{K}, \end{aligned} \tag{5.16}$$

where

$$\mathbf{N}_0 = \mathbf{V}_0 + \mathbf{V}_P(\mathbf{H}\mathrm{E}[\mathbf{P}_{source}] - \mathbf{P}_{inv0}) - \mathbf{V}_Q\mathbf{Q}_{inv0} - \mathbf{V}_K\mathbf{K}_0 \tag{5.17}$$

$$\mathbf{N}_\alpha = \mathbf{V}_Q \tag{5.18}$$

$$\mathbf{N}_\beta = \mathbf{V}_Q\,\mathrm{diag}[\mathbf{H}\mathrm{E}[\mathbf{P}_{source}]] \tag{5.19}$$

$$\mathbf{N}_K = \mathbf{V}_K. \tag{5.20}$$

If the source powers are assumed to be distributed independently over the interval of interest, the variance of the voltage magnitudes can be expressed from (5.9) as

$$\begin{aligned}\mathrm{Var}[|\tilde{\mathbf{V}}|] &\approx \mathrm{Var}[\mathbf{V}_0 - \mathbf{V}_P\mathbf{P}_{inv0} - \mathbf{V}_Q\mathbf{Q}_{inv0} - \mathbf{V}_K\mathbf{K}_0 + \mathbf{V}_Q\boldsymbol{\alpha} + \mathbf{V}_K\mathbf{K} + \mathbf{V}_P\mathbf{H}\mathbf{P}_{source} \\ &\quad + \mathbf{V}_Q\,\mathrm{diag}[\mathbf{H}\mathbf{P}_{source}]\boldsymbol{\beta}] \\ &= \mathrm{Var}[\mathbf{V}_0 - \mathbf{V}_P\mathbf{P}_{inv0} - \mathbf{V}_Q\mathbf{Q}_{inv0} - \mathbf{V}_K\mathbf{K}_0 + \mathbf{V}_Q\boldsymbol{\alpha} + \mathbf{V}_K\mathbf{K} + (\mathbf{V}_P\mathbf{H} + \mathbf{V}_Q \\ &\quad \cdot \mathrm{diag}(\boldsymbol{\beta})\mathbf{H})\mathbf{P}_{source}] \\ &= (\mathbf{V}_P\mathbf{H} + \mathbf{V}_Q\,\mathrm{diag}(\boldsymbol{\beta})\mathbf{H})^{\circ 2}\,\mathrm{Var}[\mathbf{P}_{source}], \end{aligned} \tag{5.21}$$

and the standard deviation can be written as

$$(\mathrm{Var}[|\tilde{\mathbf{V}}|])^{\circ\frac{1}{2}} \approx ((\mathbf{V}_P\mathbf{H} + \mathbf{V}_Q\,\mathrm{diag}(\boldsymbol{\beta})\mathbf{H})^{\circ 2}\mathrm{Var}[\mathbf{P}_{source}])^{\circ\frac{1}{2}}. \tag{5.22}$$

The standard deviation can be further approximated using a Taylor series around a previous estimate of $\boldsymbol{\beta}$ (i.e., $\boldsymbol{\beta}_0$):

$$\begin{aligned}(\mathrm{Var}[|\mathbf{V}|])^{\circ\frac{1}{2}} &\approx (((\mathbf{V}_P + \mathbf{V}_Q\,\mathrm{diag}[\boldsymbol{\beta}_0])\mathbf{H})^{\circ 2}\,\mathrm{Var}[\mathbf{P}_{source}])^{\circ\frac{1}{2}} + (((\mathbf{V}_P + \mathbf{V}_Q\,\mathrm{diag}[\boldsymbol{\beta}_0])\mathbf{H} \\ &\quad \cdot \mathrm{diag}[\mathrm{Var}[\mathbf{P}_{source}]]\mathbf{H}^{\mathrm{T}}) \circ \mathbf{V}_Q \circ ((((\mathbf{V}_P + \mathbf{V}_Q\,\mathrm{diag}[\boldsymbol{\beta}_0])\mathbf{H})^{\circ 2}\,\mathrm{Var}[\mathbf{P}_{source}])^{\circ\frac{1}{2}} \\ &\quad \cdot \mathbf{1}_{1\times N_{inv}})^{\circ(-1)})(\boldsymbol{\beta} - \boldsymbol{\beta}_0) \\ &= \mathbf{M}_0 + \mathbf{M}_\beta\boldsymbol{\beta}, \end{aligned} \tag{5.23}$$

where

$$\begin{aligned}\mathbf{M}_0 &= (((\mathbf{V}_P + \mathbf{V}_Q\,\mathrm{diag}[\boldsymbol{\beta}_0])\mathbf{H})^{\circ 2}\,\mathrm{Var}[\mathbf{P}_{source}])^{\circ\frac{1}{2}} - (((\mathbf{V}_P + \mathbf{V}_Q\,\mathrm{diag}[\boldsymbol{\beta}_0])\mathbf{H} \\ &\quad \cdot \mathrm{diag}[\mathrm{Var}[\mathbf{P}_{source}]]\mathbf{H}^{\mathrm{T}}) \circ \mathbf{V}_Q \circ ((((\mathbf{V}_P + \mathbf{V}_Q\,\mathrm{diag}[\boldsymbol{\beta}_0])\mathbf{H})^{\circ 2}\,\mathrm{Var}[\mathbf{P}_{source}])^{\circ\frac{1}{2}}\mathbf{1}_{1\times N_{inv}})^{\circ(-1)}) \\ &\quad \cdot \boldsymbol{\beta}_0 \end{aligned} \tag{5.24}$$

$$\begin{aligned}\mathbf{M}_\beta &= ((\mathbf{V}_P + \mathbf{V}_Q\,\mathrm{diag}[\boldsymbol{\beta}_0])\mathbf{H}\,\mathrm{diag}[\mathrm{Var}[\mathbf{P}_{source}]]\mathbf{H}^{\mathrm{T}}) \circ \mathbf{V}_Q \circ ((((\mathbf{V}_P + \mathbf{V}_Q\,\mathrm{diag}[\boldsymbol{\beta}_0])\mathbf{H})^{\circ 2} \\ &\quad \mathrm{Var}[\mathbf{P}_{source}])^{\circ\frac{1}{2}} \cdot \mathbf{1}_{1\times N_{inv}})^{\circ(-1)} \end{aligned} \tag{5.25}$$

If the node voltage magnitudes are assumed to be normally distributed over the interval of interest, the probability constraints in (5.10), which are equivalent to

$$\Pr[|\tilde{V}_i| \leq V_{min}] \leq p_{max} \tag{5.26}$$

$$\Pr[|\tilde{V}_i| \leq V_{max}] \geq 1 - p_{max}, \tag{5.27}$$

can be expressed as

$$\Phi\left(\frac{V_{min} - \mathrm{E}[|\tilde{V}_i|]}{\sqrt{\mathrm{Var}[|\tilde{V}_i|]}}\right) \leq p_{max} \tag{5.28}$$

$$\Phi\left(\frac{V_{max} - \mathrm{E}[|\tilde{V}_i|]}{\sqrt{\mathrm{Var}[|\tilde{V}_i|]}}\right) \geq 1 - p_{max}, \tag{5.29}$$

where $\Phi(\cdot)$ is the cumulative distribution function of the standard normal distribution. By substitution of (5.16) and (5.23), these constraints $\forall i \in \{1, 2, \ldots, N_{node}\}$ can be expressed as

$$\mathbf{V}_{min} - (\mathbf{N}_0 + \mathbf{N}_\alpha \boldsymbol{\alpha} + \mathbf{N}_\beta \boldsymbol{\beta} + \mathbf{N}_K \mathbf{K}) \leq \Phi^{-1}(p_{max})(\mathbf{M}_0 + \mathbf{M}_\beta \boldsymbol{\beta}), \tag{5.30}$$

$$\mathbf{V}_{max} - (\mathbf{N}_0 + \mathbf{N}_\alpha \boldsymbol{\alpha} + \mathbf{N}_\beta \boldsymbol{\beta} + \mathbf{N}_K \mathbf{K}) \geq \Phi^{-1}(1 - p_{max})(\mathbf{M}_0 + \mathbf{M}_\beta \boldsymbol{\beta}), \tag{5.31}$$

where $\mathbf{V}_{min} = V_{min}\mathbf{1}_{N_{node}\times 1}$ and $\mathbf{V}_{max} = V_{max}\mathbf{1}_{N_{node}\times 1}$. The approximation in (5.23) is only valid for $\boldsymbol{\beta}$ sufficiently close to $\boldsymbol{\beta}_0$. In particular, an additional constraint is introduced to ensure that the approximate standard deviation is nonnegative:

$$\mathbf{M}_0 + \mathbf{M}_\beta \boldsymbol{\beta} \geq \mathbf{0}. \tag{5.32}$$

The maximum expected reactive power being injected by each inverter phase is limited by the apparent power limits of the inverter phase:

$$-(\mathbf{S}_{max}^{\circ 2} - \mathbf{P}_{inv0}^{\circ 2})^{\circ \frac{1}{2}} \leq (\boldsymbol{\alpha} + \boldsymbol{\beta} \circ \mathbf{P}_{inv0}) \leq (\mathbf{S}_{max}^{\circ 2} - \mathbf{P}_{inv0}^{\circ 2})^{\circ \frac{1}{2}}, \tag{5.33}$$

where $\mathbf{S}_{max} \in \mathbb{R}^{N_{inv}\times 1}$ is a vector of the apparent power limits of the inverter phases.

By combining (5.11) and (5.30)–(5.33), the solution to the optimization problem in (5.10) can be approximated by the solution of a linear programming problem of the form

$$\begin{aligned} \min_{\mathbf{x}} \quad & \mathbf{c}^{\mathrm{T}}\mathbf{x} \\ \text{subject to} \quad & \mathbf{A}\mathbf{x} \leq \mathbf{b} \\ & \mathbf{x}_{min} \leq \mathbf{x} \leq \mathbf{x}_{max}, \end{aligned} \tag{5.34}$$

where $\mathbf{x} = [\boldsymbol{\alpha}^{\mathrm{T}}\ \boldsymbol{\beta}^{\mathrm{T}}\ \mathbf{K}^{\mathrm{T}}]^{\mathrm{T}}$, $\mathbf{c} = [\mathbf{c}_{\alpha}^{\mathrm{T}}\ \mathbf{c}_{\beta}^{\mathrm{T}}\ \mathbf{c}_{K}^{\mathrm{T}}]^{\mathrm{T}}$, and

$$\mathbf{A} = \begin{bmatrix} -\mathbf{N}_{\alpha} & -(\mathbf{N}_{\beta} + \Phi^{-1}(p_{max})\mathbf{M}_{\beta}) & -\mathbf{N}_{K} \\ \mathbf{N}_{\alpha} & \mathbf{N}_{\beta} + \Phi^{-1}(1-p_{max})\mathbf{M}_{\beta} & -\mathbf{N}_{K} \\ \mathbf{0}_{3N_{node}\times N_{inv}} & -\mathbf{M}_{\beta} & \mathbf{0}_{3N_{node}\times N_{t}} \\ \mathbf{I}_{N_{inv}} & \mathrm{diag}[\mathbf{P}_{inv0}] & \mathbf{0}_{N_{inv}\times N_{t}} \\ -\mathbf{I}_{N_{inv}} & -\mathrm{diag}[\mathbf{P}_{inv0}] & \mathbf{0}_{N_{inv}\times N_{t}} \end{bmatrix}$$

$$\mathbf{b} = \begin{bmatrix} \Phi^{-1}(p_{max})\mathbf{M}_0 - \mathbf{V}_{min} + \mathbf{N}_0 \\ -\Phi^{-1}(1-p_{max})\mathbf{M}_0 + \mathbf{V}_{min} - \mathbf{N}_0 \\ \mathbf{M}_0 \\ (\mathbf{S}_{max}^{\circ 2} - \mathbf{P}_{inv0}^{\circ 2})^{\circ \frac{1}{2}} \\ (\mathbf{S}_{max}^{\circ 2} - \mathbf{P}_{inv0}^{\circ 2})^{\circ \frac{1}{2}} \end{bmatrix},$$

where $\mathbf{0}_{m\times n}$ is the $m \times n$ matrix filled with zero.

Because the linear programming problem described by (5.34) is based on linearization about a previous estimate of the solution of the optimization problem in (5.10), the solution to the problem may not be optimal or even be feasible. However, if the previous estimate of the solution is feasible, then it can be shown that the solution to (5.34) indicates a direction in which the solution quality can be improved. In order to implement an algorithm using this approach, it is necessary to locate an initial feasible solution.

Given any candidate initial solution (e.g., $\boldsymbol{\alpha}_0 = \mathbf{0}$, $\boldsymbol{\beta}_0 = \mathbf{0}$, and $\mathbf{K}_u = \mathbf{0}$) and the assumed statistical characteristics of the source power over the interval of interest, it is possible to

linearize the system about the point with

$$\mathbf{P}_{inv0} = \mathbf{H}\mathrm{E}[\mathbf{P}_{source}] \tag{5.35}$$

$$\mathbf{Q}_{inv0} = \boldsymbol{\alpha}_0 + \boldsymbol{\beta}_0 \circ (\mathbf{H}\mathrm{E}[\mathbf{P}_{source}]). \tag{5.36}$$

With linearization, a point that is near the candidate initial solution that satisfies the linear inequality constraints associated with the candidate initial solution can be found. Because the solution is near the candidate initial solution, it is more likely to be feasible with the constraints being obtained from a nearby point. This problem can be expressed as a quadratic programming problem:

$$\begin{aligned} \min_{\mathbf{x}} \quad & \tfrac{1}{2}\mathbf{x}^{\mathrm{T}}\mathbf{Q}\mathbf{x} + \mathbf{f}^{\mathrm{T}}\mathbf{x} + C \\ \text{subject to} \quad & \mathbf{A}\mathbf{x} \leq \mathbf{b} \\ & \mathbf{x}_{min} \leq \mathbf{x} \leq \mathbf{x}_{max}, \end{aligned} \tag{5.37}$$

where

$$\begin{aligned} \frac{1}{2}\mathbf{x}^{\mathrm{T}}\mathbf{Q}\mathbf{x} + \mathbf{f}^{\mathrm{T}}\mathbf{x} + C = {} & \frac{1}{2}(\boldsymbol{\alpha} - \boldsymbol{\alpha}_0)^{\mathrm{T}} \operatorname{diag}[\mathbf{S}_{max}^{\circ(-1)}](\boldsymbol{\alpha} - \boldsymbol{\alpha}_0) \\ & + \frac{1}{2}(\boldsymbol{\beta} - \boldsymbol{\beta}_0)^{\mathrm{T}}(\boldsymbol{\beta} - \boldsymbol{\beta}_0) + \frac{1}{2}(\mathbf{K} - \mathbf{K}_0)^{\mathrm{T}} \operatorname{diag}[\mathbf{K}_{range}^{\circ(-1)}](\mathbf{K} - \mathbf{K}_0), \end{aligned} \tag{5.38}$$

where $\mathbf{K}_{range}$ is a vector indicating the magnitude of the voltage regulator tap settings (e.g., $\max\{|K_{min}|, |K_{max}|\}$).

When solving the quadratic programming problem in (5.37), the solver returns updated candidate initial solutions $\boldsymbol{\alpha}_0$, $\boldsymbol{\beta}_0$, and $\hat{\mathbf{K}}$, the last of which does not consider the integer nature of the tap settings. An unrounded estimate $\mathbf{K}_u$ is maintained and updated by determining the difference between the voltage regulator tap settings determined by the quadratic programming solver and those about which the system is linearized:

$$\boldsymbol{\Delta}\mathbf{K} := \hat{\mathbf{K}} - \mathbf{K}_0. \tag{5.39}$$

The unrounded estimate is updated using

$$\mathbf{K}_u := \mathbf{K}_u + \boldsymbol{\Delta}\mathbf{K}, \tag{5.40}$$

and the candidate initial integer vector $\mathbf{K}_0$ is updated by rounding the unrounded estimate. This process is repeated until an initial feasible solution is found as shown in the top portion of the flowchart in Figure 5.1.

Once an initial feasible solution is found, the linear programming problem in (5.34) can be solved to determine a direction in which the solution quality can be improved. By searching in this direction, a feasible solution that improves the solution quality can be located. This process can be repeated until the solution converges. This process is illustrated in the bottom portion of Figure 5.1. In the top portion, $\boldsymbol{\alpha}$, $\boldsymbol{\beta}$, and $\mathbf{K}$ represent the current feasible candidate solution. The bottom portion shows the process of finding a feasible solution (i.e., $\boldsymbol{\alpha}_0$, $\boldsymbol{\beta}_0$, and $\mathbf{K}_0$). By solving the linear programming problem, a new, possibly infeasible, candidate solution represented by $\bar{\boldsymbol{\alpha}}$, $\bar{\boldsymbol{\beta}}$, and $\bar{\mathbf{K}}$ is found. The feasibility and solution quality of points between the current candidate solution and the new candidate solution are evaluated. If necessary, the new candidate solution is moved closer to the current candidate solution using a step size constriction coefficient $\delta \in (0,1)$. When no further feasible improvement to the solution is made (in terms of relative step size $0 < \varepsilon \ll 1$), the algorithm terminates with the values $\boldsymbol{\alpha}_0$, $\boldsymbol{\beta}_0$, and $\mathbf{K}_0$.

5.4 Test System Description

The IEEE 123-node radial distribution test feeder [87] is considered as a test network to assess the performance of the proposed control strategy. This test system is shown in Figure 3.2, has a nominal voltage of 4.16 kV, and consists of 123 nodes, unbalanced loads, and four voltage regulators, which are located between Nodes 150 and 149, 9 and 14, 25 and 26, and 160 and 67. In this study, ten three-phase PV inverters are considered in the locations shown in Figure 3.2 based on a previous study [71] in which inverters situated in these locations with spatially correlated irradiance can cause significant voltage fluctuations. The power output of these inverters is based on the 1-s global horizontal irradiance data collected by the National Renewable Energy Laboratory Solar Measurement Grid in

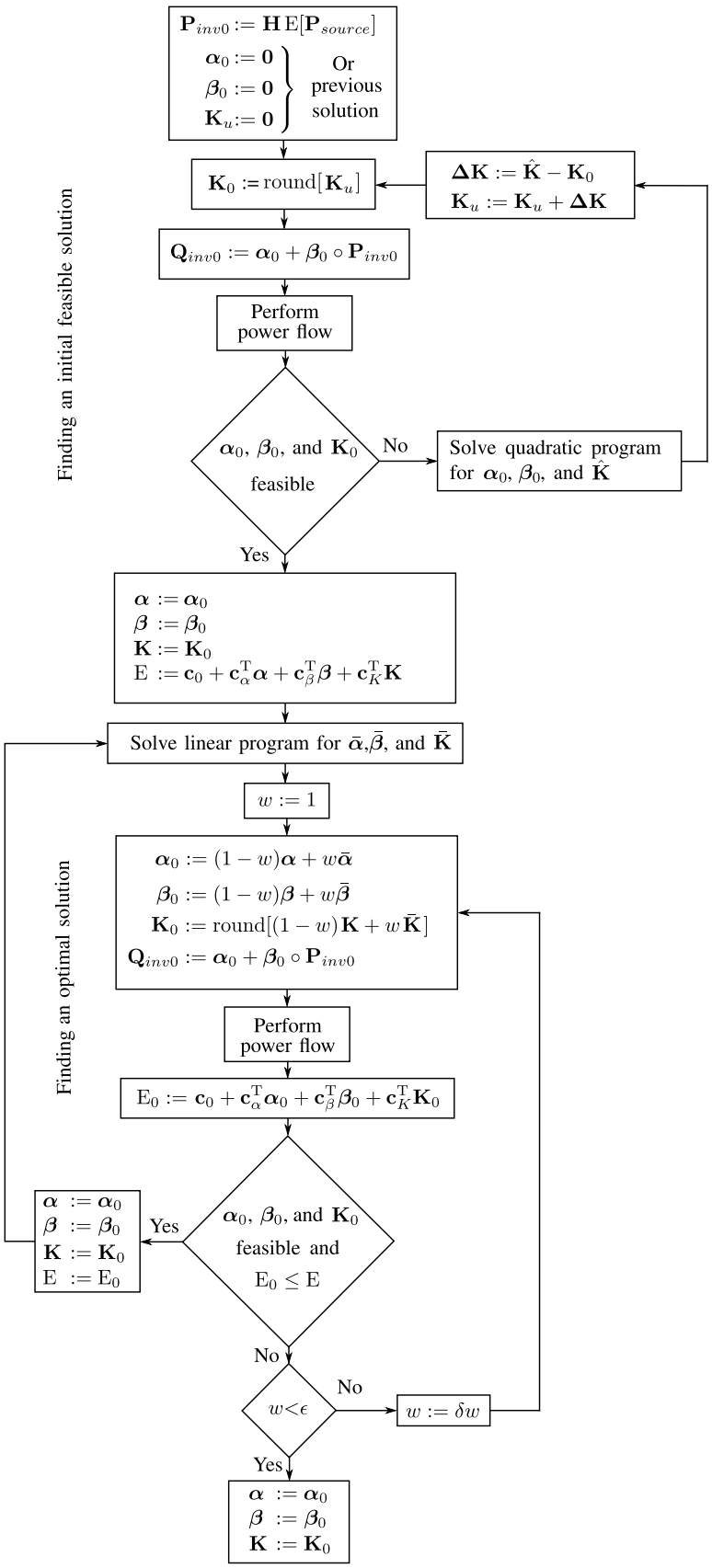

Figure 5.1: Flowchart of proposed solution algorithm

Table 5.1: Inverter parameters

Node Location	Rated Solar Power (kW)	Irradiance Data Source
1	300	DH1
7	300	DH2
8	300	DH3
13	300	DH4
18	300	DH5
52	300	DH6
53	300	DH7
54	300	DH8
55	300	DH9
56	300	DH10

Oahu, Hawaii [88]. In particular, the active power output of each inverter in proportional to the irradiance, with rated power output at an irradiance of 1500 W/m^2. The inverter locations, ratings, and data sources are given in Table 5.1.

To evaluate the proposed method, the 14-hour period from 5:00 AM to 7:00 PM on 22 July 2010 is considered. During this period, the active power injection varies significantly, exhibiting high variance and spatial correlation between nearby PV sources. The system loading is based on the load observed by the Electric Reliability Council of Texas [95] over the same period. The load data is normalized such that the peak load during the period corresponds to maximum system load. The load at each node is updated every 15 minutes. The total load and PV power generation over the period are shown in Figure 5.2.

In this work, suitable PV generation forecast methodologies are assumed to be applied [90, 96, 97]. The expected values and variances of the PV sources are assumed to be known in advance over the next period of interest, but the moment-by-moment source power injections are not assumed to be known in advance.

OpenDSS is used to perform power flow calculations [98]. The acceptable voltage magnitude range of all nodes is 118–126 V on a 120-V scale [26]. When performing optimization, the maximum acceptable probability of voltage magnitude violations during

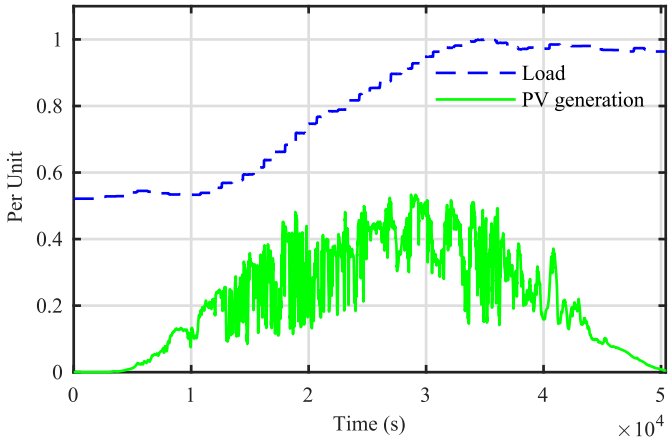

Figure 5.2: Load profile and PV active power injection.

the optimization interval p_{max} of 5% is used. When assessing the results, the range of acceptable voltage magnitudes is slightly expanded to 117.95–126.05 V to avoid penalizing methods for extremely small deviations (e.g., due to non-linearity, non-normal distributions, and correlation between sources).

All of the optimization problems are solved using an open-source linear programming solver (Coin-OR Linear Programming) and an open-source quadratic programming solver (Object Orientated Quadratic Programming). A workstation with an Intel Core i7-3770 processor operating at 3.40 GHz with 8 GB of memory was used to perform the results and simulations. To control the convergence of the algorithm, the values $\delta = 0.8$ and $\varepsilon = 10^{-4}$ are used herein. The average time required to find $\boldsymbol{\alpha}$, $\boldsymbol{\beta}$, and $\mathbf{K}$ for each 15-minute interval over the entire 14-hour period is recorded as 180 seconds for the IEEE 123-node radial distribution test feeder, which is significantly smaller than the 15-minute cycle time.

In order to examine the proposed method, three versions of three different methods are considered. The three versions of these methods vary based on which variables are considered. In the first version (V1), only the voltage regulator tap settings $\mathbf{K}$ are adjusted, and the fixed and variable reactive power output of the PV inverters are zero (i.e., $\boldsymbol{\alpha} = \boldsymbol{\beta} = \mathbf{0}$). This version is similar to conventional volt-var control methods in which only utility equipment is controlled [99]. In the second version (V2), the voltage regulator tap settings

$\mathbf{K}$ and the inverter fixed reactive power output $\boldsymbol{\alpha}$ are adjusted, but the inverter variable reactive power output does not change during the interval (i.e., $\boldsymbol{\beta} = \mathbf{0}$). This version is similar to approaches in which reactive power is dispatched over certain intervals [44, 57]. In the third version (V3), the voltage regulator tap settings $\mathbf{K}$ and the inverter fixed and variable reactive power outputs ($\boldsymbol{\alpha}$ and $\boldsymbol{\beta}$) are adjusted.

While the three versions listed above differ with respect to which decision variables are considered, the three methods differ according to how they determine the values of these variables. The first method, the static method (SM), involves solving (5.10) over an interval corresponding to the entire 14-hour period using average load. In the second method, the dynamic method (DM), the expected losses are minimized over 15-minute intervals subject to the constraint that the expected voltage magnitudes are within the acceptable range of $[V_{min}, V_{max}]$ and the expected reactive power is within the apparent power limits of the inverter phase. The variability of the PV source power injections is not considered in this optimization problem. When the variable reactive power output is considered (i.e., the V3), it is determined in a second layer based on minimizing the sensitivity of the local voltage magnitudes to fluctuations in active power injection [71], which corresponds to the dual-layer approach proposed in [75]. As in [75], 20% of the reactive power capability is reserved in the first layer for use in the second layer. For the third method, the integrated method (IM), which is the method presented herein, (5.10) is solved over 15-minute intervals.

The nine instances representing each combination of the three versions and the three methods set forth herein are denoted using nine abbreviations. Each abbreviation indicates the method and version. For example, DMV2 indicates the dynamic method version 2.

5.5 Simulation Results and Discussion

The nine instances set forth above are simulated over the scenario mentioned above, and the simulation results are reported in Table 5.2. For each instance, the total number of

Table 5.2: Simulation Results for All Instances

Instance	Violated node phases	Violation time (s)	Violation percentage (%)	Mean loss (kW)	Worst-case 15-min violation percentage (%)	Worst-case violated node phase
SMV1	88	20731	41	45.86	—	—
SMV2	72	23860	47	41.98	—	—
SMV3	114	43200	54	42.83	—	—
DMV1	43	5266	4.7	44.82	55	104 c-phase
DMV2	24	3629	3.4	40.90	43	104 c-phase
DMV3	0	0	0	41.10	0	—
IMV1	18	1077	1.2	44.82	23	114 a-phase
IMV2	13	922	0.86	40.88	30	114 a-phase
IMV3	0	0	0	40.81	0	—

violated node phases (i.e., nodes with phase voltage magnitudes outside of the acceptable range) is recorded. Also, the total time in which any violation is experienced in the system is observed. For each node phase, two voltage violation percentages are calculated: one for voltage magnitude over the acceptable limit, and the other for voltage magnitude under the acceptable limit, corresponding to the constraints in (5.10). The largest of these violation percentages across the system is presented. Mean loss is determined using power calculated every second over the 14-hour period. The DM and IM both operate on a 15-minute interval, so worst-case violations in any 15-minute interval are also considered for these methods. The worst-case violation percentage is the violation percentage during the worst 15-minute interval for a given instance. The node phase experiencing this worst-case violation is also recorded.

As seen in Table 5.2, the SM results in many phases having voltage magnitude violations and the system experiencing such violations for a large fraction of the considered interval. Even using the chance constraints in (5.10), the violation percentages are very large with all versions. This occurs because this method does not account for any changes over the day. In particular, it does not consider how load varies, including how it is corre-

lated over longer periods of time with the PV generation, which is shown in Figure 5.3 (a). It can be seen that because of variations in loading, voltage magnitudes drift outside of the acceptable range for large periods of time. However, it can also be seen that using variable reactive power (i.e., V3), the voltage magnitudes are smoother. The SMV1 is a basic baseline, but it is not particularly realistic because it does not correspond to how such systems are ordinarily operated (e.g., tap changes by voltage regulators).

DMV1 is a more realistic baseline, with its behavior more closely representing distribution system volt-var control. It adjusts the tap settings each 15 minutes to minimize system losses while maintaining expected voltage magnitudes within acceptable limits. It can be seen in Table 5.2 that it is generally successful with reducing the overall violation percentage, but it does experience 15-minute intervals in which it is not able to control the voltage magnitudes effectively. Even DMV2, which uses fixed reactive power output in each 15-minute interval cannot prevent the system from experiencing unacceptable 15-minute intervals. This can be seen in Figure 5.3 (b). It can also be seen that using the reactive power capability of the PV inverters results in smoother voltage magnitudes compared with using tap changes alone. It can be seen in Table 5.2, that the DM versions are more effective at reducing both voltage magnitude violations and losses than the analogous SM versions. This is expected because the DM is making decisions every 15 minutes compared with a single decision being made by the SM.

The proposed IM versions are also shown in Table 5.2. The IM versions also make a decision every 15 minutes, but they formulate voltage magnitude limits as chance constraints. It can be seen that they are more capable than the analogous DM versions at reducing both voltage magnitude violations and losses. Figure 5.3 (c) indicates that IMV1 and IMV2 both maintain voltage magnitudes in most intervals, but that the system still experiences unacceptable 15-minute intervals because the violation percentage is larger than $p_{max} = 5\%$. From Table 5.2, the severity of these intervals for the IM versions is less than that of the DM versions. Another observation that can be made from these results is that the worst-

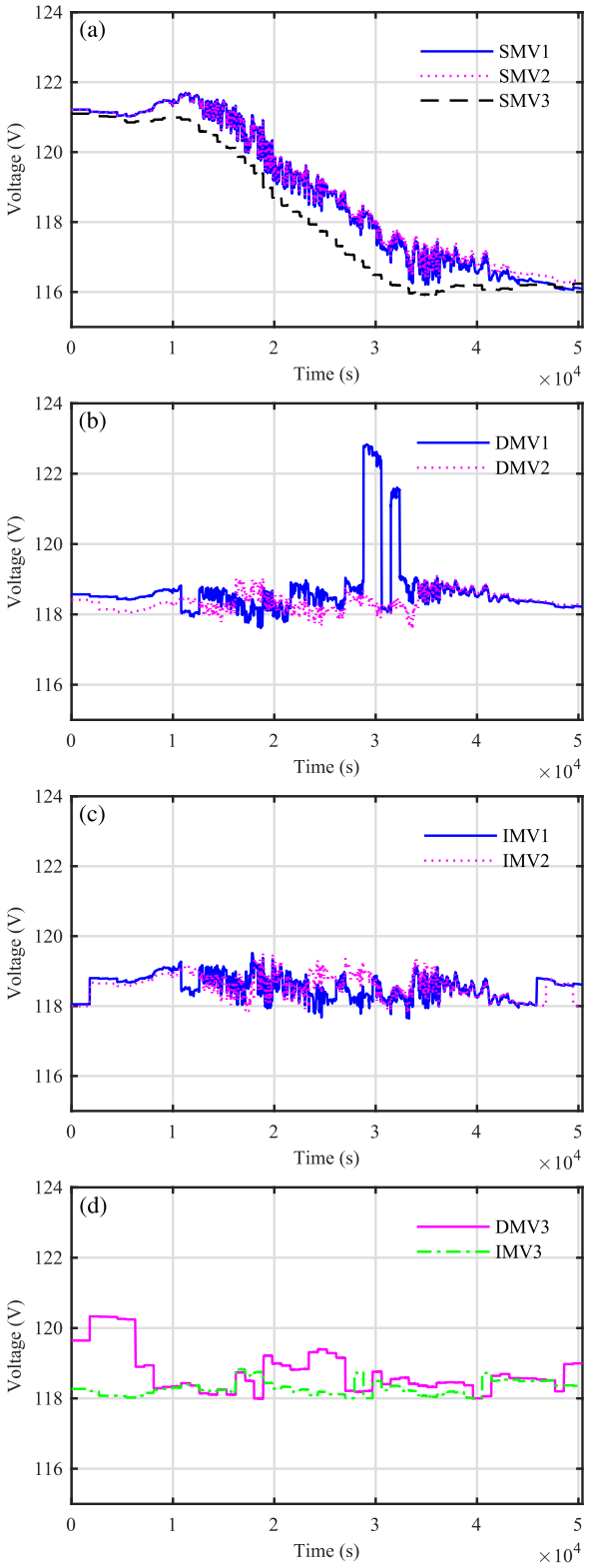

Figure 5.3: (a) Node 114 *a*-phase voltage magnitude for SM, (b) Node 104 *c*-phase voltage magnitude for DMV1 and DMV2, (c) Node 114 *a*-phase voltage magnitude for IMV1 and IMV2, and (d) Node 104 *c*-phase voltage magnitude for DMV3 and IMV3.

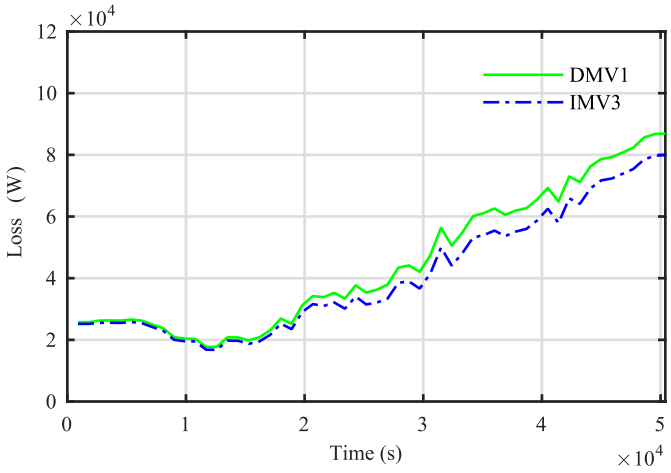

Figure 5.4: Losses for DMV1 and IMV3.

case 15-minute violation percentages for these instances should be less than approximately $p_{max} = 5\%$. A potential explanation for this discrepancy is that variable reactive power injection (i.e., $\boldsymbol{\beta}$) is not used in IMV1 or IMV2.

The DMV3 seeks to keep the voltage magnitude within acceptable limits as shown in Figure 5.3 (d) with no violation over the interval of interest and with successful reduction in mean losses of 8.30% with respect to DMV1 as can be seen in Table 5.2. In DMV3, the first layer is used to minimize the system loss, reserving some of the PV reactive power capability for use in the second layer but not coordinating with the second layer. Consequently, the DMV3 is somewhat conservative with respect to loss minimization (because of the reserved capability) and results in less smooth voltages (because of the lack of coordination). Alternatively, the IMV3 is formulated as an integrated control method in which the use of inverter reactive power capability with the operation of voltage regulators is coordinated to control voltage magnitude violations and reduce losses. It also exhibits no voltage violations over the interval of interest, is able to further reduce losses (8.97% with respect to DMV1 as shown in Figure 5.4 or an additional 8.07% reduction with respect to the reduction obtained with DMV3), and results in smoother voltage magnitudes than other instances as shown in Figure 5.3 (d).

The proposed IMV3 coordinates the actions of the distribution system equipment (e.g.,

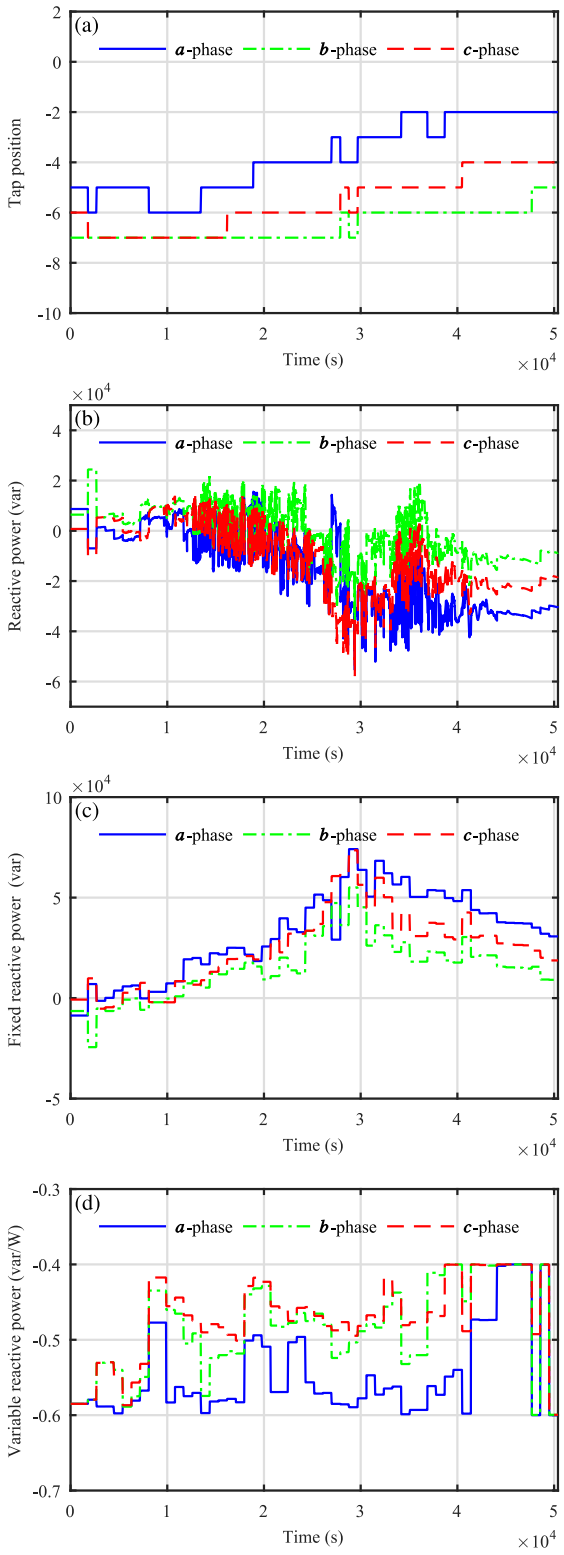

Figure 5.5: (a) Tap positions for the voltage regulator connected to Node 160 for IMV3, (b) PV inverter three-phase reactive power injection at Node 55, and (c) and (d) the PV inverter three-phase fixed and variable reactive power injection ($\boldsymbol{\alpha}$ and $\boldsymbol{\beta}$) at Node 55 for IMV3.

Table 5.3: The tap change operations of DM and IM versions over the interval of interest

Voltage regulators (V.R)	Phase	Instance					
		DMV1	DMV2	DMV3	IMV1	IMV2	IMV3
$V.R_{150-149}$	*abc*	2	2	3	2	5	1
$V.R_{9-14}$	*a*	3	3	6	7	2	1
$V.R_{25-26}$	*a*	4	6	6	8	5	5
	c	5	1	4	5	2	3
$V.R_{160-67}$	*a*	7	9	14	7	5	11
	b	6	4	8	8	2	4
	c	7	3	11	11	6	6
Total number of tap changes		34	28	52	48	27	31

voltage regulators) with those of the PV inverters. Too frequently occurring tap change operations is a maintenance concern for distribution system operators. While it is not an explicit goal of the proposed method, it can help reduce tap change operations. The control strategy used herein adjusts the voltage regulators infrequently (i.e., at most every 15 minutes over the 14-hour period) and the solution method in Figure 5.1 begins its search for each interval from the solution for the previous interval. To study the effectiveness of the IMV3 in terms of tap change operation reduction, the tap changing operations of the IM and DM versions over the 14-hour period are shown in Table 5.3. Also, the tap settings of one of the voltage regulators using IMV3 are shown in Figure 5.5 (a). It can be seen that the tap settings are adjusted relatively infrequently during the course of the day in order to improve losses and maintain voltages in response to changing load and PV injections. As a result, IMV3 has fewer tap change operations in comparison with DMV3, which is the instance with the most comparable performance. The proposed method is able to function in this way because it uses variable PV reactive power injections to compensate for rapid changes. The three-phase reactive power output of one of the PV inverters and its control parameters ($\boldsymbol{\alpha}$ and $\boldsymbol{\beta}$) are shown in Figure 5.5 (b),(c), and (d). It can be seen that whenever the PV generation has a significant fluctuation as shown in Figure 5.2, PV inverters provide or consume reactive power based on the PV generation patterns. The proposed method is

Table 5.4: Accuracy of the proposed method (i.e., optimal solutions)

15-minute interval	Mean loss (kW) of the IMV3 using MINLP	Mean loss (kW) of the IMV3 using the proposed algorithm
5:00 AM to 5:15 AM	25.085	25.1
7:30 AM to 7:45 AM	19.547	19.548
10:00 AM to 10:15 AM	23.454	23.454
10:30 AM to 10:45 AM	31.603	31.603
3:00 PM to 3:15 PM	53.622	53.623

Table 5.5: The sensitivity of the proposed method (i.e., initial solutions)

15-minute interval	Mean loss (kW) of the IMV3 using MINLP	Mean loss (kW) of the IMV3 using the proposed algorithm
5:00 AM to 5:15 AM	26.351	25.184
7:30 AM to 7:45 AM	20.782	19.553
10:00 AM to 10:15 AM	28	23.545
10:30 AM to 10:45 AM	37.16	32.03
3:00 PM to 3:15 PM	60.215	53.68

able to minimize losses and maintain system voltages more effectively by coordinating the response of the distribution system equipment with that of the PV inverters.

Because the proposed method is a supervisory control method targeting the performance of the entire system, the most effective means of validating its performance is with system studies. In this case, a widely available and acceptable test system (i.e., the IEEE 123-node test feeder from the IEEE PES Distribution System Analysis Subcommittee) is used to validate the method. To validate the accuracy of the proposed method to find the optimal solution for the control parameters, the mixed-integer nonlinear programming (MINLP) solver is used to solve the proposed problem directly. The results show that the proposed method matches the results obtained from the MINLP solver (within the tolerances used by the method) with much less computational time. For example, the five 15-minute intervals have been randomly chosen from the interval of interest, and it is assumed that the MINLP uses the optimal solutions of the proposed method as initial solutions. The

Table 5.6: Performance of IM

Method		Violated node phases	Violation time (s)	Violation percentage (%)	Mean loss (kW)	Worst-case 15-min violation percentage(%)	Worst-case violated node phase
IMV1	Expected	–	–	0.18	44.63	0.62	114 a-phase
	Synthetic	4	13	0.2	44.66	0.66	114 a-phase
	Actual	18	1077	1.2	44.82	23	114 a-phase
IMV2	Expected	–	–	0.07	40.70	2.04	114 a-phase
	Synthetic	3	34	0.04	40.73	2.0	114 a-phase
	Actual	13	922	0.86	40.88	30	114 a-phase
IMV3	Expected	–	–	0	40.60	0	—
	Synthetic	0	0	0	40.63	0	—
	Actual	0	0	0	40.81	0	—

results shown in Table 5.4 clearly indicate that optimal solutions of the proposed method are very close to optimal solutions obtained by the MINLP. To better understand the performance of the proposed method and the MINLP in terms of initial solutions, it is assumed that the proposed method and the MINLP have the same initial solutions (i.e., zero initial solutions). As can be seen in Table 5.5, the MINLP solver is far more sensitive to the initial solution than the proposed method. This is expected because this type of problem might mostly be non-convex with several local minima that are suboptimal solutions to non-convex problems.

5.5.1 Sensitivity to Distribution Assumptions

The sensitivity of the IM is evaluated with respect to assumptions (i.e., the normality and independence of the PV source powers). Statistical tests (e.g., the Anderson-Darling normality and Pearson correlation coefficient test) are used to measure both the normality of the irradiance during the interval of interest and the linear correlation of PV sources. These tests reject the hypothesis in which the irradiance during the interval of interest is normally distributed and indicate a strong linear correlation between PV sources. In order to assess the degree to which the proposed method fails to satisfy the assumptions, synthetic PV

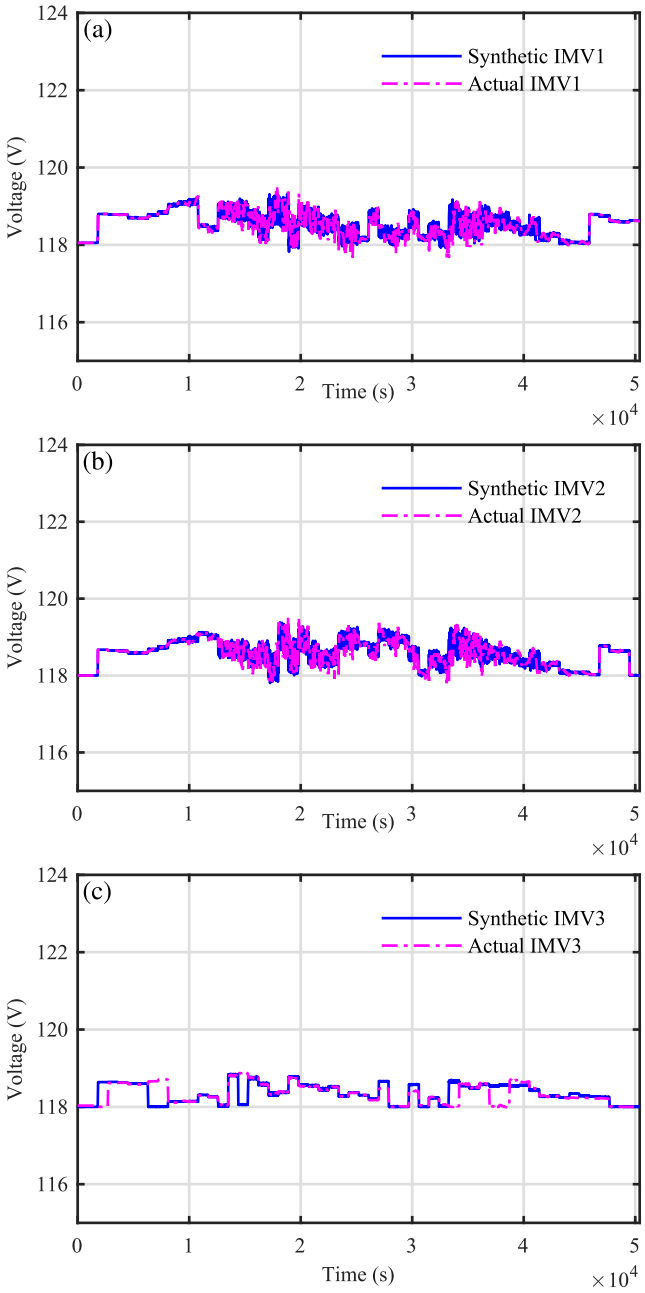

Figure 5.6: (a) Node 114 *a*-phase voltage magnitude for synthetic and actual case of the IMV1, (b) Node 114 *a*-phase voltage magnitude for synthetic and actual case of the IMV2, and (c) Node 114 *a*-phase voltage magnitude for for synthetic and actual case of the IMV3.

source powers are constructed that have the same statistical characteristics (i.e., mean values and variances) as those in the actual PV source powers. However, the synthetic values are constructed to be independent and normally distributed. It is possible to compare the expected values (considered when computing the IM solution) to the simulation performances of the IM in both the synthetic and the actual PV source powers. Table 5.6 for the actual case indicates that the assumptions actually hold for the PV sources in the IMV1 and IMV2 (i.e., a maximum acceptable probability of voltage magnitude violation pmax of 5% at every 15-min), and do not hold with acceptable performance of the IMV3 because of the variable PV reactive power output [85]. From Table 5.6, the IMV1 and IMV2 in the synthetic case result in less node phases having voltage magnitude violations at some point during the case and a lower period of time in which at least one node phase experiences an unacceptable voltage magnitude. Another observation that can be made from Table 5.6 is that the IMV3 in both the synthetic and actual case results in no node phases having voltage magnitude violations. In terms of the violation percentage, the IM versions in the synthetic case more carefully seek to match the expected violation percentage. This is expected because the IM versions in the synthetic case more carefully match the assumptions upon which the expected value is calculated. The lower value during the IM versions in the synthetic case indicates improved voltage quality, but it also represents a more conservative solution to the optimization problem because p_{max} is 5%. When compared with the actual case, the IMV1 and IMV2 are less accurate to match the expected violation percentage while the IMV3 matches the expected violation percentage. In terms of the mean loss, the IMV1, IMV2, and IMV3 in the synthetic case carefully seek to match the expected value of the mean loss, but in the actual case are relatively worse. In terms of the worst-case 15-min violation percentage, the IMV1, IMV2, and IMV3 in the synthetic case are relatively close to matching the expected value, but the IMV1 and IMV2 in the actual case fail to satisfy the the assumption herein (i.e., a maximum acceptable probability of voltage magnitude violation pmax of 5% at every 15-min) because these methods are highly sensitive to the

assumptions (i.e., the normality and independence of the PV source powers) without considering the variable PV reactive power output used to mitigate the variation of PV source powers. When taken together, the results indicate that the IMV3 is not highly sensitive to the assumptions regarding the normality and independence of the PV source powers.

The resulting voltage magnitude at the *a* phase of Node 114 is shown as an example in Figure 5.6 for the synthetic and actual case. Figure 5.6 (a) and (b) indicate that the voltage magnitude of the IMV1 and the IMV2 using the synthetic case has a shorter excursion under the acceptable lower limit (117.95 V) than in the actual case. Figure 5.6 (c) also indicates that the voltage magnitude of the IMV3 in both the synthetic and actual case does not draft outside the acceptable ranges because it is not highly sensitive to the assumptions used in this work, and exhibits a smoother voltage magnitude than the IMV1 and the IMV2 over the interval of interest because of the use of the variable PV reactive power output.

5.6 Conclusion

An integrated control method, formulated as a mixed-integer, nonlinear, chance-constrained optimization problem, is presented to minimize the expected value of a figure of merit while constraining the probability of unacceptable voltage magnitudes and considering the uncertainty of PV power injections over the interval of interest. The integrated control method combines the capabilities of distribution system equipment with the reactive power capabilities of PV inverters to minimize system losses and constrain the probability of voltage violations. The proposed method uses suitable PV generation forecast methodologies that include the expected values and variances of the PV sources, but not the moment-by-moment values. The sensitivity of the proposed method IMV3 to the distribution assumptions is considered, and it is found that the method is not highly sensitive to these assumptions. The performance of the proposed method is evaluated using the IEEE 123-node radial distribution test feeder under changing load and irradiance conditions, and it is compared against two different existing methods. The results showed the capability of the

proposed method to minimize the system losses and mitigate voltage fluctuations.

Chapter 6

Coordination of PV Inverters and Voltage Regulators Considering Generation Correlation and Voltage Quality Constraints for Loss Minimization

6.1 Introduction

In this chapter, a coordinated volt-var control method is proposed to achieve the optimal expected performance (i.e., system losses and voltage profiles), while considering spatial correlations among the DGs. It also seeks to maintain voltage magnitudes within an acceptable range, by formulating chance constraints on the voltage magnitude and considering the uncertainty of DG power injections, over the interval of interest. Although the volt-var control proposed herein uses infrequent communication between the distribution system operator and voltage regulator settings, it can respond successfully to a rapid change in irradiance conditions, by using DG control parameters. Thus, allowing them to respond to such changes in real time. The control strategy is formulated as a mixed-integer, nonlinear, chance-constrained optimization problem, and a heuristic approach, using power

flow solutions and linearization to find optimal solutions. The proposed method is based on previous work [85], where this method only used the reactive power output of DGs to improve the system performance, and to previous work [93], where this method used distribution system equipment including PV inverters, to improve the system performance. The main improvements of this work are: a consideration of the spatial correlation among DGs, improved voltage magnitude profiles by limiting the variation of voltage magnitudes, evaluation of the system performance over longer periods, and a more thorough comparison with existing methods to achieve a reasonable benchmark for comparison.

Despite the fact that the proposed method mainly targets the improvement of the system performance (i.e., the system losses and voltage magnitude profiles), a frequent operation of voltage regulators can be indirectly remedied using an effective approach. This approach involves reducing the number of possible interactions between DGs and voltage regulators. This can be achieved by adjusting the voltage regulators every 15 minutes, over the 14-hour period, and restarting the proposed solution algorithm from a previous optimal solution.

The DG source powers are distributed near each other in this work. Therefore, the DG source powers are highly correlated with each other, based on statistical tests used to measure the normality of irradiance during this interval and the linear correlation of DG sources. Consequently, the impact of spatial correlations among DG source powers on the accuracy of the proposed method and the voltage profile enhancement is mainly studied in this chapter. The proposed method is validated using an IEEE 123-node radial distribution system. The results showed that the proposed method is promising for improving the system performance and voltage magnitude profile with intermittent renewable resources.

The remainder of this chapter is described as follows. Section 6.2 presents the system description and approximation for the figure of merit and the system voltage magnitudes. The problem formulation is provided in Section 6.3. Section 6.4 describes the test system description based on the IEEE 123-node radial distribution test feeder [87]. Simulation results and discussion are explored in Section 6.5. Finally, conclusions are given in Sec-

tion 6.6.

6.2 System Description and Approximation

A coordinated volt-var control method using the PV inverters and voltage regulators is presented herein to minimize the expected value of a figure of merit U and mitigate the voltage magnitude fluctuations, while considering the spatial correlation among DGs and constraining the probability of unacceptable voltage magnitudes in the distribution systems. The strategy used herein is based on solving nonlinear problems using power flow solutions and approximations derived from power flow solutions in a heuristic method. The equations that explain the system description and approximation for the figure of merit and the system voltage magnitudes mentioned in 5.2 will be used in this section.

6.3 Problem Formulation

The proposed method is formulated as a nonlinear, mixed-integer, chance-constrained problem with predefined probabilistic constraints. The proposed method seeks to improve the expected value of a figure of merit including optimal expected inverter control parameters and voltage regulator settings, while ensuring that the probability of unacceptable

voltage magnitudes over the interval of interest is satisfied[1]:

$$\begin{array}{ll} \min_{\boldsymbol{\alpha},\boldsymbol{\beta},\mathbf{K}} & \mathrm{E}[U] \\ \text{subject to} & \Pr[|\tilde{V}_i| \leq V_{min}] \leq p_{max} \\ \forall i \in \{1,2,\ldots,N_{node}\} & \Pr[|\tilde{V}_i| \geq V_{max}] \leq p_{max} \\ & \mathbf{0} \leq (\mathrm{Var}[|\mathbf{V}|])^{\circ\frac{1}{2}} \leq \boldsymbol{\sigma}_{max} \\ & (\mathrm{E}[\mathbf{P}_{inv}]^{\circ 2} + \mathrm{E}[\mathbf{Q}_{inv}]^{\circ 2})^{\circ\frac{1}{2}} \leq \mathbf{S}_{max} \\ & \boldsymbol{\alpha}_{min} \leq \boldsymbol{\alpha} \leq \boldsymbol{\alpha}_{max} \\ & \boldsymbol{\beta}_{min} \leq \boldsymbol{\beta} \leq \boldsymbol{\beta}_{max} \\ & \mathbf{K}_{min} \leq \mathbf{K} \leq \mathbf{K}_{max}, \end{array} \tag{6.1}$$

where $\tilde{V}_i$ is the voltage at node phase i, p_{max} is the maximum acceptable probability for a node phase voltage magnitude to exceed V_{max} or to fall below V_{min}, $\boldsymbol{\sigma}_{max} = \sigma_{max}\mathbf{1}_{N_{node}\times 1}$ is the vector of the maximum expected standard deviation of the voltage magnitudes, $\mathbf{S}_{max} \in \mathbb{R}^{N_{inv}\times 1}$ is a vector of the apparent power limits of the inverter phases, $\boldsymbol{\alpha}_{min}$, $\boldsymbol{\beta}_{min}$, $\boldsymbol{\alpha}_{max}$, $\boldsymbol{\beta}_{max}$ are minimal and maximal allowable inverter control parameters, and $\mathbf{K}_{min}$ and $\mathbf{K}_{max}$ are minimal and maximal allowable voltage regulator tap settings.

It is assumed that the expected value and the variance of each source power, i.e., $\mathrm{E}[\mathbf{P}_{source}]$ and $\mathrm{Var}[\mathbf{P}_{source}]$, are known over the interval of interest. This nonlinear problem is solved iteratively, and is solved based on a linearization about the previous solution estimate (i.e., $\boldsymbol{\alpha}_0$, $\boldsymbol{\beta}_0$, and $\mathbf{K}_0$).

It is possible to approximate $\mathrm{E}[U]$ using (5.8):

$$\begin{aligned} \mathrm{E}[U] &\approx U_0 + \mathbf{U}_P^{\mathrm{T}}(\mathbf{H}\,\mathrm{E}[\mathbf{P}_{source}] - \mathbf{P}_{inv0}) - \mathbf{U}_Q^{\mathrm{T}}\mathbf{Q}_{inv0} - \mathbf{U}_K^{\mathrm{T}}\mathbf{K}_0 \\ &\quad + \mathbf{U}_Q^{\mathrm{T}}\boldsymbol{\alpha} + \mathbf{U}_Q^{\mathrm{T}}\,\mathrm{diag}[\mathbf{H}\,\mathrm{E}[\mathbf{P}_{source}]]\boldsymbol{\beta} + \mathbf{U}_K^{\mathrm{T}}\mathbf{K} \\ &= \mathbf{c}_0 + \mathbf{c}_\alpha^{\mathrm{T}}\boldsymbol{\alpha} + \mathbf{c}_\beta^{\mathrm{T}}\boldsymbol{\beta} + \mathbf{c}_K^{\mathrm{T}}\mathbf{K}, \end{aligned} \tag{6.2}$$

[1] E is the expectation operator

where

$$\mathbf{c}_0 = U_0 + \mathbf{U}_P^{\mathrm{T}}(\mathbf{H}\mathrm{E}[\mathbf{P}_{source}] - \mathbf{P}_{inv0}) - \mathbf{U}_Q^{\mathrm{T}}\mathbf{Q}_{inv0} - \mathbf{U}_K^{\mathrm{T}}\mathbf{K}_0 \tag{6.3}$$

$$\mathbf{c}_\alpha = \mathbf{U}_Q \tag{6.4}$$

$$\mathbf{c}_\beta = \mathrm{diag}[\mathbf{H}\mathrm{E}[\mathbf{P}_{source}]]\mathbf{U}_Q \tag{6.5}$$

$$\mathbf{c}_K = \mathbf{U}_K. \tag{6.6}$$

The expected voltage magnitudes along the distribution feeder can be expressed from (5.9) as

$$\begin{aligned}\mathrm{E}[|\tilde{\mathbf{V}}|] \approx{}& \mathbf{V}_0 + \mathbf{V}_P(\mathbf{H}\mathrm{E}[\mathbf{P}_{source}] - \mathbf{P}_{inv0}) - \mathbf{V}_Q\mathbf{Q}_{inv0} - \mathbf{V}_K\mathbf{K}_0 \\ &+ \mathbf{V}_Q\boldsymbol{\alpha} + \mathbf{V}_Q\,\mathrm{diag}[\mathbf{H}\mathrm{E}[\mathbf{P}_{source}]]\boldsymbol{\beta} + \mathbf{V}_K\mathbf{K} \\ ={}& \mathbf{N}_0 + \mathbf{N}_\alpha\boldsymbol{\alpha} + \mathbf{N}_\beta\boldsymbol{\beta} + \mathbf{N}_K\mathbf{K},\end{aligned} \tag{6.7}$$

where

$$\mathbf{N}_0 = \mathbf{V}_0 + \mathbf{V}_P(\mathbf{H}\mathrm{E}[\mathbf{P}_{source}] - \mathbf{P}_{inv0}) - \mathbf{V}_Q\mathbf{Q}_{inv0} - \mathbf{V}_K\mathbf{K}_0 \tag{6.8}$$

$$\mathbf{N}_\alpha = \mathbf{V}_Q \tag{6.9}$$

$$\mathbf{N}_\beta = \mathbf{V}_Q\,\mathrm{diag}[\mathbf{H}\mathrm{E}[\mathbf{P}_{source}]] \tag{6.10}$$

$$\mathbf{N}_K = \mathbf{V}_K. \tag{6.11}$$

In order to explore the influence of the spatial correlation among the PV source powers, the covariance matrix among the PV source powers is considered when expressing the variance of the voltage magnitudes [100]. Accordingly, the source powers are assumed to be distributed dependently over the interval of interest, and the variance of the voltage magnitudes can be expressed from (5.9) as[2]

$$\mathrm{Var}[|\tilde{\mathbf{V}}|] \approx (\mathbf{V}_P\mathbf{H} + \mathbf{V}_Q\,\mathrm{diag}(\boldsymbol{\beta})\mathbf{H})\,\mathrm{Cov}[\mathbf{P}_{source}](\mathbf{V}_P\mathbf{H} + \mathbf{V}_Q\,\mathrm{diag}(\boldsymbol{\beta})\mathbf{H})^{\mathrm{T}}, \tag{6.12}$$

where $\mathrm{Cov}[\mathbf{P}_{source}]$ is the covariance matrix among PV source powers, and the standard deviation can be written as

[2]Cov is the covariance operator.

$$(\mathrm{Var}[|\tilde{\mathbf{V}}|])^{\circ\frac{1}{2}} \approx ((((\mathbf{V}_P\mathbf{H}+\mathbf{V}_Q\,\mathrm{diag}[\boldsymbol{\beta}]\mathbf{H})\,\mathrm{Cov}[\mathbf{P}_{source}](\mathbf{V}_P\mathbf{H}+\mathbf{V}_Q\,\mathrm{diag}[\boldsymbol{\beta}]\mathbf{H})^{\mathrm{T}})\circ\mathbf{I}_{N_{node}})$$
$$\circ\mathbf{1}_{N_{node}\times 1})^{\circ\frac{1}{2}}. \tag{6.13}$$

The standard deviation can be further approximated using a Taylor series around a previous estimate of $\boldsymbol{\beta}$ (i.e., $\boldsymbol{\beta}_0$):

$$\begin{aligned}(\mathrm{Var}[|\mathbf{V}|])^{\circ\frac{1}{2}} \approx{}& ((((\mathbf{V}_P\mathbf{H}+\mathbf{V}_Q\,\mathrm{diag}[\boldsymbol{\beta}_0]\mathbf{H})\,\mathrm{Cov}[\mathbf{P}_{source}](\mathbf{V}_P\mathbf{H}+\mathbf{V}_Q\,\mathrm{diag}[\boldsymbol{\beta}]\mathbf{H})^{\mathrm{T}})\circ\mathbf{I}_{N_{node}})\\
&\circ\mathbf{1}_{N_{node}\times 1})^{\circ\frac{1}{2}}+\frac{1}{2}((\mathbf{V}_P\mathbf{H}\,\mathrm{Cov}[\mathbf{P}_{source}]\mathbf{H}^{\mathrm{T}}\circ\mathbf{V}_Q+(\mathbf{H}\,\mathrm{Cov}[\mathbf{P}_{source}]\mathbf{H}^{\mathrm{T}}\mathbf{V}_P^{\mathrm{T}})^{\mathrm{T}}\circ\mathbf{V}_Q\\
&+(\mathbf{H}\,\mathrm{Cov}[\mathbf{P}_{source}]\mathbf{H}^{\mathrm{T}}(\mathbf{V}_Q\,\mathrm{diag}[\boldsymbol{\beta}_0])^{\mathrm{T}})^{\mathrm{T}}2\circ\mathbf{V}_Q)\circ((((((\mathbf{V}_P\mathbf{H}+\mathbf{V}_Q\,\mathrm{diag}[\boldsymbol{\beta}_0]\mathbf{H})\\
&\cdot\mathrm{Cov}[\mathbf{P}_{source}](\mathbf{V}_P\mathbf{H}+\mathbf{V}_Q\,\mathrm{diag}[\boldsymbol{\beta}_0]\mathbf{H})^{\mathrm{T}})\circ\mathbf{I}_{N_{node}})\circ\mathbf{1}_{N_{node}\times 1})^{\circ\frac{1}{2}}\mathbf{1}_{1\times N_{inv}})^{\circ(-1)}))\\
&\cdot(\boldsymbol{\beta}-\boldsymbol{\beta}_0)\\
={}&\mathbf{M}_0+\mathbf{M}_\beta\boldsymbol{\beta},\end{aligned} \tag{6.14}$$

where

$$\begin{aligned}\mathbf{M}_0 ={}& ((((\mathbf{V}_P\mathbf{H}+\mathbf{V}_Q\,\mathrm{diag}[\boldsymbol{\beta}_0]\mathbf{H})\,\mathrm{Cov}[\mathbf{P}_{source}](\mathbf{V}_P\mathbf{H}+\mathbf{V}_Q\,\mathrm{diag}[\boldsymbol{\beta}]\mathbf{H})^{\mathrm{T}})\circ\mathbf{I}_{N_{node}})\circ\mathbf{1}_{N_{node}\times 1})^{\circ\frac{1}{2}}\\
&-\frac{1}{2}((\mathbf{V}_P\mathbf{H}\,\mathrm{Cov}[\mathbf{P}_{source}]\mathbf{H}^{\mathrm{T}}\circ\mathbf{V}_Q+(\mathbf{H}\,\mathrm{Cov}[\mathbf{P}_{source}]\mathbf{H}^{\mathrm{T}}\mathbf{V}_P^{\mathrm{T}})^{\mathrm{T}}\circ\mathbf{V}_Q+(\mathbf{H}\,\mathrm{Cov}[\mathbf{P}_{source}]\mathbf{H}^{\mathrm{T}}\\
&\cdot(\mathbf{V}_Q\,\mathrm{diag}[\boldsymbol{\beta}_0])^{\mathrm{T}})^{\mathrm{T}}2\circ\mathbf{V}_Q)\circ((((((\mathbf{V}_P\mathbf{H}+\mathbf{V}_Q\,\mathrm{diag}[\boldsymbol{\beta}_0]\mathbf{H})\,\mathrm{Cov}[\mathbf{P}_{source}](\mathbf{V}_P\mathbf{H}+\mathbf{V}_Q\\
&\cdot\mathrm{diag}[\boldsymbol{\beta}_0]\mathbf{H})^{\mathrm{T}})\circ\mathbf{I}_{N_{node}})\circ\mathbf{1}_{N_{node}\times 1})^{\circ\frac{1}{2}}\mathbf{1}_{1\times N_{inv}})^{\circ(-1)})\boldsymbol{\beta}_0\end{aligned} \tag{6.15}$$

$$\begin{aligned}\mathbf{M}_\beta ={}&\frac{1}{2}((\mathbf{V}_P\mathbf{H}\,\mathrm{Cov}[\mathbf{P}_{source}]\mathbf{H}^{\mathrm{T}}\circ\mathbf{V}_Q+(\mathbf{H}\,\mathrm{Cov}[\mathbf{P}_{source}]\mathbf{H}^{\mathrm{T}}\mathbf{V}_P^{\mathrm{T}})^{\mathrm{T}}\circ\mathbf{V}_Q+(\mathbf{H}\,\mathrm{Cov}[\mathbf{P}_{source}]\mathbf{H}^{\mathrm{T}}\\
&\cdot(\mathbf{V}_Q\,\mathrm{diag}[\boldsymbol{\beta}_0])^{\mathrm{T}})^{\mathrm{T}}2\circ\mathbf{V}_Q)\circ((((((\mathbf{V}_P\mathbf{H}+\mathbf{V}_Q\,\mathrm{diag}[\boldsymbol{\beta}_0]\mathbf{H})\,\mathrm{Cov}[\mathbf{P}_{source}](\mathbf{V}_P\mathbf{H}+\mathbf{V}_Q\\
&\cdot\mathrm{diag}[\boldsymbol{\beta}_0]\mathbf{H})^{\mathrm{T}})\circ\mathbf{I}_{N_{node}})\circ\mathbf{1}_{N_{node}\times 1})^{\circ\frac{1}{2}}\mathbf{1}_{1\times N_{inv}})^{\circ(-1)}))\end{aligned} \tag{6.16}$$

If the node voltage magnitudes are assumed to be normally distributed over the interval of interest, the probability constraints in (6.1), which are equivalent to

$$\Pr[|\tilde{V}_i|\le V_{min}]\le p_{max} \tag{6.17}$$

$$\Pr[|\tilde{V}_i|\le V_{max}]\ge 1-p_{max}, \tag{6.18}$$

can be expressed as

$$\Phi\left(\frac{V_{min}-\mathrm{E}[|\tilde{V}_i|]}{\sqrt{\mathrm{Var}[|\tilde{V}_i|]}}\right) \leq p_{max} \tag{6.19}$$

$$\Phi\left(\frac{V_{max}-\mathrm{E}[|\tilde{V}_i|]}{\sqrt{\mathrm{Var}[|\tilde{V}_i|]}}\right) \geq 1-p_{max}, \tag{6.20}$$

where $\Phi(\cdot)$ is the cumulative distribution function of the standard normal distribution. By substitution of (6.7) and (6.14), these constraints $\forall i \in \{1,2,\ldots,N_{node}\}$ can be expressed as

$$\mathbf{V}_{min}-(\mathbf{N}_0+\mathbf{N}_\alpha\boldsymbol{\alpha}+\mathbf{N}_\beta\boldsymbol{\beta}+\mathbf{N}_K\mathbf{K}) \leq \Phi^{-1}(p_{max})(\mathbf{M}_0+\mathbf{M}_\beta\boldsymbol{\beta}), \tag{6.21}$$

$$\mathbf{V}_{max}-(\mathbf{N}_0+\mathbf{N}_\alpha\boldsymbol{\alpha}+\mathbf{N}_\beta\boldsymbol{\beta}+\mathbf{N}_K\mathbf{K}) \geq \Phi^{-1}(1-p_{max})(\mathbf{M}_0+\mathbf{M}_\beta\boldsymbol{\beta}), \tag{6.22}$$

where $\mathbf{V}_{min}=V_{min}\mathbf{1}_{N_{node}\times 1}$ and $\mathbf{V}_{max}=V_{max}\mathbf{1}_{N_{node}\times 1}$. The approximation in (6.14) is only valid for $\boldsymbol{\beta}$ sufficiently close to $\boldsymbol{\beta}_0$. Specifically, an additional constraint is introduced to ensure that the approximate standard deviation is non negative:

$$\mathbf{0} \leq \mathbf{M}_0+\mathbf{M}_\beta\boldsymbol{\beta} \leq \boldsymbol{\sigma}_{max}, \tag{6.23}$$

The maximum expected reactive power being injected by each inverter phase is limited by the apparent power limits of the inverter phase:

$$-(\mathbf{S}_{max}^{\circ 2}-\mathbf{P}_{inv0}^{\circ 2})^{\circ\frac{1}{2}} \leq (\boldsymbol{\alpha}+\boldsymbol{\beta}\circ\mathbf{P}_{inv0}) \leq (\mathbf{S}_{max}^{\circ 2}-\mathbf{P}_{inv0}^{\circ 2})^{\circ\frac{1}{2}}, \tag{6.24}$$

By combining (6.2) and (6.21)–(6.24), the solution to the optimization problem in (6.1) can be approximated by the solution of a linear programming problem of the form

$$\begin{aligned} \min_{\mathbf{x}} \quad & \mathbf{c}^{\mathrm{T}}\mathbf{x} \\ \text{subject to} \quad & \mathbf{A}\mathbf{x} \leq \mathbf{b} \\ & \mathbf{x}_{min} \leq \mathbf{x} \leq \mathbf{x}_{max}, \end{aligned} \tag{6.25}$$

where $\mathbf{x}=[\boldsymbol{\alpha}^{\mathrm{T}}\ \boldsymbol{\beta}^{\mathrm{T}}\ \mathbf{K}^{\mathrm{T}}]^{\mathrm{T}}$, $\mathbf{c}=[\mathbf{c}_\alpha^{\mathrm{T}}\ \mathbf{c}_\beta^{\mathrm{T}}\ \mathbf{c}_K^{\mathrm{T}}]^{\mathrm{T}}$, and

$$\mathbf{A} = \begin{bmatrix} -\mathbf{N}_\alpha & -(\mathbf{N}_\beta + \Phi^{-1}(p_{max})\mathbf{M}_\beta) & -\mathbf{N}_K \\ \mathbf{N}_\alpha & \mathbf{N}_\beta + \Phi^{-1}(1-p_{max})\mathbf{M}_\beta & -\mathbf{N}_K \\ \mathbf{0}_{3N_{node}\times N_{inv}} & -\mathbf{M}_\beta & \mathbf{0}_{3N_{node}\times N_t} \\ \mathbf{0}_{3N_{node}\times N_{inv}} & \mathbf{M}_\beta & \mathbf{0}_{3N_{node}\times N_t} \\ \mathbf{I}_{N_{inv}} & \text{diag}[\mathbf{P}_{inv0}] & \mathbf{0}_{N_{inv}\times N_t} \\ -\mathbf{I}_{N_{inv}} & -\text{diag}[\mathbf{P}_{inv0}] & \mathbf{0}_{N_{inv}\times N_t} \end{bmatrix}$$

$$\mathbf{b} = \begin{bmatrix} \Phi^{-1}(p_{max})\mathbf{M}_0 - \mathbf{V}_{min} + \mathbf{N}_0 \\ -\Phi^{-1}(1-p_{max})\mathbf{M}_0 + \mathbf{V}_{min} - \mathbf{N}_0 \\ \mathbf{M}_0 \\ \boldsymbol{\sigma}_{max} - \mathbf{M}_0 \\ (\mathbf{S}_{max}^{\circ 2} - \mathbf{P}_{inv0}^{\circ 2})^{\circ \frac{1}{2}} \\ (\mathbf{S}_{max}^{\circ 2} - \mathbf{P}_{inv0}^{\circ 2})^{\circ \frac{1}{2}} \end{bmatrix},$$

where $\mathbf{0}_{m\times n}$ is the $m \times n$ matrix filled with zero. The algorithm that describes the scenario of finding optimal solutions for the optimization problem given in (6.1) is mentioned in 5.3.

6.4 Test System Description

To examine the performance of the proposed volt-var control, six methods, based on unbalanced three-phase distribution test system, are studied, by using the modified IEEE 123-node radial distribution test feeder [87]. The test feeder is described in Figure 3.2. This test system used herein has a nominal voltage of 4.16 kV and consists of 123 nodes. It also has unbalanced loads, and four voltage regulators for voltage control between Nodes 150 and 149, 9 and 14, 25 and 26, and 160 and 67. In this study, ten three-phase four wire PV inverters are connected to nodes 1, 7, 8, 13, 18, 52, 53, 54, 55, and 56. Their

locations are based on a previous study [71] that showed inverters situated in these locations with spatially correlated irradiance can cause significant voltage fluctuations. The PV inverters injected at specified nodes can adjust the fixed and variable reactive power output for each phase independently. The rated solar power of all PV inverters is 300 kW. For the power generation of these PV inverters, one-second global horizontal irradiance data collected by the National Renewable Energy Laboratory Solar Measurement Grid in Oahu, Hawaii is used herein [88]. The solar irradiance data sources are measured based on ten irradiance sensors placed in different locations (e.g., DH1–DH10). In particular, the active power output of each inverter is proportional to the irradiance with rated power output at an irradiance of 1500 W/m^2. For the study proposed herein, irradiance data from 5:00 AM to 7:00 PM on 22 July 2010 is used. During this period, the active power injection varies significantly, exhibiting high variance and spatial correlation between nearby PV sources. The system loading is based on the load observed by the Electric Reliability Council of Texas [95] over the same period. The load data is normalized such that the peak load during the period corresponds to maximum system load. The load at each node is updated every 15 minutes. The total load and PV power generation are illustrated in Figure 5.2 for a 14-hour period. In this study, suitable PV generation forecast methodologies are assumed to be applied [90,96,97]. The expected values and variances of the PV sources are assumed to be known in advance over the next period of interest, but the moment-by-moment source power injections are not assumed to be known in advance.

OpenDSS is used to perform power flow calculations [98]. The voltage magnitude limits of all nodes are assumed to be 118–126 V on a base of a 120-V scale [26]. When performing optimization, the maximum acceptable probability of voltage magnitude violations during the optimization interval p_{max} of 5% is used. When assessing the results, the range of acceptable voltage magnitudes is slightly expanded to 117.9995–126.0005 V to avoid penalizing methods for extremely small deviations (e.g., due to non-normal distributions).

In order to examine the proposed method, six different methods are considered. In first method, the baseline method (BM), the voltage regulator tap settings $\mathbf{K}$ are only adjusted, and the fixed and variable reactive power output of the PV inverters are zero (i.e., $\boldsymbol{\alpha} = \boldsymbol{\beta} = \mathbf{0}$). In this optimization problem, the tap settings are adjusted every 15 minutes to minimize system losses while maintaining expected voltage magnitudes within acceptable limits, and the variability of the PV source power output injections is not considered. For the rest of the methods, the voltage regulator tap settings $\mathbf{K}$ and the inverter fixed and variable reactive power outputs ($\boldsymbol{\alpha}$ and $\boldsymbol{\beta}$) are adjusted every 15 minutes. In the second method, the dynamic method (DM), the expected losses are minimized over 15-minute intervals subject to the constraint that the expected voltage magnitudes are within the acceptable range of $[V_{min}, V_{max}]$ and the maximum expected reactive power is within the apparent power limits of the inverter phase. The variability of the PV source power injections is not considered in this optimization problem. When the variable reactive power output is considered, it is determined in a second layer based on minimizing the sensitivity of the local voltage magnitudes to fluctuations in active power injection [71], which corresponds to the dual-layer approach proposed in [75]. As in [75], 20% of the reactive power capability is reserved in the first layer for use in the second layer. For the third method, the integrated method (IM), (6.1) is solved over 15-minute intervals with considering the variability of the PV source power injections. For the fourth method, the limited integrated method (LIM), (6.1) is solved over 15-minute intervals, by considering the variability of the PV source power injections and limiting the variation of voltage magnitudes. For the fifth method, the correlated integrated method (CIM),which is the method presented herein, (6.1) is solved over 15-minute intervals, by considering the spatial correlations among the PV source powers. For the sixth method, the limited correlated integrated method (LCIM), (6.1) is solved over 15-minute intervals, by considering the spatial correlations among the PV source powers and limiting the variation of voltage magnitudes.

6.5 Simulation Results and Discussion

The six methods are simulated over the scenario mentioned above, and the simulation results are reported in Table 6.1. For each method, the total number of violated node phases (i.e., nodes with phase voltage magnitudes outside of the acceptable range) is recorded. Also, the total time in which any violation is experienced in the system is observed. For each node phase, two voltage violation percentages are calculated: one for voltage magnitude over the acceptable limit, and the other for voltage magnitude under the acceptable limit. The largest of these violation percentages across the system is presented. Mean loss is determined using power calculated every second over the 14-hour period. All methods operate on a 15-minute interval, so the worst-case violations in any 15-minute interval are also considered for these methods. The worst-case violation percentage is the violation percentage during the worst 15-minute interval for a given method. The node phase experiencing this worst-case violation is also recorded.

The voltage magnitude variation can be constrained based on the desirable standard deviation of the voltage magnitudes in (6.23). This efficient constraint helps the proposed method to match assumptions made in this work and mitigate the impact of non-normal distributions on the proposed method. In order to evaluate the performance of the proposed method in terms of the voltage magnitude variation, all methods are studied to understand the performance of these methods on the distribution voltage magnitude variations. All methods are compared with each other and evaluated on their performance based on several metrics. The metrics are described as follows. The mean violation time is the average of the violation time for all nodes experienced a voltage magnitude outside of the acceptable limits during the case. The voltage magnitude violation indicates each node phase voltage magnitude is over the acceptable limit, a certain fraction of the voltage magnitude during the case, and under the acceptable limit, a certain fraction of the voltage magnitude. The mean voltage magnitude violation is the mean of the aforementioned fraction. The largest

Table 6.1: Simulation results for all methods

method	Violated node phases	Violation time (s)	Violation percentage (%)	Mean loss (kW)	Worst-case 15-min violation percentage (%)	Worst-case violated node phase
BM	49	8516	7	44.82	62	104 *c*-phase
DM	2	900	1.63	41.10	66	104 *c*-phase
IM	3	1683	2.47	40.81	32	114 *a*-phase
LIM	4	738	1.06	40.84	16.45	114 *a*-phase
CIM	5	515	0.47	40.82	8	114 *a*-phase
LCIM	1	60	0.12	40.83	4.4	114 *a*-phase

such fraction is the maximum voltage magnitude violation. The standard deviation of the voltage magnitudes of Node i over the time interval m is used and defined below

$$\sigma_{im} = \sqrt{\frac{1}{T_{in}} \sum_{t=1}^{T_{in}} (|\tilde{\mathbf{V}}_{im}(t)| - |\tilde{\mathbf{V}}^{\star}_{im}|)^2}, \tag{6.26}$$

where $|\tilde{\mathbf{V}}^{\star}_{im}|$ is the mean of the voltage magnitudes of Node i during the time interval m, $i \in \{1,2,...,N_{node}\}$, $t \in \{1,2,...,T_{in}\}$ and T_{in} is the time interval, and $m = \{1,2,...,M\}$ and M is the total number of the time interval over the interval of interest. The standard deviation of the voltage magnitudes each time interval can be expressed as

$$\sigma_m = \sqrt{\frac{1}{N_{node}} \sum_{i=1}^{N_{node}} \sigma^2_{im}}. \tag{6.27}$$

The maximum standard deviation over the interval of interest is given by

$$\max_{m \in M} \max_{i \in \{1,2,...,N_{node}\}} \sigma_{im}, \tag{6.28}$$

where $\sigma_{im} \in \mathbb{R}^M_+$ is a standard deviation of the voltage magnitudes over the time interval m, and the average standard deviation over the interval of interest is given by

$$\frac{1}{M} \sum_{m=1}^{M} \sigma_m. \tag{6.29}$$

As it can be seen in Table 6.1, the BM failed to maintain the overall violation percentages within the acceptable range because the violation percentage is larger than $p_{max} = 5\%$.

Also, the voltage magnitudes drift outside of the acceptable range for larger periods of time than the other methods as seen in Figure 6.1 (a). Table 6.1 also shows that the DM is more effective than the BM in reducing both voltage magnitude violations and system losses. This is expected because the DM makes its decision every 15 minutes, but it uses the inverter fixed and variable reactive power outputs ($\boldsymbol{\alpha}$ and $\boldsymbol{\beta}$) to improve system performance, compared with a single decision being made by the BM (i.e., $\mathbf{K}$). However, the DM is somewhat conservative with respect to loss minimization because of the reserved capability of PV inverters. The lack of coordination between the two layers in the DM causes the voltage magnitudes to have unacceptable 15-minute intervals and be less smooth during the interval of interest as shown in Figure 6.1 (b) compared with the LCIM.

The IM also makes its decision every 15 minutes and uses the inverter fixed and variable reactive power outputs ($\boldsymbol{\alpha}$ and $\boldsymbol{\beta}$) to improve system performance, but it formulates voltage magnitude limits as chance constraints. From Table 6.1, the IM is obviously more capable of reducing system losses, albeit the IM is less capable than the DM in reducing voltage magnitude violations. This is expected because the IM formulates the voltage magnitude limits as chance constraints to reduce system losses. In order to mitigate the impact of non-normal distribution of irradiance data used herein, the variation of the voltage magnitudes is limited in the IM (i.e., the LIM). Consequently, as noticed in Table 6.1, the performance of the IM is relatively improved in terms of violation time, violation percentage, and the unacceptable 15-minute interval. However, there is a trade off between limiting the variation of the voltage magnitudes, which also restricts chance constraints, and reducing system losses as noticed in Table 6.1. Another observation that can be made from Table 6.1 is that the IM still experiences unacceptable 15-minute intervals due to non-linearity, non-normal distributions, and the spatial correlations among PV sources. Consequently, the main advantage obtained using the LIM is that, in addition to improving the system performance, the LIM has less voltage magnitude variability than the IM in most of the interval of interest as seen in Figure 6.1 (c).

The CIM is the method proposed herein in this chapter. It also makes its decision every 15 minutes and formulates voltage magnitude limits as chance constraints, but it considers spatial correlations among the PV sources. The simulation results in Table 6.1 indicate that the performance of the CIM to match assumptions is sufficiently higher than the aforementioned methods. As seen in Table 6.1, the CIM results in a lower period of time in which at least one node phase experiences an unacceptable voltage magnitude with more reduction of the overall violation percentage. Table 6.1 also indicates that the severity of the worst-case 15-minute violation percentages for the CIM is less than that of others, but it still experiences unacceptable 15-minute intervals. This is expected because of non-normal distribution of irradiance data. Although the CIM is also effective in reducing mean loss with respect to the BM, the CIM still is somewhat more conservative with respect to loss minimization than the IM (0.022% more). The LCIM is also shown in Table 6.1. In the CIM, the variation of the voltage magnitudes is also limited to mitigate the impact of a non-normal distribution of irradiance data (i.e., the LCIM). Therefore, as seen in Table 6.1, the LCIM results in less node phase having voltage magnitude violations than the other methods, and a lower period of time in which at least one node phase experiences an unacceptable voltage magnitude with also more reduction of the overall violation percentage. Another observation that can be made from these results is that the worst-case 15-minute violation percentage for the LCIM is less than $p_{max} = 5\%$. The results also show that the LCIM has slightly worse losses than the CIM (0.022% more with respect to the BM). This is expected due to limiting the variability of the voltage magnitudes that somewhat makes the LCIM conservative in loss reduction. The overall conclusion is that the simulation results in Table 6.1 indicate that the performance improvement of the LCIM to match assumptions has been observed in both voltage magnitude violations and the worst-case 15-minute violation percentage. Also, it can be noticed from Figure 6.1 (d) that the LCIM has smoother voltage magnitudes than the CIM in most of the interval of interest.

The performance of all the methods during the interval of interest to mitigate a voltage

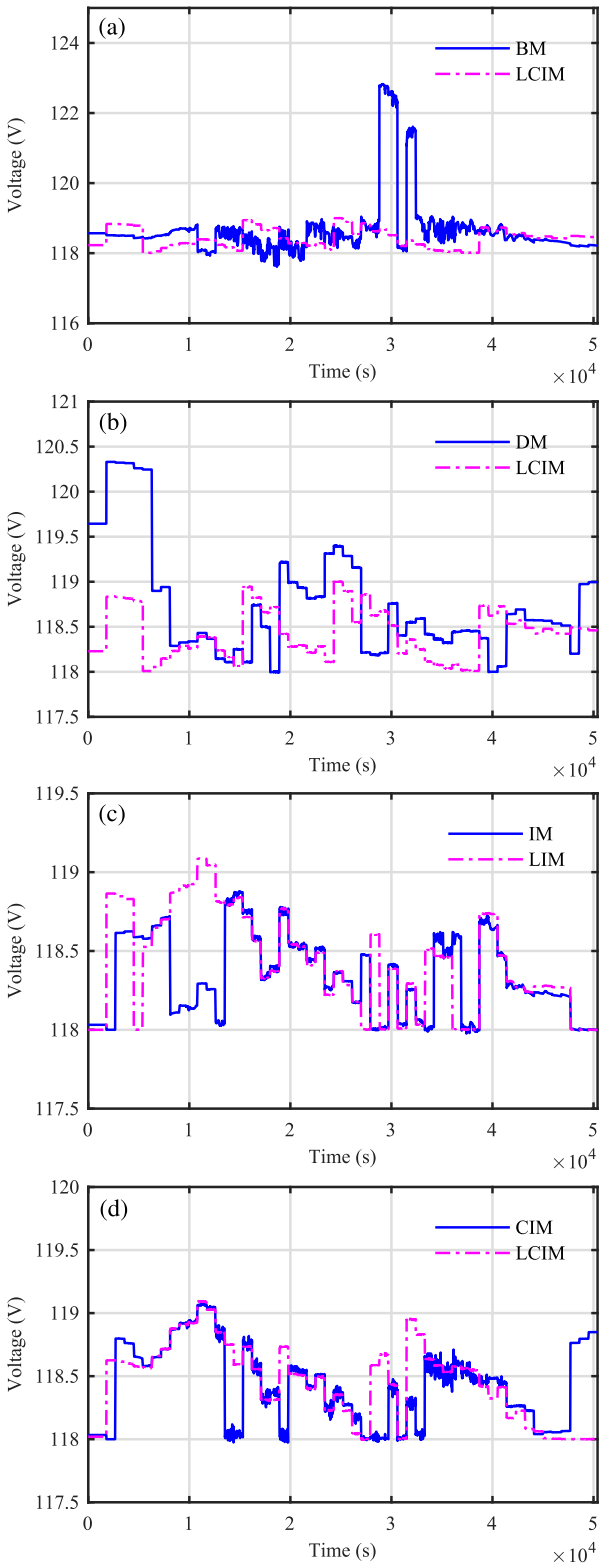

Figure 6.1: (a) Node 104 *c*-phase voltage magnitude for BM and LCIM, (b) Node 104 *c*-phase voltage magnitude for the DM and LCIM, (c) Node 114 *a*-phase voltage magnitude for the IM and LIM, and (d) Node 114 *a*-phase voltage magnitude for the CIM and LCIM.

Table 6.2: Simulation results for voltage magnitude violations

method	Mean violation time (s)	Mean violation (mV)	Maximum violation (mV)	Mean standard deviation (mV)	Maximum standard deviation (mV)
BM	118	225×10^{-3}	499	89.5	259.8
DM	3.3	1.65×10^{-4}	7.3	1.4	4.3
IM	6.12	4.6×10^{-4}	23.5	4.7	12.83
LIM	2.68	8.1×10^{-5}	7.15	1.67	3.92
CIM	2.04	3.1×10^{-4}	45	12.61	42.5
LCIM	0.22	1.26×10^{-5}	9.6	2.22	3.67

variation is shown in Table 6.2. In terms of mean violation time, the LCIM is successful in reducing the overall mean violation time. Also, the Table 6.2 indicates that the LCIM has the best improvement in a mean voltage magnitude violation. Furthermore, it matches the desirable constraint of standard deviations of the voltage magnitudes during the interval of interest (e.g., σ_{max} = 3.5 mV on a base of 120-V scale chosen based on the best reduction in the system loss and improvement in the voltage magnitude profile for the LCIM and LIM).

To study the behavior of the LCIM and LIM in this chapter further, the worst-case 15-min standard deviation of voltage magnitude resulting at the *a* phase of Node 114 for CIM and IM is shown as an example in Figure 6.2 compared with the LCIM and LIM. As seen in Figure 6.2 (a) and (b) that without limiting the standard deviation of the voltage magnitude over the interval of interest, the CIM and IM experience more observable voltage magnitude variations than the LCIM and LIM. As a result, limiting the standard deviation of the voltage magnitude over the interval of interest helps to mitigate the voltage magnitude violation and improve the voltage magnitude profile of all system nodes.

The rapid fluctuation in PV output powers results in an excessive number of tap change operations of voltage regulators. While the main goal of the proposed method is not to reduce tap change operations, this efficient strategy used herein helps to reduce that. The control strategy adjusts the voltage regulators infrequently (i.e., at most every 15 minutes

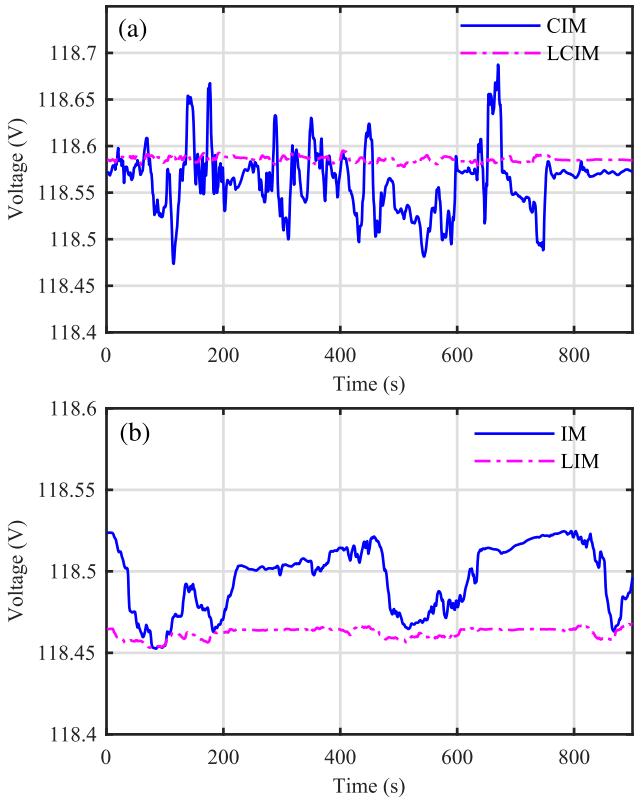

Figure 6.2: The worst 15-minute standard deviation of voltage magnitude of Node 114 *a*-phase voltage magnitude for the CIM and LCIM in (a) and for the IM and LIM in (b).

over the 14-hour period) and the solution method in Figure 5.1 begins its search for each interval from the solution for the previous interval. To study the effectiveness of the LCIM in terms of a tap change operation reduction, the total number of tap changing operations of all methods over the 14-hour period are shown in Table 6.3. Also, the tap settings of one of the voltage regulators using the CIM and LCIM is shown in Figure 6.3. Figure 6.3 (b) shows that constraining the voltage magnitude variations helps to adjust tap change operations relatively infrequently compared with Figure 6.3 (a) during the course of the day in order to improve losses, enhance the voltage profiles, and maintain voltages in response to changing load and PV injections. As a result, the LCIM has fewer tap change operations in comparison with the other methods as shown in Table 6.3.

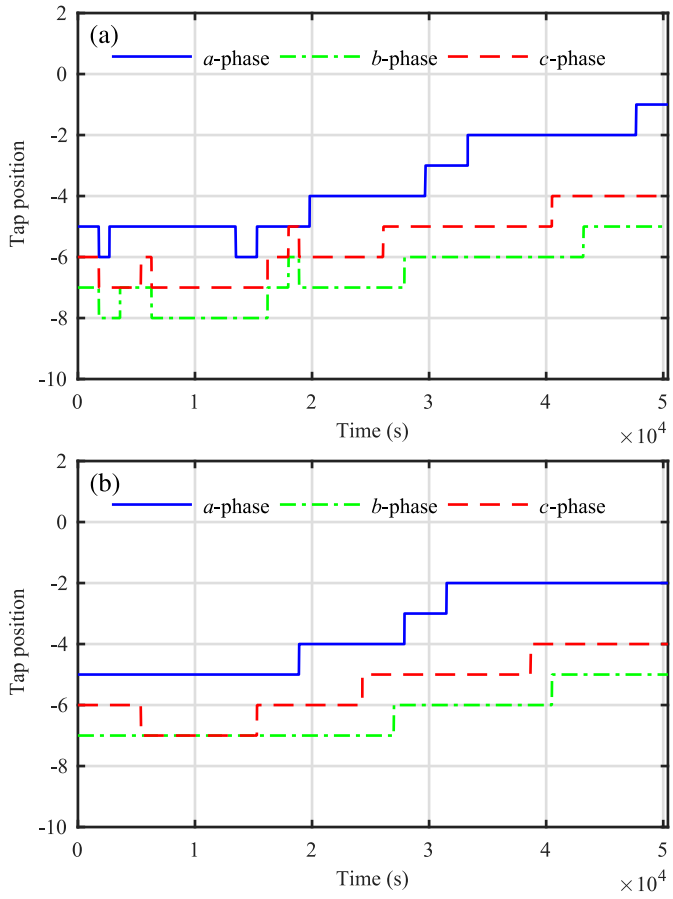

Figure 6.3: Tap positions for the voltage regulator connected to Node 160 for the CIM in (a) and for the LCIM in (b).

Table 6.3: Total number of tap change operations of all methods over the interval of interest

Voltage regulators (V.R)	Phase	Method					
		BM	DM	IM	LIM	CIM	LCIM
$V.R_{150-149}$	*abc*	2	3	1	1	1	1
$V.R_{9-14}$	*a*	3	6	1	2	1	1
$V.R_{25-26}$	*a*	4	6	5	11	6	4
	c	5	4	3	3	2	2
$V.R_{160-67}$	*a*	7	14	11	10	8	3
	b	6	8	4	4	8	2
	c	7	11	6	8	8	4
Total number of tap changes		34	52	31	39	34	17

6.6 Conclusion

A correlated integrated method that is formulated as a mixed-integer, nonlinear, chance-constrained optimization problem is proposed to optimize the expected performance of a distribution system. It optimizes this performance while considering the spatial correlation among PV sources, maintaining acceptable system voltage magnitudes, and considering the uncertainty of PV power injections. The proposed method uses both the PV inverter capability to inject or absorb a reactive power and the voltage control equipment to minimize the system losses, mitigate voltage magnitude fluctuations, improve voltage magnitude profiles, and indirectly reduce tap operations of voltage regulators. The proposed method formulated the voltage magnitude requirements as chance constraints. The performance is assessed using IEEE 123-node radial distribution test feeder under load and irradiance changing, and more thoroughly by the consideration of longer periods of time and comparison with existing methods. The final results demonstrated that the proposed method can effectively improve the system performance of distribution systems with PV sources.

Chapter 7

Conclusion and Future Work

7.1 Conclusion

In this dissertation, several volt-var control methods using voltage and reactive power control equipment are proposed to provide applicable solutions to mitigate the adverse effects that DGs might have. In Chapter 3, a method of achieving optimal expected performance while maintaining appropriate system voltage magnitudes is proposed. Specifically, this technique is used to optimize only the reactive power output of DGs to improve expected system performance (i.e., the operating profit) and to compensate for variations in active power injections during an upcoming interval. Three different cases are studied to understand the performance of the proposed method under various conditions (i.e., the cloudy case, sunny case, and transient case). Each of these cases represents a 15-minute interval over which the operation of traditional voltage regulation equipment (i.e., capacitor banks and voltage regulators) is considered fixed. The proposed chance-constrained optimization (CCO) method is examined against three other methods. The baseline method involves the inverters only providing active power without any reactive power. The local voltage control (LVC) method involves using a volt-var control to maintain the system voltage magnitudes within acceptable limits and coordinates the injecting or the absorbing of reactive power among several distributed generators with a piecewise linear droop characteristic. The global violation unbalanced (GVU) method is formulated to inject independent reac-

tive powers based on real power injections into each phase to mitigate voltage violations. The CCO is compared to baseline, LVC, and GVU methods on the IEEE 123-node radial distribution feeder under various generation conditions. Three cases were considered, corresponding to cloudy, sunny, and transient conditions. The results showed that in each of these cases, the CCO method is able to improve the average operating profit over the other methods while maintaining acceptable voltage magnitudes and reducing distribution system losses. When performance of the proposed method is examined in terms of sensitivity to the distribution assumptions made in this chapter, the results showed that the CCO method is not highly sensitive to these assumptions.

In Chapter 4, the integrated chance-constrained optimization (ICCO) is proposed. The ICCO combines the conventional voltage control equipment (e.g., voltage regulators) and the capability of PV inverters to inject reactive power along with active power to maximize the expected value of a figure of merit (i.e., the operating profit) while constraining the probability of unacceptable voltage magnitudes. The ICCO uses short-term forecasts that include the expected mean and variance of the active power injection and expected load and formulates the voltage magnitude requirements as chance constraints. The optimal voltage regulator tap settings and PV inverter reactive parameters can be transmitted periodically from a centralized control center (e.g., every 15 minutes) via local communication channels. The ICCO method is examined against three other methods. The baseline method involves the PV inverters only providing active power without reactive power. The CCO method seeks to find optimal expected performance with respect to a figure of merit of interest while maintaining appropriate system voltage magnitudes without considering the optimal voltage regulator tap settings. The dual global violation unbalanced (DGVU) method involves calculating the optimal control settings in the first layer (e.g., voltage regulation tap settings and reference reactive power of PV inverters), and they are kept constant for the second layer. In the second layer, PV inverter reactive power is used to mitigate voltage variations. The ICCO is compared to baseline, CCO, and DGVU methods on the

IEEE 123-node radial distribution feeder under various generation conditions. Using the same three cases mentioned above, the results showed that the ICCO method was effective in both improving performance with respect to the figure of merit and constraining the probability of voltage magnitude violations.

In Chapter 5, a supervisory volt-var control method focusing on system optimization is proposed. The proposed method is addressing a figure of merit of interest to the distribution system operator (e.g., system loss) while constraining the probability of unacceptable voltage magnitudes occurring during the interval of interest. The proposed method performs this control by adjusting parameters associated with the fixed and variable reactive power produced by the inverter and the voltage regulator tap settings, by formulating chance constraints on the voltage magnitudes. The proposed method includes an enhanced solution algorithm to the mixed-integer problem that accounts for the discrete nature of voltage regulator tap settings and accelerates the process of finding initial feasible points. The performance of the proposed method is also evaluated more thoroughly by consideration of longer periods of time, and, by comparison, with existing methods. Although the proposed method does not explicitly seek to reduce the number of tap change operations, the proposed control method uses an efficient approach to limit the number of tap change operations indirectly. The strategy used herein helps the voltage regulators to be infrequently adjusted (i.e., every 15 minutes over the 14-hour period) and proposes restarting the algorithm from the previous solution, helping with reducing tap change operations as well. This volt-var control strategy also requires both infrequent communication with the distribution system operator and infrequent changes to voltage regulator settings. However, it can respond to rapidly changing conditions by providing control parameters to the inverters to allow them to respond to such changes in real time, a capability that is available in smart inverters. In order to examine the proposed method, three different methods that control the variable and fixed reactive power output of the DG inverters and the voltage regulator tap settings are considered. These methods are mainly defined by static method, dynamic

method, and integrated method. Each of these methods involves three versions which vary based on which variables are considered. The performance of the proposed method is evaluated using the IEEE 123-node radial distribution test feeder under changing load and irradiance conditions. To better understand the performance of the proposed method in terms of sensitivity to the distribution assumptions made in this chapter after considering the voltage regulator tap setting as a control variable, the sensitivity of the proposed method to the distribution assumptions is considered. The results showed that the method is not highly sensitive to these assumptions. The results also showed the effectiveness of the proposed method to minimize the system losses and mitigate voltage fluctuations.

In Chapter 6, a coordinated control of voltage regulators and PV inverters considering PV generation correlations to achieve the optimal expected performance is proposed. The proposed method performs this integrated control by using existing PV inverters and the voltage control equipment to improve the expected system performance while considering the spatial correlation among PV source powers. Six different methods are studied to understand the performance of the proposed method under various conditions. In the baseline method (BM), the voltage regulator tap settings are only adjusted every 15-minute period while keeping the expected voltage magnitudes within acceptable ranges without considering the variability of the PV source power injections. The dynamic method (DM) involves the fixed and variable PV inverter parameters and the voltage regulator tap settings are adjusted every 15-minute period while maintaining the expected voltage magnitudes within acceptable limits without considering the variability of the PV source power injections. The integrated method (IM) involves the fixed and variable reactive power output of PV inverters and the voltage regulator tap settings are adjusted every 15-minute period while maintaining the expected voltage magnitudes within acceptable limits, by formulating the voltage magnitudes as chance constraints and considering the variability of the PV source power injection. The limited integrated method (LIM) involves the IM used with constraining the expected variation of voltage magnitudes by a desirable standard deviation. The

correlated integrated method (CIM) involves the voltage regulator tap settings and the PV inverter reactive power output parameters are adjusted every 15-minute period while maintaining the expected voltage magnitudes within acceptable limits and considering the spatial correlation among the PV source powers. In the limited correlated integrated method (LCIM), the CIM is used with constraining the expected variation of voltage magnitudes within a desirable standard deviation. The performance of the proposed method is assessed using IEEE 123-node radial distribution test feeder under load and irradiance changing, and compared with five methods for comparison purpose. The final results showed that the proposed method is promising for improving the system performance and voltage magnitude profile with intermittent renewable resources.

7.2 Future Work

For the volt-var control method discussed in Chapter 3, which only used the reactive power outputs of PV inverters to optimize the system performance, the price for reactive power injected is ignored when formulating the proposed method. In future work, the price for reactive power injected by the PV inverter will be added to the figure of merit equation to make the proposed method more realistic. The modified figure of merit will be expressed as

$$U = \sum_{i=1}^{N_{load}} C^{load} P_{load,i} - \sum_{i=1}^{N_{pv}} C^{pv} P_{pv,i} - \sum_{i=1}^{N_{pv}} C^{qv} Q_{pv,i} - \sum_{i=1}^{N_{in}} C^{in} P_{in,i}, \tag{7.1}$$

where C^{qv} is the price paid for reactive power received from PV sources and $Q_{pv,i}$ is a reactive power received from a PV phase i.

For all volt-var control methods described in this dissertation, the most significant assumptions are the normality and independence of the PV source powers. Under these assumptions and when modeled in this linearized way, the voltage magnitudes will be normally distributed over the interval of interest. For the volt-var control methods described in Chapter 5 and 6, when assessing the results, the range of acceptable voltage magnitudes

is slightly expanded to avoid penalizing methods for extremely small deviations (e.g., non-normal distributions). In order to obtain accurate results that match these assumptions, it is recommended to use the Gaussian mixture distribution instead of using the normal Gaussian distribution for future work to fit the real data used in this dissertation.

All volt-var control methods proposed in this dissertation mostly relied on the DG reactive power parameters (i.e., the fixed and variable reactive power outputs) and the voltage control equipment (e.g., voltage regulators) to improve the system performance while maintaining the voltage magnitudes within acceptable ranges. In order to obtain a comprehensive volt-var control method, the voltage control method that controls the voltage magnitudes locally at point of common coupling is proposed for future work. The problem formulation will be expressed as

$$\begin{aligned}
&\min_{\boldsymbol{\alpha},\boldsymbol{\beta},\mathbf{K},\boldsymbol{\gamma}} && \mathrm{E}[U] \\
&\text{subject to} && \Pr[|\tilde{V}_i| \leq V_{min}] \leq p_{max} \\
&\forall i \in \{1,2,\ldots,N_{node}\} && \Pr[|\tilde{V}_i| \geq V_{max}] \leq p_{max} \\
& && \boldsymbol{\alpha}_{min} \leq \boldsymbol{\alpha} \leq \boldsymbol{\alpha}_{max} \\
& && \boldsymbol{\beta}_{min} \leq \boldsymbol{\beta} \leq \boldsymbol{\beta}_{max} \\
& && \mathbf{K}_{min} \leq \mathbf{K} \leq \mathbf{K}_{max} \\
& && \boldsymbol{\gamma}_{min} \leq \boldsymbol{\gamma} \leq \boldsymbol{\gamma}_{max},
\end{aligned} \tag{7.2}$$

where $\boldsymbol{\gamma}$ is the voltage substitution rates, $\boldsymbol{\gamma}_{min} = \gamma_{min}\mathbf{1}_{N_{inv}} \times 1$ and $\boldsymbol{\gamma}_{max} = \gamma_{max}\mathbf{1}_{N_{inv}} \times 1$, and γ_{min} and γ_{max} are minimal and maximal allowable voltage substitution rates. The reactive power injected into each inverter phase will be expressed using a modified affine control equation:

$$\mathbf{Q}_{inv} = \boldsymbol{\alpha} + \boldsymbol{\beta} \circ \mathbf{P}_{inv} + \boldsymbol{\gamma} \circ (\mathbf{S}|\tilde{\mathbf{V}}|), \tag{7.3}$$

where $\mathbf{S}$ is the $N_{inv} \times N_{node}$, a selector matrix filled with zeros and ones. This method provides a good insight as to what the performance is of the rest of the system in terms of voltage magnitudes and also gives us a degree of freedom to react towards, for example, minimizing the system losses while the $\boldsymbol{\gamma}$ can be used to maintain the probability constraints.

In this method, the set of decisions is expanded to solve the same problem proposed in this dissertation (i.e., $\boldsymbol{\alpha}$, $\boldsymbol{\beta}$, and $\boldsymbol{\gamma}$), which $\boldsymbol{\gamma}$ helps to sense the voltage magnitudes locally and react accordingly. This coordinated voltage and reactive power control can be implemented to utilize the full capability of existing voltage and reactive power control equipment. This control method provides grid-support to mitigate negative impacts that are associated with integration of the DGs and thus accommodates more DGs into the distribution systems.

Bibliography

[1] W. H. Kersting, *Distribution System Modeling and Analysis*. Boca Raton,NY: CRC Press, 2012.

[2] G. Pepermans *et al.*, "Distributed generation: definition, benefits and issues," *Energy Policy*, vol. 33, no. 6, p. 787–798, July 2005.

[3] M. Hasheminamin *et al.*, "Impact study of high PV penetration in low and medium-voltage networks when considering residential and industrial load profile," in *2013 International Conf. on Renewable Energy Research and Applications (ICRERA)*, Oct 2013, pp. 347–352.

[4] P. P. Barker and R. W. D. Mello, "Determining the impact of distributed generation on power systems. i. radial distribution systems," in *2000 Power Engineering Society Summer Meeting (Cat. No.00CH37134)*, vol. 3, 2000, pp. 1645–1656 vol. 3.

[5] J. P. Lopes *et al.*, "Integrating distributed generation into electric power systems: A review of drivers, challenges and opportunities," *Electric Power Syst. Res.*, vol. 77, no. 9, p. 1189–1203, July 2007.

[6] W. El-Khattam and M. Salama, "Distributed generation technologies, definitions and benefits," *Electric Power Syst. Res.*, vol. 71, pp. 119–128, Oct 2004.

[7] P. Chiradeja and R. Ramakumar, "An approach to quantify the technical benefits of distributed generation," *IEEE Trans. Energy Convers.*, vol. 19, no. 4, pp. 764–773, Dec 2004.

[8] M. A. Kashem and G. Ledwich, "Multiple distributed generators for distribution feeder voltage support," *IEEE Trans. Energy Convers.*, vol. 20, no. 3, pp. 676–684, Sept 2005.

[9] P. N. Vovos *et al.*, "Centralized and distributed voltage control: Impact on distributed generation penetration," *IEEE Trans. Power Syst.*, vol. 22, no. 1, pp. 476–483, Feb 2007.

[10] W. H. Kersting, "Distribution feeder voltage regulation control," *IEEE Trans. Ind. Appl.*, vol. 46, no. 2, pp. 620–626, March 2010.

[11] R.-H. Liang and Y.-S. Wang, "Fuzzy-based reactive power and voltage control in a distribution system," *IEEE Trans. Power Del.*, vol. 18, no. 2, pp. 610–618, April 2003.

[12] S. Pal and S. Nath, "An intelligent on line voltage regulation in power distribution system," in *2010 International Conf. on Power, Control and Embedded Systems*, Nov 2010, pp. 1–5.

[13] M. Tahir *et al.*, "A review of volt/var control techniques in passive and active power distribution networks," in *2016 IEEE Smart Energy Grid Engineering (SEGE)*, Aug 2016, pp. 57–63.

[14] R. A. Walling *et al.*, "Summary of distributed resources impact on power delivery systems," *IEEE Trans. Power Del.*, vol. 23, no. 3, pp. 1636–1644, July 2008.

[15] R. J. Bravo *et al.*, "Var support from solar PV inverters," in *40th IEEE Photovolt. Specialist Conf.*, June 2014, pp. 2672–2676.

[16] M. A. G. de Brito *et al.*, "Evaluation of the main MPPT techniques for photovoltaic applications," *IEEE Trans. Ind. Electron.*, vol. 60, no. 3, pp. 1156–1167, March 2013.

[17] E. Bianconi *et al.*, "A fast current-based MPPT technique employing sliding mode control," *IEEE Trans. Ind. Electron.*, vol. 60, no. 3, pp. 1168–1178, March 2013.

[18] H. Li *et al.*, "Adaptive voltage control with distributed energy resources: Algorithm, theoretical analysis, simulation, and field test verification," *IEEE Trans. Power Syst.*, vol. 25, no. 3, pp. 1638–1647, Aug 2010.

[19] S. Uaroon *et al.*, "Reactive power compensation for solving voltage problems in PV farm based upon IEC-61850," in *2017 14th Int. Conf. on Electrical Engineering/-Electronics, Computer, Telecommunications and Information Technology (ECTI-CON)*, June 2017, pp. 353–356.

[20] R. G. Wandhare and V. Agarwal, "Reactive power capacity enhancement of a PV-grid system to increase PV penetration level in smart grid scenario," *IEEE Trans. Smart Grid*, vol. 5, no. 4, pp. 1845–1854, July 2014.

[21] I. Abdelmotteleb *et al.*, "Benefits of PV inverter volt-var control on distribution network operation," in *2017 IEEE Manchester PowerTech*, June 2017, pp. 1–6.

[22] M. Farivar *et al.*, "Optimal inverter var control in distribution systems with high PV penetration," in *2012 IEEE Power and Energy Society General Meeting*, July 2012, pp. 1–7.

[23] K. Turitsyn *et al.*, "Options for control of reactive power by distributed photovoltaic generators," *Proc. IEEE*, vol. 99, no. 6, pp. 1063–1073, June 2011.

[24] Y. Liu *et al.*, "Distribution system voltage performance analysis for high-penetration PV," in *2008 IEEE Energy 2030 Conference*, Nov 2008, pp. 1–8.

[25] H. J. Liu and T. J. Overbye, "Smart-grid-enabled distributed reactive power support with conservation voltage reduction," in *Power and Energy Conf. at Illinois (PECI), 2014*, Feb 2014, pp. 1–5.

[26] *The American National Standards Institute ANSI, American national standard for electric power-systems and equipment voltage ratings (60) hertz*, ANSI Std. C84.1, 1995-1996.

[27] K. P. Schneider *et al.*, "Evaluations of conservation voltage reduction (cvr) on a national level," Pacific Nortwest National Laboratory PNNL Report, United States Department of Energy under Contract DE-AC05-76RL01830 19596, 2010.

[28] M. Braun, "Reactive power supplied by PV inverters - cost-benefit-analysis," in *22nd European Photovolt. Solar Energy Conf. and Exhibition*, Sept. 2007, pp. 1–7.

[29] P. Juanuwattanakul and M. A. S. Masoum, "Increasing distributed generation penetration in multiphase distribution networks considering grid losses, maximum loading factor and bus voltage limits," *IET Gener. Transm. Distrib.*, vol. 6, no. 12, pp. 1262–1271, December 2012.

[30] W. El-Khattam and M. Salama, "Distributed generation technologies, definitions and benefits," *Electric Power Syst. Res.*, vol. 71, no. 2, pp. 119 – 128, 2004.

[31] Y. P. Agalgaonkar *et al.*, "Distribution voltage control considering the impact of PV generation on tap changers and autonomous regulators," *IEEE Trans. Power Syst.*, vol. 29, no. 1, pp. 182–192, Jan 2014.

[32] F. Giraud and Z. M. Salameh, "Analysis of the effects of a passing cloud on a grid-interactive photovoltaic system with battery storage using neural networks," *IEEE Trans. Energy Convers.*, vol. 14, no. 4, pp. 1572–1577, Dec 1999.

[33] M. Lave1 *et al.*, "High-frequency irradiance fluctuations and geographic smoothing," *Solar Energy*, vol. 86, no. 8, pp. 2190–2199, Aug 2012.

[34] J. H. R. Enslin *et al.*, "Integrated photovoltaic maximum power point tracking converter," *IEEE Trans. Ind. Electron.*, vol. 44, no. 6, pp. 769–773, Dec 1997.

[35] D. Cheng *et al.*, "Photovoltaic PV impact assessment for very high penetration levels," *IEEE J. Photovolt.*, vol. 6, no. 1, pp. 295–300, Jan 2016.

[36] D. B. Arnold *et al.*, "Model-free optimal control of var resources in distribution systems: An extremum seeking approach," *IEEE Trans. Power Syst.*, vol. 31, no. 5, pp. 3583–3593, Sept 2016.

[37] W. Sheng *et al.*, "Reactive power coordinated optimisation method with renewable distributed generation based on improved harmony search," *IET Gener. Transm. Distrib.*, vol. 10, no. 13, pp. 3152–3162, 2016.

[38] S. Chen *et al.*, "Optimal reactive power and voltage control in distribution networks with distributed generators by fuzzy adaptive hybrid particle swarm optimisation method," *IET Gener. Transm. Distrib.*, vol. 9, no. 11, pp. 1096–1103, 2015.

[39] A. O'Connell and A. Keane, "Var curves for photovoltaic inverters in distribution systems," *IET Gener. Transm. Distrib.*, vol. 11, no. 3, pp. 730–739, 2017.

[40] R. Kabiri *et al.*, "Lv grid voltage regulation using transformer electronic tap changing, with PV inverter reactive power injection," *IEEE J. Emerging and Sel. Topics Power Electron.*, vol. 3, no. 4, pp. 1182–1192, Dec 2015.

[41] F. A. Viawan and D. Karlsson, "Combined local and remote voltage and reactive power control in the presence of induction machine distributed generation," *IEEE Trans. Power Syst.*, vol. 22, no. 4, pp. 2003–2012, Nov 2007.

[42] N. Daratha *et al.*, "Coordination between OLTC and SVC for voltage regulation in unbalanced distribution system distributed generation," *IEEE Trans. Power Syst.*, vol. 29, no. 1, pp. 289–299, Jan 2014.

[43] B. Milosevic and M. Begovic, "Capacitor placement for conservative voltage reduction on distribution feeders," *IEEE Trans. Power Del.*, vol. 19, no. 3, pp. 1360–1367, July 2004.

[44] E. A. Paaso *et al.*, "Formulation and solution of distribution system voltage and var control with distributed generation as a mixed integer non-linear programming problem," *Electric Power Syst. Res.*, vol. 108, no. 8-10, pp. 164–169, Mar 2014.

[45] A. A. S. Algarni and K. Bhattacharya, "Disco operation considering DG units and their goodness factors," *IEEE Trans. Power Syst.*, vol. 24, no. 4, pp. 1831–1840, Nov 2009.

[46] A. Safdarian *et al.*, "Integration of price-based demand response in discos' short-term decision model," *IEEE Trans. Smart Grid*, vol. 5, no. 5, pp. 2235–2245, Sept 2014.

[47] P. M. Sotkiewicz and J. M. Vignolo, "Nodal pricing for distribution networks: efficient pricing for efficiency enhancing DG," *IEEE Trans.Power Syst.*, vol. 21, no. 2, pp. 1013–1014, May 2006.

[48] A. Cagnano *et al.*, "Online optimal reactive power control strategy of PV inverters," *IEEE Trans. Ind. Electron.*, vol. 58, no. 10, pp. 4549–4558, Oct 2011.

[49] S. Weckx *et al.*, "Reducing grid losses and voltage unbalance with PV inverters," in *2014 IEEE PES General Meeting — Conf. Expos.*, July 2014, pp. 1–5.

[50] D. Chaudhary *et al.*, "Chance-constrained real-time volt/var optimization using simulated annealing," in *2015 IEEE Power and Energy Soc. General Meeting*, July 2015, pp. 1–5.

[51] L. F. Ochoa and G. P. Harrison, "Minimizing energy losses: Optimal accommodation and smart operation of renewable distributed generation," *IEEE Trans. Power Syst.*, vol. 26, no. 1, pp. 198–205, Feb 2011.

[52] A. A. A. de Souza *et al.*, "Impact of distributed generation on the operational planning of low voltage distribution networks using genetic algorithms," in *2013 IEEE PES Conf. on Innovative Smart Grid Technologies (ISGT Latin America)*, April 2013, pp. 1–7.

[53] P. Li *et al.*, "A coordinated control method of voltage and reactive power for active distribution networks based on soft open point," *IEEE Trans. Sustain. Energy*, vol. PP, no. 99, pp. 1–12, 2017.

[54] Z. Wang *et al.*, "Mpc-based voltage/var optimization for distribution circuits with distributed generators and exponential load models," *IEEE Trans. Smart Grid*, vol. 5, no. 5, pp. 2412–2420, Sept 2014.

[55] Y. M. Atwa *et al.*, "Optimal renewable resources mix for distribution system energy loss minimization," *IEEE Trans. Power Syst.*, vol. 25, no. 1, pp. 360–370, Feb 2010.

[56] A. Keane *et al.*, "Enhanced utilization of voltage control resources with distributed generation," *IEEE Trans. Power Syst.*, vol. 26, no. 1, pp. 252–260, Feb 2011.

[57] M. Chamana *et al.*, "Distributed control of voltage regulating devices in the presence of high PV penetration to mitigate ramp-rate issues," *IEEE Trans. Smart Grid*, vol. PP, no. 99, pp. 1–1, 2017.

[58] M. Z. Degefa *et al.*, "Optimal voltage control strategies for day-ahead active distribution network operation," *Electric Power Syst. Res.*, vol. 127, pp. 41–52, Oct 2015.

[59] H. J. Liu *et al.*, "Distributed voltage control in distribution networks: Online and robust implementations," *IEEE Trans. Smart Grid*, vol. PP, no. 99, pp. 1–1, 2017.

[60] T. Senjyu *et al.*, "Optimal distribution voltage control and coordination with distributed generation," *IEEE Trans. Power Del.*, vol. 23, no. 2, pp. 1236–1242, April 2008.

[61] S. Weckx *et al.*, "Combined central and local active and reactive power control of PV inverters," *IEEE Trans. Sustain. Energy*, vol. 5, no. 3, pp. 776–784, July 2014.

[62] P. Jahangiri and D. C. Aliprantis, "Distributed volt/var control by PV inverters," *IEEE Trans. Power Syst.*, vol. 28, no. 3, pp. 3429–3439, Aug 2013.

[63] H. G. Yeh *et al.*, "Adaptive var control for distribution circuits with photovoltaic generators," *IEEE Trans. Power Syst.*, vol. 27, no. 3, pp. 1656–1663, Aug 2012.

[64] M. Ibrahim and M. M. A. Salama, "Smart distribution system volt/var control using distributed intelligence and wireless communication," *IET Gener. Transm. Distrib.*, vol. 9, no. 4, pp. 307–318, 2015.

[65] R. A. Shayani and M. A. G. de Oliveira, "Photovoltaic generation penetration limits in radial distribution systems," *IEEE Trans. Power Syst.*, vol. 26, no. 3, pp. 1625–1631, Aug 2011.

[66] A. R. Malekpour and A. Pahwa, "A dynamic operational scheme for residential PV smart inverters," *IEEE Trans. Smart Grid*, vol. 8, no. 5, pp. 2258–2267, Sept 2017.

[67] H. E. Farag and E. F. El-Saadany, "Voltage regulation in distribution feeders with high DG penetration: From traditional to smart," in *2011 IEEE Power and Energy Soc. General Meeting*, July 2011, pp. 1–8.

[68] F. Katiraei and J. R. Aguero, "Solar PV integration challenges," *IEEE Power Energy Mag.*, vol. 9, no. 3, pp. 62–71, May 2011.

[69] D. Ranamuka *et al.*, "Online coordinated voltage control in distribution systems subjected to structural changes and DG availability," *IEEE Trans. Smart Grid*, vol. 7, no. 2, pp. 580–591, March 2016.

[70] M. A. Ghasemi and M. Parniani, "Prevention of distribution network overvoltage by adaptive droop-based active and reactive power control of PV systems," *Electric Power Syst. Res.*, vol. 133, pp. 313–327, Apr 2016.

[71] X. Liu *et al.*, "Reactive power control methods for photovoltaic inverters to mitigate short-term voltage magnitude fluctuations," *Electric Power Syst. Res.*, vol. 127, pp. 213–220, Oct 2015.

[72] E. Demirok *et al.*, "Local reactive power control methods for overvoltage prevention of distributed solar inverters in low-voltage grids," *IEEE Journal of Photovoltaics*, vol. 1, no. 2, pp. 174–182, Oct 2011.

[73] A. Safayet *et al.*, "Reactive power management for overvoltage prevention at high PV penetration in a low-voltage distribution system," *IEEE Trans. Ind. Appl.*, vol. 53, no. 6, pp. 5786–5794, Nov 2017.

[74] M. J. E. Alam *et al.*, "A multi-mode control strategy for var support by solar PV inverters in distribution networks," *IEEE Trans. Power Syst.*, vol. 30, no. 3, pp. 1316–1326, May 2015.

[75] E. A. Paaso *et al.*, "Dual-layer voltage and var control approach with active participation from distributed solar generations," *Electr. Power Compon. Syst.*, vol. 43, no. 8-10, pp. 854–865, Mar 2015.

[76] J. M. Guerrero *et al.*, "Advanced control architectures for intelligent microgrids; part i: Decentralized and hierarchical control," *IEEE Trans. Ind. Electron.*, vol. 60, no. 4, pp. 1254–1262, April 2013.

[77] H. R. Baghaee *et al.*, "A decentralized power management and sliding mode control strategy for hybrid ac/dc microgrids including renewable energy resources," *IEEE Trans. Ind. Informat.*, vol. PP, no. 99, pp. 1–1, 2017.

[78] N. Yang *et al.*, "An investigation of reactive power planning based on chance constrained programming," *Electric Power Syst. Res.*, vol. 151, pp. 650–656, Nov 2007.

[79] B. Odetayo *et al.*, "A chance constrained programming approach to integrated planning of distributed power generation and natural gas network," *Electric Power Syst. Res.*, vol. 151, pp. 197–207, Oct 2017.

[80] M. Lubin *et al.*, "A robust approach to chance constrained optimal power flow with renewable generation," *IEEE Trans. Power Syst.*, vol. 31, no. 5, pp. 3840–3849, Sept 2016.

[81] K. Baker and B. Toomey, "Efficient relaxations for joint chance constrained AC optimal power flow," *Electric Power Syst. Res.*, vol. 148, pp. 230–236, July 2017.

[82] Y. Zhang *et al.*, "Distributionally robust chance-constrained optimal power flow with uncertain renewables and uncertain reserves provided by loads," *IEEE Trans. Power Syst.*, vol. 32, no. 2, pp. 1378–1388, March 2017.

[83] L. Roald and G. Andersson, "Chance-constrained ac optimal power flow: Reformulations and efficient algorithms," *IEEE Trans. Power Syst.*, vol. PP, no. 99, pp. 1–1, 2017.

[84] E. Dall'Anese *et al.*, "Chance-constrained ac optimal power flow for distribution systems with renewables," *Electric Power Syst. Res.*, vol. 32, no. 5, pp. 3427–3438, Sept 2017.

[85] S. Ibrahim *et al.*, "PV inverter reactive power control for chance-constrained distribution system performance optimisation," *IET Gener. Transm. Distrib.*, vol. 12, no. 5, pp. 1089–1098, 2018.

[86] Q. Yang *et al.*, "Communication infrastructures for distributed control of power distribution networks," *IEEE Trans. Ind. Informat.*, vol. 7, no. 2, pp. 316–327, May 2011.

[87] W. H. Kersting, "Radial distribution test feeders," *IEEE Trans. Power Syst.*, vol. 6, no. 3, pp. 975–985, Aug 1991.

[88] M. Sengupta and Andreas. (2010) Solar measurement grid (1.5-year archive) 1-second global horizontal irradiance oahu, hawaii. [Online]. Available: http://www.nrel.gov/midc/oahu-archive/

[89] (2016) U.s. energy information administration (EIA). [Online]. Available: http://www.eia.gov/

[90] L. Chong *et al.*, "Short-term PV generation forecasting based on weather type clustering and improved GPR model," in *2016 Chin. Int. Conf. on Electricity Distribution (CICED)*, Aug 2016, pp. 1–5.

[91] A. Tascikaraoglu *et al.*, "Compressive spatio-temporal forecasting of meteorological quantities and photovoltaic power," *IEEE Trans. Sustain. Energy*, vol. 7, no. 3, pp. 1295–1305, July 2016.

[92] T.W.Anderson and D.A.Darling, "Asymptotic theory of certain goodness of fit criteria based on stochastic processes," *IEEE Trans. Sustain. Energy*, vol. 2, no. 23, pp. 193–212, 1952.

[93] S. K. Ibrahim *et al.*, "Integrated distribution system optimization using a chance-constrained formulation," in *2017 North American Power Symp. (NAPS)*, Sept 2017, pp. 1–6.

[94] F. Tamp and P. Ciufo, "A sensitivity analysis toolkit for the simplification of MV distribution network voltage management," *IEEE Trans. Smart Grid*, vol. 5, no. 2, pp. 559–568, March 2014.

[95] Electric Reliability Council of Texas available at: http://www.ercot.com, accessed 15 August 2017.

[96] C. Yang *et al.*, "Multitime-scale data-driven spatio-temporal forecast of photovoltaic generation," *IEEE Trans. Sustain. Energy*, vol. 6, no. 1, pp. 104–112, Jan 2015.

[97] C. M. Huang *et al.*, "One-day-ahead hourly forecasting for photovoltaic power generation using an intelligent method with weather-based forecasting models," *IET Gener. Transm. Distrib.*, vol. 9, no. 14, pp. 1874–1882, 2015.

[98] R. C. Dugan, "Reference guide: The open distribution system simulator (OpenDSS)," *EPRI, Tech. Rep*, Jun 2013.

[99] Y. P. Agalgaonkar *et al.*, "Distribution voltage control considering the impact of PV generation on tap changers and autonomous regulators," *IEEE Trans. Power Syst.*, vol. 29, no. 1, pp. 182–192, Jan 2014.

[100] K. Yasunami and T. Washio, "An accuracy evaluation of PV power output estimation method using covariance between solar radiation intensity and power flow," in *2015 IEEE Innovative Smart Grid Technologies - Asia (ISGT ASIA)*, Nov 2015, pp. 1–6.

Vita

Sarmad K. Ibrahim received the B.Sc. degree in electrical engineering from the University of Babylon, Babylon, Iraq, in 2002, the M.Sc. degree in electrical power engineering from the University of Technology, Baghdad, Iraq, in 2005, and he is currently pursuing the Ph.D. degree in electrical engineering from University of Kentucky, USA.

Publications

1. Sarmad Ibrahim, Aaron Cramer, Xiao Liu, and Yuan Liao: 'Photovoltaic Inverter Reactive Power Control for Chance-Constrained Distribution System Performance Optimization', *IET Generation, Transmission and Distribution*, 2018, 12, (5), pp. 1089–1098.

2. Sarmad K. Ibrahim, Aaron Cramer, and Yuan Liao: 'Integrated distribution system optimization using a chance-constrained formulation', *2017 IEEE North American Power Symposium (NAPS)*, 2017, pp. 1–6.

3. Sarmad Ibrahim, Aaron Cramer, and Yuan Liao: 'Integrated Control of Voltage Regulators and Distributed Generation Inverters', *Submitted: Electric Power Systems Research*, 2017.